

Department of Environmental, Land and Infrastructure Engineering

Master of Science in Georesources and Geoenergy Engineering

Parametric Analysis of EoS

By

Aktoty Kauzhanova

S330789

Supervisors

Prof. Dario Viberti Supervisor Dott.ssa Marialuna Loffredo Co-Supervisor

> Politecnico di Torino October, 2025

Summary

This work presents a parametric analysis and practical comparison of four cubic equations of state (EoS): Soave – Redlich – Kwong (SRK), Soave – Redlich – Kwong – Peneloux (SRKP), Peng – Robinson (PR) , and Peng – Robinson – Peneloux (PRP) using a QA/QC-verified PVT dataset from the Volve field provided by the technical literature.

The aim is to compare the results of four EoS-based PVT simulations with experimental data, and to correlate the deviations to the physical meaning of the EoS parameters.

The first step in the workflow was the validation of the bottom hole sample reliability through a material balance assessment. Furthermore, an equilibrium consistency check was performed using Hoffman and Buckley plots to verify the validity of the phase behaviour predictions.

The four models with default parameters were run on 23 component compositions to perform the EoS parametric analysis. PR underestimated P_{sat} by approximately 9% compared to experimental data, while SRK overestimated Psat by about 5%. PR and PRP showed a better match for the Constant Composition Expansion (CCE). However, SRK and SRKP predicted Differential Liberation parameters better compared to PR and PRP. Overall, the study showed a systematic offset between PR and SRK consistent with the different formulations of the attractive and repulsive terms.

Following this, plus-fluid regression was applied on 23 components mixture to improve heavy end characterization. The composition was then lumped to 8 components and tuned within acceptable tolerances.

The study demonstrates that each EoS has its own strengths and limitations. Furthermore, a workflow for fit- for- purpose EoS methodology is presented. In this study we focused on a single composition, however in practice, field wide EoS is tuned using multiple samples to obtain a representative EoS model.

Acknowledgment

I would like to express my sincere gratitude to Professor Dario Viberti for his clear and inspiring explanations of PVT during the course. His enthusiasm for teaching motivated me to study more deeply, and his support throughout my thesis was invaluable. I am also deeply grateful to Dr. Marialuna Loffredo for her thorough review, guidance, and great patience throughout the writing process. Her direction improved the quality of this work. I acknowledge all the professors whose guidance helped me acquire knowledge. I am especially thankful to my family for their support and encouragement. I also acknowledge ENI Corporate University for the scholarship and institutional support, and NCOC for their sustained support throughout my studies. Finally, I would like to thank my classmates for their friendship and helping one another, especially during exams, their support and camaraderie made this experience memorable.

Contents

1.	Contents		3
2.	Chapter 1.		1
3.	-	Review of Equation	
			1
	1.1 C	orresponding States Principles	1
		centric Factor	
		Phase envelope	
		ubic Equation of State	
	1.4.1	The van der Waals Equation of State	7
	1.4.2		
	1.4.3	Soave-Redlich-Kwong Equation of State	
	1.4.4	Peng-Robinson Equation of State	
	1.4.5	Peneloux Volume Correction	
	1.5 F	lash and Phase Envelope Calculations	16
4.	Chapter 2.		19
5.	2	Workflow of Parametric Analysi	s of EoS
			19
	2.1 Q	uality Control of Black Oil Laboratory Data	19
	2.1.1	Material Balance Check	20
	2.1.2	Thermodynamic Consistency Check of Composition	21
	2.2 E	oS Comparison and Definition of PVT Properties	23
	2.2.1	Composition Preparation for Modelling	23
	2.2.2		
	2.2.3	Comparison of Equations of State	
	2.3 P	lus Fluid Regression	32
	2.4 L	umping and Calibration	33
	2.4.1	Lumping scheme	34

	2.4.2	Lumping in PVT sim	34
	2.4.3	Calibration of the 8 component EoS	36
6.	Chapter 3		38
7.	3		Real data
	3.1 Qu	ality Control of Laboratory Data	38
	3.1.1	Material Balance Check	38
	3.1.2	Thermodynamic Consistency Check of Composition	40
	3.2 Eo	S Comparison	42
	3.2.1	Input Data for PVT Simulation	42
	3.2.2	Comparison of EoS Results with Experimental Data	
	3.3 Plu	ıs Fluid Regression	52
	3.4 Lui	mping and Calibration of PR-P	60
	3.4.1	Lumping of 23 Components to 8 Components	60
	3.4.2	Calibration of 8 Component EoS (PR-P)	65
8.	Conclusion		3—1
9.	References.		3—2
10.			

List of Tables

Table 2.1: Standard characterization -SRK [Pedersen et al.,1989 and 1992].24
Table 2.2: Standard characterization – PR [Pedersen et al.,2002]24
Table 2.3: Heavy oil characterization – SRK [Pedersen et al.,2002]24
Table 2.4: Heavy oil characterization – PR [Pedersen et al.,2002]25
Table 2.5: Splitting of plus fraction into carbon number fractions [Calsep Tech
Talk #19]25
Table 2.6: Summary of the key differences between SRK and PR formulations
[Soave 1972; Danesh 1998]; [Peng & Robinson 1976; Pedersen 2007]32
Table 3.1: Composition of the bottom hole sample39
Table 3.2: Single stage flush results
Table 3.3: 23 Component mixture used for the modelling of EoS [Lab. Report
Well 15/9-19SR DST 1]42
Table 3.4: Constant mass expansion results [Lab. Report Well 15/9-19SR DST
1]43
Table 3.5: Differential liberation results [Lab. Report Well 15/9-19SR DST 1].
43
Table 3.6: Differential liberation results [Lab. Report Well 15/9-19SR DST 1].
44
Table 3.7: Viscosity correction factor adjustment. Plus fluid regression55
Table 3.8: Summary of regressed parameters of Option 1 (stepwise regression)
and Option 2 (combined regression)76
Table 3.9: Results of Option 1 (stepwise regression) and Option 2 (combined
regression). Weight indicates the relative importance assigned during regression;
AAD is the mean absolute difference between pre- and post-tuning predictions .77

List of Figures

Figure 1.1: Generalized compressibility factor correlation applicable across the
full range of reduced pressures $Pr, Vr = V/RTc/Pc$ [Nelson et al., 1954]
Figure 1.2: Schematic P-T diagram of a binary mixture [Danesh, 1998]
Figure 1.3: Schematic P-V diagram of a binary mixture [Danesh, 1998]
Figure 1.4: Phase diagram of ethane-normal heptane [Danesh 1998]
Figure 1.5: Phase envelope of a multicomponent mixture [Danesh 1998]6
Figure 1.6: PV curve for pure component
Figure 1.7: PV isotherms of a pure substance at subcritical, critical, and
supercritical temperatures predicted by a van der Waals EoS10
Figure 1.8: Schematic representation of P-T flash process for a hydrocarbon
reservoir mixture [Pedersen, 2007]
Figure 2.1: Material balance plot for PVT compositions. Green markers show
YiZiandXiZi computed from laboratory data; red markers useYiZiandXiZi with
calculated Zi. Plotted data demonstrate alignment of laboratory and calculated data
Figure 2.2: Demonstration of Hoffman plot with valid data [Seyed Mohammac
et al., 2020]
Figure 2.3: Demonstration of Buckley plot with valid data [Seyed Mohammac
riguic 2.5. Demonstration of Duckley plot with valid data [Seyed Monaninal
et al., 2020]23
et al., 2020]

Figure 3.3: Buckley plot41
Figure 3.4: Phase envelope comparison modelled by PR and SRK. Deviation
of the modelled Psat from experimental Psat
Figure 3.5: CCE. Relative volume comparison. (a) – Deviation from
experiment (%). (b) – Relative volume vs. pressure (bar)
Figure 3.6: CCE. Compressibility comparison. (a) – Deviation from
experiment (%). (b) – Compressibility vs. pressure (bar)
Figure 3.7: CCE. Y-Factor comparison. (a) – Deviation from experiment (%).
(b) – Y-Factor vs. pressure (bar)
Figure 3.8: DL oil formation volume factor. (a) – Deviation from experiment
(%). (b) – Oil formation volume factor vs. pressure (bar)
Figure 3.9: DL Solution GOR. (a) – Deviation from experiment (%). (b) –
Solution GOR vs. pressure (bar)
Figure 3.10: DL oil density. (a) – Deviation from experiment (%). (b) – Oil
density vs. pressure (bar)
Figure 3.11: DL Z- factor. (a) – Deviation from experiment (%). (b) – Z- factor
vs. pressure (bar)51
Figure 3.12: DL Gas viscosity. (a) – Deviation from experiment (%). (b) – DL
gas viscosity vs. pressure (bar)
Figure 3.13: Oil viscosity. (a) – Deviation from experiment (%). (b) – Oil
viscosity vs. pressure (bar)
Figure 3.14: Molecular weight adjustment. Plus fluid regression53
Figure 3.15: Critical Pressure adjustment. Plus fluid regression53
Figure 3.16: Critical temperature adjustment. Plus fluid regression54
Figure 3.17: Recomputed cPen values due to MW change. Plus fluid regression.
Figure 3.18: Acentric factor adjustment. Plus fluid regression55
Figure 3.19: CCE Relative volume – before and after tuning
Figure 3.20: CCE Compressibility result – before and after tuning56
Figure 3.21: CCE Y-factor – before and after tuning
Figure 3.22: DL Oil FVF – before and after tuning
Figure 3.23: DL Gas FVF – before and after tuning
Figure 3.24: Oil density – before and after tuning
Figure 3.25: Gas Z-factor – before and after tuning
Figure 3.26: Gas Z-factor – before and after tuning
Figure 3.27: Oil viscosity – before and after tuning60
Figure 3.28:Phasae envelope comparison between 23 Component model (post
plus fluid regression) and 8 component lumped model61

Figure 3.47: DL Oil Formation Volume Factor. Difference between Post
lumping and Option 1(1-Step and2-Step Regression) and Option 2 (combined
Regression)
Figure 3.48: DL Oil density. Difference between Post lumping and Option 1(1-
Step and 2-Step Regression) and Option 2 (combined Regression)
Figure 3.49: DL Gas Z-Factor. Difference between Post lumping and Option
1(1-Step and2-Step Regression) and Option 2 (combined Regression)74
Figure 3.50: DL Gas Viscosity. Difference between Post lumping and Option
1(1-Step and2-Step Regression) and Option 2 (combined Regression)74
Figure 3.51: Oil Viscosity. Difference between Post lumping and Option 1(1-
Step and 2-Step Regression) and Option 2 (combined Regression)
Figure 3.52: Oil density. Post Peneloux correction regression applied on Option
1

Chapter 1

1. Review of Equation of State

Equations of state (EoS) play an important role in thermodynamics, fluid mechanics and reservoir engineering. These models give a mathematical description of the behavior of substances as the pressure, temperature and volume are varied. In reservoir engineering, Peng-Robinson (PR) and Soave-Redlich-Kwong (SRK) are probably the most commonly used EoS models for simulating hydrocarbon phase behaviors, interpreting production strategy and modeling PVT property. During the last century, numerous empirical equations of state (EoS) formulations have been developed and optimized to capture the complex thermodynamic properties of a mixture of hydrocarbons.

This chapter follows the development of EoSs, summarizes the theoretical aspects of EoSs analysis, and presents recent innovations with respect to parameter optimization and characterization and also describes the specific case of volatile oils and gas condensates.

1.1 Corresponding States Principles

The corresponding states principle (CSP) states that fluids whether pure components or mixtures evaluated at the same non-dimensional reduced temperature $(T_r = T/T_c)$ and reduced pressure $(P_r = P/P_c)$ exhibit approximately the same deviation from the ideal gas behaviour.

In a general, two parameter form [Poling et al., 2001], CSP can be expressed as

$$P_r = P_r(V_r, T_r), \tag{1.1}$$

where V_r and T_r denote the reduced (specific) volume and reduced temperature, respectively.

This formulation is most reliable for groups of substances with broadly similar molecular structures. To extend applicability across dissimilar groups, a third parameter is introduced – the compressibility factor (Z - Factor). Z-Factor is a

measurement of how much a real gas deviates from an ideal gas behaviour. For an ideal gas Z equals 1. For non-ideal gas, Z may attain values below or above 1. It is a dimensionless ratio and in thermodynamics is defined as [Poling et al., 2001]:

$$Z = \frac{PV}{RT}. ag{1.2}$$

The compressibility factor may be expressed in a fully non-dimensional form:

$$Z = Z_c P_r V_r, T_r \tag{1.3}$$

using the critical compressibility factor (Eq. 1.7) and its reduced form (Eq.1.8).

$$Z_c = \frac{P_c V_c}{RT_c}; (1.4)$$

$$Z_r = \frac{Z}{Z_c} = \frac{P_r V_r}{T_r}. ag{1.5}$$

Following [Bejan, 2006], pure substances can be described by a two-parameter CSP and a compressibility factor. It enables eliminating V_r from the above equation to obtain the following 3-parameter relationship:

$$Z = Z(T_r, P_r, Z_c), \tag{1.6}$$

where Z_c may serves as the parameter reflecting aspects of molecular constitution [Bejan, 2006].

Consequently, the behaviour of many fluids can be generalized in a single chart. The chart shown in Figure 1.5 is the Nelson-Obert correlation, constructed from experimental PVT measurements for multiple substances [Nelson et al., 1954]. It is broadly applicable to most non-polar fluids; however, it should not be used for strongly polar compounds or for helium, hydrogen, or neon unless modified critical constants are employed [Poling et al., 2001].

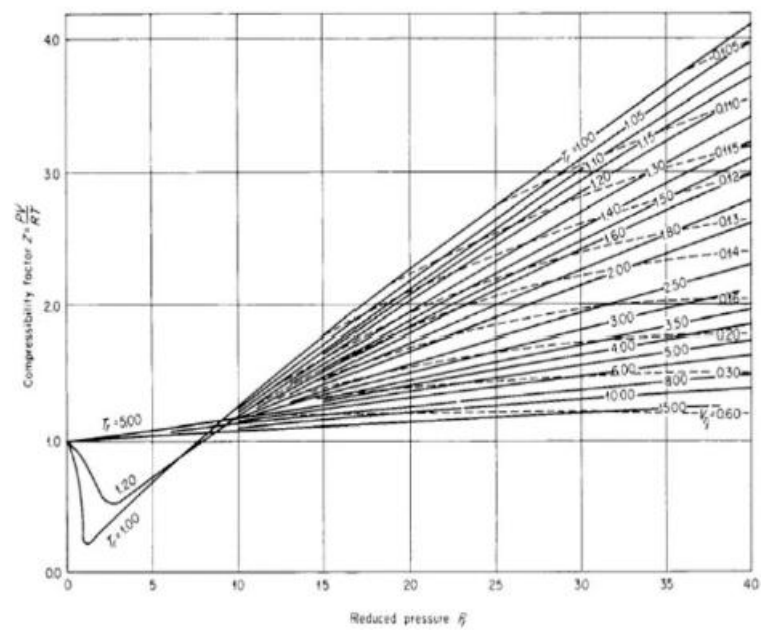


Figure 1.1: Generalized compressibility factor correlation applicable across the full range of reduced pressures P_r , $V_r = V/(RT_c/P_c)$ [Nelson et al., 1954]

1.2 Acentric Factor

An alternative approach was proposed by Pitzer [Pitzer et al. 1955]. In his work he introduced the use of the acentric ω , defined as:

$$\omega = -\log_{10} P_r - 1 \quad \text{for} \quad T_r = 0.7.$$
 (1.7)

This formulation assigns the value $\omega = 0$ to so-called "simple fluids", which Pitzer described as permanent gases with heavy molecules, such as Ar, Xe, and Ne [Bejan, 2006].

The acentric factor is determined from the deviation of a fluid's experimental vapor-pressure curve from that of a reference substance composed of small, spherical molecules. It increases with molecular complexity and non-sphericity. For hydrocarbons, ω rises with carbon number and with structural features such as branching, cyclization, and aromaticity. So heavier hydrocarbons and the C_7 + pseudo-components that represent them typically exhibit substantially larger ω acentric factors than small, nearly spherical alkanes (e.g., CH_4 , C_2H_6) [Poling et al.,2001]

Based on this concept, the three-parameter corresponding states principle (CSP) can be expressed as:

$$Z = Z(T_r, P_r, \omega). \tag{1.8}$$

Moreover, ω enters directly into cubic equation of state and mixing rules: it determines the temperature dependent attractive parameter a(T). These

applications ensure accurate predictions of phase behaviour in complex, non-ideal reservoir fluids.

1.3 Phase envelope

A real reservoir fluid is multicomponent, so its phase behaviour is more involved than that of a single pure compound. However, because most reservoir hydrocarbons have similar structures and sizes, the overall behaviour is usually not highly complicated [Danesh, 1998].

Binary mixtures (two components) are useful as examples since they capture the essential features of hydrocarbon phase behaviour and often look very similar to a full multicomponent system. For that reason, binaries are a good, simple stand-in for explaining the qualitative behaviour of reservoir fluids [Danesh,1998].

In a binary vapor—liquid system the phase rule gives two degrees of freedom, so temperature and pressure can be varied independently (Figure 1.1). The phase envelope on a pressure-temperature diagram (P-T diagram) is bounded by the bubble-point and dew-point curves, inside which vapor and liquid coexist. These curves meet at the critical point (C), where the two phases become indistinguishable. Mixtures can exhibit two phases even above the critical temperature or pressure of the pure components. The phase envelope attains its highest pressure at the cricondenbar (B) and highest temperature at the cricondentherm (D).

Figure 1.2 illustrates the pressure volume diagram (P-V diagram) of a binary mixture at fixed temperature. Unlike a pure component, which holds pressure constant through the two-phase region—the mixture's pressure decreases during isothermal expansion from the bubble point to the dew point.

A mixture's phase diagram is set by its overall composition. For the ethane—heptane system (Figure 1.3), the mixture critical temperature lies between the pure-component critical temperatures, whereas the mixture critical pressure commonly lies above both pure-component values. As composition varies, the set of critical states traces a critical locus (dashed line) [Danesh,1998; Pedersen et al., 2014].

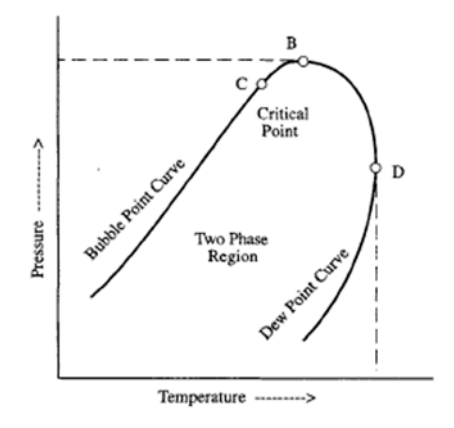


Figure 1.2: Schematic P-T diagram of a binary mixture [Danesh, 1998].

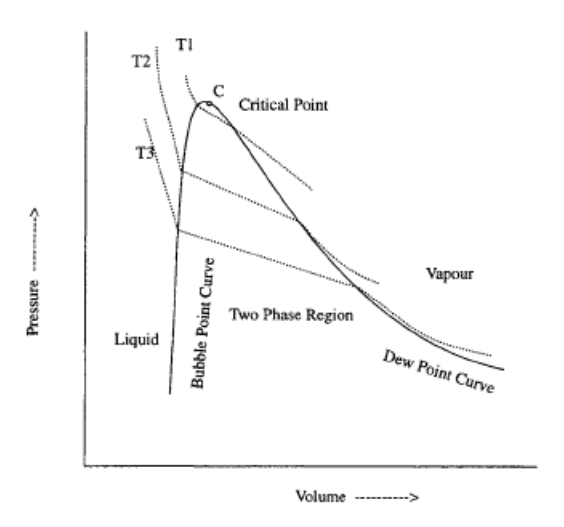


Figure 1.3: Schematic P-V diagram of a binary mixture [Danesh, 1998].

A binary mixture's critical pressure tends to increase as the separation between the pure-component critical points grows. As indicated in Figure 1.3, two-phase states occur only within the region bounded by the critical-point locus (the critical line connecting the pure-component critical points); outside this envelope the mixture is single phase.

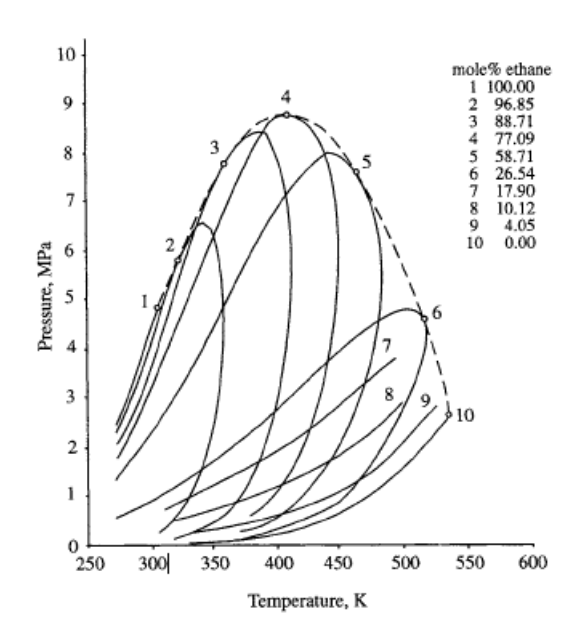


Figure 1.4: Phase diagram of ethane-normal heptane [Danesh 1998].

The principle of corresponding states for pure fluids can be extended to mixtures by replacing true critical properties with pseudo-critical (mixture) values. These pseudo-critical properties are obtained from the pure-component critical data using a mixing rule. The most common choice is Kay's mixing rule [Kay, 1936] (simple mole-fraction averaging):

$$\widehat{\Phi_c} = \sum_i z_i \; \Phi_{c,i}, \tag{1.9}$$

where z_i is the mole fraction of component i; $\Phi_{c,i}$ is a critical property of component i (e.g $T_{c,i}$, $P_{c,i}$, $V_{c,i}$,); and $\widehat{\Phi}_c$ is the corresponding pseudo-critical mixture value $(\widehat{T}_c, \widehat{P}_c, \widehat{V}_c)$.

Therefore, the pseudo-critical properties for the mixture are defined as:

$$T_r^{\rm ps} = \frac{T}{\widehat{T}_c}; \tag{1.10}$$

$$P_r^{\rm ps} = \frac{\tilde{P}}{\widehat{P}_c}.\tag{1.11}$$

These pseudo-reduced quantities let applying pure-fluid correlations to multicomponent systems.

Figure 1.4 presents a constant-composition phase diagram for a multicomponent mixture. Within the phase envelope, liquid and vapor coexist; outside it, the fluid is single phase. Lines of constant vapor quality (or liquid/mixture volume ratio) are shown inside the envelope. These iso-quality lines crowd together as the critical point is approached, indicating that very small changes in pressure or temperature near critical conditions produce large changes in phase proportions.

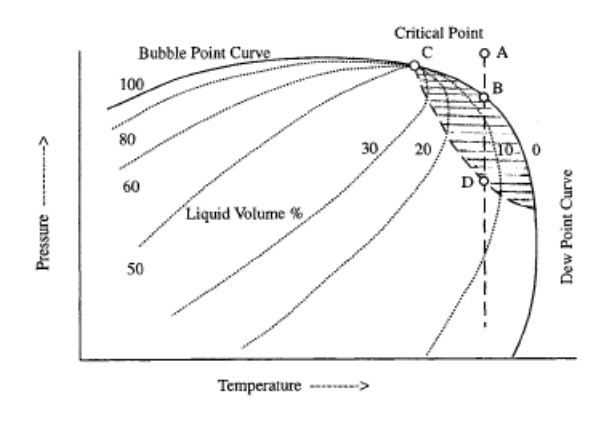


Figure 1.5: Phase envelope of a multicomponent mixture [Danesh 1998].

1.4 Cubic Equation of State

Most of the PVT calculations in oil and gas mixtures are based upon cubic EoS which has been around for over a century since the work of van der Waals (Van der Waals, 1873). From Van der Waals equation, a number of cubic models have modified terms over the years in an attempt to more accurately predict phase behavior and physical properties of hydrocarbon systems. A cross-cutting and dominant version was created by Redlich and Kwong in 1949. In the 1970s, this

model was improved by Soave (1972) and Peng-Robinson (1976, 1978). Later, in 1982, Peneloux et al. presented a volume-shift concept to improve the liquid-density predictions. Rigorous cubic formulations have gained popularity in the last four decades thanks to cheaper computing technology which allows to generate millions of multicomponent phase-equilibrium and property calculations in seconds.

1.4.1 The van der Waals Equation of State

The starting point for Van der Waals' EoS was the phase behavior of a pure component. Figure (1.6) displays pressure (P) vs. molar volume (V) curves for a pure component at various temperatures. At temperatures above the critical one, the PV curves show a hyperbolic shape suggesting that the pressure is inversely proportional to the molar volume. This behavior is known from the ideal gas law:

$$P = \frac{RT}{V},\tag{1.12}$$

where R is the gas constant and T is the absolute temperature. According to the ideal gas law, the molar volume of a component approaches to zero as the pressure tends to be infinite. However, as shown in Figure 1.6, this is not what happens when dealing with real gases since increasing pressure, the molar volume tends to a limiting value, which van der Waals named b. By considering this behavior of real gases, van der Waals [van Der Waals, 1913] modified the ideal gas law as follows:

$$V = \frac{RT}{P} + b. ag{1.13}$$

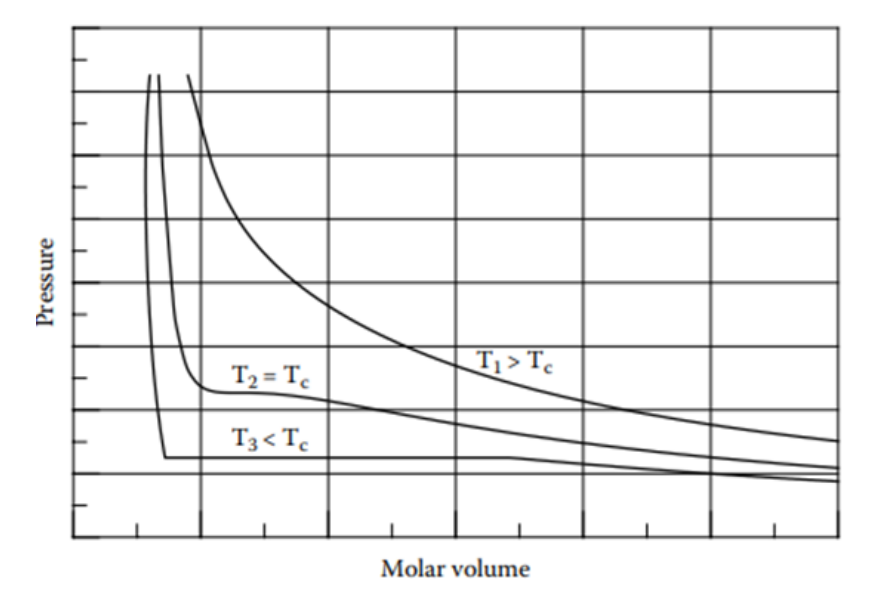


Figure 1.6: PV curve for pure component

Therefore, the pressure is obtained as:

$$P = \frac{RT}{V - h}. ag{1.14}$$

At temperatures below the critical point (T3 in Figure 1.6) a vapor-to-liquid phase transition may take place. The phase transition from a gaseous state where the molecules are far apart to a liquid state where the molecules are much closer suggests the presence of attractive forces between the molecules. These attractive forces are not accounted for in Eq.1.14, which is therefore not capable of describing a vapor-to-liquid phase transition. The force acting between two volume elements is proportional to the molecular concentration, which is inversely proportional to the molar volume, suggesting a dependence on $\frac{1}{V^2}$. Based on this, van der Waals proposed an attractive term proportional to $\frac{1}{V^2}$, obtaining the following EoS formulation:

$$P = \frac{RT}{V - b} - \frac{a}{V^2}.\tag{1.15}$$

The van der Waals equation can be written in terms of volume to find the molar volume from pressure and temperature:

$$V^{3} - \left(b + \frac{RT}{P}\right)V^{2} + \frac{a}{P}V - \frac{ab}{P} = 0.$$
 (1.15)

At the critical point of a pure component, the isothermal first and second derivatives of pressure with respect to volume are zero:

$$\left(\frac{\partial P}{\partial V}\right)_{P_c, V_c, T_c} = \left(\frac{\partial^2 P}{\partial V^2}\right)_{P_c, V_c, T_c} = 0 \tag{1.17}$$

Accordingly, the critical isotherm has a horizontal point of inflection at the critical state from Eq 1.15.

$$\left(\frac{\partial P}{\partial V}\right)_T = -\frac{RT}{(V-b)^2} + \frac{2a}{V^3};\tag{1.18}$$

$$\left(\frac{\partial^2 P}{\partial V^2}\right)_T = \frac{2RT}{(V-b)^3} - \frac{6a}{V^4}.$$
(1.19)

At the critical point we have:

$$\left(\frac{\partial P}{\partial V}\right)_{P_c, V_c, T_c} = -\frac{RT_c}{(V_c - b)^2} + \frac{2a}{V_c^3} = 0;$$
 (1.20)

$$\left(\frac{\partial^2 P}{\partial V^2}\right)_{P_c, V_c, T_c} = \frac{2RT_c}{(V_c - b)^3} - \frac{6a}{V_c^4} = 0.$$
(1.21)

From Eq. 1.20 and Eq. 1.21 knowing that at the critical point V equals the critical molar volume V_c , a and b can be expressed as follows:

$$b = \frac{V_c}{3} = \frac{0.125 \, RT_c}{P_c}; \tag{1.22}$$

$$a = \frac{9}{8}T_c V = \frac{0.4218 R^2 T_c^2}{P_c}.$$
 (1.23)

For cubic EoS at subcritical temperatures (Eq. 1.16) gives three roots for volume or compressibility factor. The largest root corresponds to saturated vapor, the smallest root to saturated liquid. The intermediate root has no physical meaning since it implies a positive value $\left(\frac{\partial P}{\partial V}\right)_T$, which is impossible for a pure component. Whereas for a single component, increasing pressure must reduce the molar volume, so $\left(\frac{\partial P}{\partial V}\right)_T$ should be a large negative value. In the case of the liquid phase, at high pressures the variation of molar volume is very small and $\left(\frac{\partial P}{\partial V}\right)_T$ is relatively high for the liquid phase.

At temperatures above the critical temperature, the Van der Waals EoS produces one real root and two complex roots (discarded). The single root represents the fluid: if it lies close to b the state is compressed liquid, whereas if it is near RT/P, the state is gas or superheated vapor. At the critical temperature all three roots are equal and represents the critical volume.

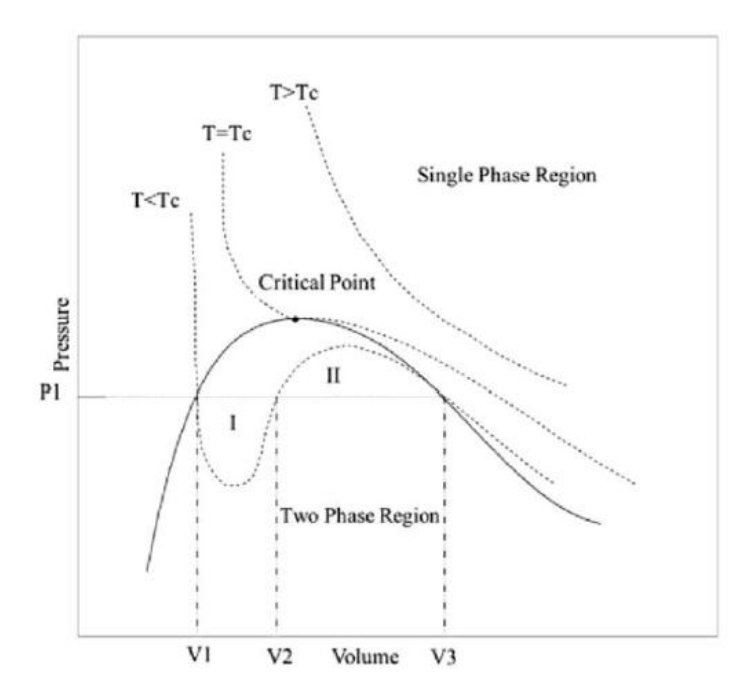


Figure 1.7: PV isotherms of a pure substance at subcritical, critical, and supercritical temperatures predicted by a van der Waals EoS.

The Van der Waals equation can also be written in terms of compressibility factor:

$$Z^{3} - \left(1 + \frac{Pb}{RT}\right)Z^{2} + \frac{Pa}{R^{2}T^{2}}Z - \frac{P^{2}}{R^{3}T^{3}}ab = 0.$$
(1.24)

From Eq. 1.25 it is possible to calculate the value of Z_c for which we obtain:

$$Z_c = \frac{3}{8} = 0.375. \tag{1.25}$$

However, experimental evidence shows that the critical compressibility factor for pure fluids is between $Z_c^{(H_2O)} = 0.23$ to $Z_c^{(H_2)} = 0.30$ [Poling et al., 2001], which justifies the need for improvements.

Indeed, this equation is not suited to describe the behavior of dense fluids and several different variations to improve its performance have been proposed, in which the attractive and repulsive terms have been varied.

Later developments of cubic equations of state have primarily focused on improving the quantitative predictions of vapor pressure and phase properties. In addition, considerable efforts have been done to extend the application area of cubic equations of state from pure components to mixtures.

1.4.2 Redlich-Kwong Equation of State

The equation of Redlich and Kwong (1949) [Redlich et al., 1949] is, by many, considered the first modern equation of state and takes the following form:

$$P = \frac{RT}{V - b} - \frac{a}{\sqrt{T}V(V + b)}.$$
(1.26)

In this case attractive term differs from the one in the van der Waals equation (Equation 1.13) for the following reasons:

- it has a more complex dependence on temperature, improving the accuracy of vapor pressure predictions;
- the denominator of the attractive term, originally expressed as V^2 in the van der Waals model, is modified to V(V + b) in order to improve the estimation of liquid-phase molar volumes.

The parameters a and b are calculated according to the following equations:

$$a_c = \frac{0.42748R^2T_c^2}{P_c}; (1.27)$$

$$b = \frac{0.08664RT_c}{P_c}. (1.28)$$

Redlich and Kwong (1949) applied classical van der Waals one fluid mixing rules to handle mixtures [Pedersen&Christensen, 2007]. For a N-component mixture, the parameters a and b are found using the following mixing rules [van der Waals, 1873]:

$$a = \sum_{i} \sum_{j} z_i z_j \ a_{ij}; \tag{1.29}$$

$$b = \sum_{i} z_i b_i, \tag{1.30}$$

where z_i and z_j denote the mole fractions of components i and j respectively. The parameter b_i corresponds to the b value of component i, obtained from Eq 1.28. The cross-compressibility factor and critical volume are defined as follows:

$$Z_{c,ij} = \frac{Z_{c,i} + Z_{c,j}}{2}; (1.31)$$

$$V_{cij} = \left(\frac{V_{ci}^{1/3} + V_{cj}^{1/3}}{2}\right)^{3},$$
(1.32)

where $Z_{c,i}$ and $Z_{c,j}$ represent the compressibility factors of components i and i at their respective pure-component critical points. The mixing rule applied for the critical volume relies on the assumption that the molecular dimensions of components i and j are proportional to the cubic roots of V_{ci} and V_{cj} respectively. Consequently, the term within the parentheses in Eq. 1.32 corresponds to the average linear dimension of the molecules of i and i.

Using the definition of the critical compressibility factor the cross critical pressure is expressed as:

$$P_{c,ij} = \frac{Z_{c,ij} R T_{c,ij}}{V_{c,ij}}. (1.33)$$

 $T_{c,ij}$ c is the cross critical temperature defined by Berhelot type geometric mean of the pure component critical temperature. Barner and Quinlan (1969) proposed use of k_{ij} in definition of $T_{c,ij}$ [Poling et al.,2001]. It is derived from considerations of the attractive energy between two molecules or two bodies. The use of k_{ij} in cubic EoS mixing rules was introduced by Chueh and Prausnitz (1967) [Chueh & Prausnitz, 1967]:

$$T_{c,ij} = \sqrt{T_{c,i} T_{c,j}} (1 - k_{ij}). \tag{1.34}$$

Finally, a_{ij} , attractive term, between pairs of non-similar molecules, is determined

$$a_{ij} = \frac{0.42748R^2T_{c,ij}^{2.5}}{P_{c,ij}}. (1.35)$$

Eq. 1.35 has the same form as Eq.1.27 except that the critical temperature and pressure of the pure component T_c and P_c are replaced by the corresponding cross terms $T_{c,ij}$ and $P_{c,ij}$.

 k_{ij} is the binary interaction parameter that accounts for the interaction between components i and j. By definition $k_{ij}=0$ when the two components are identical. For mixtures of nonpolar compounds k_{ij} is typically zero or close to zero, whereas for mixtures containing at least one polar component, nonzero values of k_{ij} are often necessary [Pedersen&Christensen, 2007].

1.4.3 Soave-Redlich-Kwong Equation of State

Soave (1972) identified limitations in the accuracy of Redlich-Kwong (RK) equation of state for pure-component vapor pressure predictions obtained. To address this issue, he proposed a more general form of the temperature-dependent

term in the attractive term. Therefore, we obtain the Soave–Redlich–Kwong (SRK) EoS [Soave, 1972]:

$$P = \frac{RT}{V - b} - \frac{a(T)}{V(V + b)}. (1.37)$$

Using $\sqrt{\frac{a}{a_c}}$ values determined directly from experimental vapor pressure measurements, in his work Soave analysed $\sqrt{\frac{a}{a_c}}$ vs. $\sqrt{\frac{T}{T_c}}$ for different pure hydrocarbons. His results showed an approximately linear trend, suggesting that a linear relationship should be adopted between the square root of the a-parameter ratio and the square root of the reduced temperature, defined as $T_r = \frac{T}{T_c}$. Based on this observation, Soave proposed the following functional temperature dependence:

$$a(T) = a_c \alpha (T), \tag{1.38}$$

where:

$$a_c = \frac{0.42747R^2T_c^2}{P_c};\tag{1.39}$$

$$b = \frac{0.08664RT_c}{P_c}; (1.40)$$

$$\alpha(T) = (1 + m\left(1 - \sqrt{\frac{T}{T_c}}\right))^2; \tag{1.41}$$

$$m = 0.480 + 1.547\omega - 0.176\omega^2. \tag{1.42}$$

In equation 1.42, ω is the acentric factor (Eq. 1.10). By combining Eq. 1.38, Eq. 1.41 we get:

$$\sqrt{\frac{a(T)}{a_c}} = (1+m) - m\sqrt{\frac{T}{T_c}},$$
(1.43)

which in accordance with Soave's observations reflects a liner relationship between $\sqrt{\frac{a}{a_c}}$ and $\sqrt{\frac{T}{T_c}}$. The coefficients in the expression for m (Eq. 1.42) were obtained by fitting the model to experimental vapor pressure data of nine pure hydrocarbons.

Eq. 1.37 may be written in terms of Z yielding the cubic expression as follows:

$$Z^{3} - Z^{2} + (A - B + B^{2})Z - AB = 0$$
(1.44)

The parameters A and B are defined by Equations (1.45) and (1.46), respectively:

$$A = \frac{a(T)P}{R^2T^2},\tag{1.45}$$

$$B = \frac{bP}{RT}. ag{1.46}$$

Within the framework of the SRK equation, the compressibility factor of a pure component at its critical point assumes a constant value of 0.333. For an N-component system, Soave recommended evaluating the parameters *a* and *b* through the mixing rules defined below [Pedersen&Christensen, 2007]:

$$a = \sum_{i=1}^{N} \sum_{j=1}^{N} z_i z_j a_{ij}; \tag{1.47}$$

$$b = \sum_{i=1}^{N} z_i b_i, (1.48)$$

And

$$a_{ij} = \sqrt{a_i a_j} (1 - k_{ij}). \tag{1.49}$$

The parameter k_{ij} represents a binary interaction coefficient, analogous to that used in the RK mixing rule of Eq. 1.34. The mixing rule applied to parameter b implies that pure-component molar volumes at high pressures are assumed to be additive.

1.4.4 Peng-Robinson Equation of State

The SRK equation has its limitations too, in particular such equation tends to underestimate liquid-phase densities. Peng and Robinson (1976) attributed this limitation to the SRK model's assumption that the pure-component critical compressibility factor is equal to 0.333. Instead, from experimental data the critical compressibility factors of C1-C10 *n*-paraffins should fall in the range of 0.25-0.29 [Poling et al., 2001], which are lower than those predicted by the SRK equation. To address this discrepancy, Peng and Robinson [Peng&Robinson, 1976] proposed a modified equation of state:

$$P = \frac{RT}{V - b} - \frac{a(T)}{V(V + b) + b(V - b)},$$
(1.50)

where

$$a(T) = a_c \alpha (T); \tag{1.51}$$

$$a_c = \frac{0.45724R^2T_c^2}{P_c}; (1.52)$$

$$\alpha(T) = (1 + m\left(1 - \sqrt{\frac{T}{T_c}}\right))^2; \tag{1.53}$$

$$m = 0.37464 + 1.54226\omega - 0.26992\omega^{2}; \tag{1.54}$$

$$b = \frac{0.0778RT_c}{P_c}. (1.55)$$

By imposing the critical point conditions and calculating the parameters a and b, a critical compressibility factor equal to 0.307 is obtained. Although this value is lower than the one predicted by the SRK equation, it is still higher than the corresponding experimental values.

For mixtures, Peng and Robinson recommended determining the parameters a and b through mixing rules reported in Eqs. 1.47 and 1.48. Two years later, in 1978, they proposed a modification of Eq. 1.55 to be applied for compounds with an acentric factor ω >0.49 [Peng&Robinson, 1978]:

$$m = 0.379642 + 1.48503\omega - 0.164423\omega^2 + 0.016666\omega^3. \tag{1.56}$$

1.4.5 Peneloux Volume Correction

Prior to 1982, the SRK equation was primarily applied to phase equilibrium and gas-phase density calculations [Pedersen&Christensen, 2007]. Due to its poor performance in predicting liquid densities, it was often used in combination with liquid density correlations. This approach created difficulties, particularly for near-critical systems where distinguishing between the gas and liquid phases is challenging. In 1982, Peneloux et al. [Peneloux et al., 1982] introduced a modification of the SRK equation incorporating a volume translation parameter. This revised formulation, commonly referred to as the Peneloux equation (SRK-Peneloux), is expressed as:

$$P = \frac{RT}{V - b} - \frac{a(T)}{(V + c) + (V + b + 2c)}.$$
 (1.57)

The parameter *c* is the volume translation or volume shift parameter and it is applied to SRK:

$$V_{Pen} = V_{SRK} - c; (1.58)$$

$$b_{Pen} = b_{SRK} - c, \tag{1.59}$$

where the subindex SRK stands for SRK equation and Pen for SRK-Peneloux equation.

The volume translation approach proposed by Peneloux is not restricted to the SRK equation. It can also be applied to the Peng-Robinson equation. When incorporating the Peneloux volume correction, the PR equation is expressed in the following form (PR-Peneloux):

$$p = \frac{RT}{V - b} - \frac{a(T)}{(V + c)(V + 2c + b) + (b + c)(V - b)}.$$
 (1.60)

The Peneloux volume translation parameter c does not affect gas—liquid phase equilibrium calculations, but the aim is to correct liquid molar volumes and densities so that calculated values better match experimental data [Pedersen, 2007]. For the SRK equation, the correction is particularly important, as the unmodified SRK consistently underpredicts liquid densities, especially for heavier hydrocarbons such as propane and n-hexane. Incorporating the Peneloux correction (SRK—Peneloux) significantly improves the match with experimental liquid density data across a wide temperature range, including near-critical conditions [Pedersen&Christensen, 2007].

For the PR equation, the need for a Peneloux correction is less pronounced. The PR model was originally formulated with greater emphasis on liquid density predictions and thus performs better than SRK for this property. However, discrepancies remain: PR tends to overpredict liquid densities for lighter hydrocarbons (e.g., methane and propane) at low temperatures, while results for heavier hydrocarbons (e.g., n-hexane) are more accurate but still not as good as those obtained with SRK–Peneloux [Pedersen&Christensen, 2007].

Overall, the Peneloux modification greatly enhances liquid density predictions for the SRK equation and provides moderate improvements for the PR equation, without altering phase equilibrium behaviour.

1.5 Flash and Phase Envelope Calculations

Figure 1.8 sketches a standard P-T flash. A feed containing N components enters a separator held at fixed pressure and temperature; two phases form, with gas

withdrawn from the top and liquid from the bottom. Given P, T and the feed composition z_i the flash calculation returns:

- The number of phases,
- The phase split (vapor fraction β and liquid fraction $1-\beta$),
- The phase compositions, y_i in the vapor and x_i in the liquid.

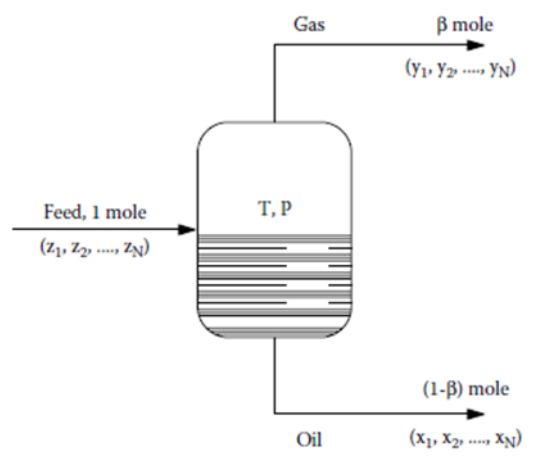


Figure 1.8: Schematic representation of P-T flash process for a hydrocarbon reservoir mixture [Pedersen, 2007].

The phase mole fractions sum to one and is often written in the form suggested by Rachford and Rice (1952) [Rachford &Rise, 1952]:

$$\sum_{i=1}^{N} (y_i - x_i) = 0. (1.61)$$

For a two-phase state, the following relations apply for two phases in equilibrium:

$$\frac{y_i}{x_i} = \frac{\phi_i^L}{\phi_i^V}, \qquad i = 1, 2, ..., N,$$
 (1.62)

where ϕ_i^L and ϕ_i^V are the fugacity coefficients, a measure of non-ideality of component i in the liquid and vapor phases, respectively, and are computed from EoS via its mixing rules. For an ideal gas $\phi_i = 1$.

Overall material balance for each component yields:

$$z_i = (1 - \beta)x_i + \beta y_i \quad i = 1, 2, ..., N,$$
 (1.63)

where z_i is the total mole fraction of component i and β is the vapor fraction. Combining this normalisation with the material balance leads to a single equation for the vapor fraction β , known as the Rachford-Tice relation (1952) [Rachford & Rise, 1952]:

$$\sum_{i=1}^{N} (y_i - x_i) = \sum_{i=1}^{N} \frac{z_i (K_i - 1)}{1 + \beta (K_i - 1)} = 0,$$
(1.65)

where K_i is the equilibrium ratio defined as:

$$K_i = y_i/x_i. (1.66)$$

It represents the ratio of a component's molar composition in the vapor phase to that in the liquid phase when equilibrium is reached.

A P-T flash determines how a reservoir mixture with overall composition Z_i distributes between vapor and liquid at a specific pressure and temperature. The task is to decide whether one or two phases are stable, in the two-phase case, to compute the vapor fraction β , the liquid fraction $(1-\beta)$, and the phase composition y_i and x_i [Prausnitz et al.,1998; Michelsen &Mollerup, 2007].

This single nonlinear equation determines the vapor fraction for given K_i .

A quick phase-existence check evaluates the Rachford-Rice function at the endpoints: $F(0) = \sum_i z_i (K_i - 1)$ and $F(1) = \sum_i z_i (K_i - 1) / K_i$. If these values have the same sign, the mixture is single phase at the specified P, T. If they have opposite signs, a two-phase solution exists and the root for β lies in [0.1].

In an EoS-based flash, the computation proceeds iteratively. Reasonable K_i estimates are used to solve Rachford–Rice equation for β . The resulting x_i and y_i are then used in EoS to update fugacity coefficients ϕ_i^L , ϕ_i^V which in turn update $K_i = \phi_i^L/\phi_i^V$. This iteration continues until changes in β , x_i , y_i and the fugacity residuals are within tolerance.

Once the flash has converged, the outputs are the phase split β and $(1-\beta)$, the compositions x_i and y_i and phase properties computed from the EoS: compressibility factors, densities and enthalpies.

Chapter 2

2 Workflow of Parametric Analysis of EoS

Cubic EoS are the standard in compositional reservoir simulators used to predict the phase behaviour of petroleum reservoir fluids. This thesis evaluates four EoS: Soave – Redlich – Kwong (SRK), Soave – Redlich – Kwong – Peneloux (SRK-Peneloux), Peng – Robinson (PR), and Peng – Robinson – Peneloux (PR-Peneloux) to predict phase behavior and volumetric properties of hydrocarbon fluids on Volve field data.

This chapter describes the workflow used for development of the thesis. In particular, the steps are the following:

- 1) Quality control of black oil laboratory data: this step was required to validate the laboratory data to be used for the comparative study of the EoS.
- 2) EoS comparison and definition of PVT properties.
- 3) Plus fluid regression.
- 4) Lumping and calibration of the 8 component EoS.

A comparison of the EoS on real data are performed following the workflow described in this chapter. The results of the study are provided in the Chapter 3.

2.1 Quality Control of Black Oil Laboratory Data

Poor quality PVT data introduce significant uncertainty in development of EoS. To confirm the accuracy of PVT data and determine representative PVT samples consistency check should be carried out. In this work, we followed the procedure for fluid composition analysis of reservoir fluid proposed by [Seyed Mohammad et al., 2020]. The first step is to verify the composition of each reported component and ensure that the sum of all components equals 100%. Along with this basic check, two complementary approaches are commonly used:

- 1) Material balance check to verify the accuracy of flashed component compositions and reported Gas Oil Ratio (GOR) of Single Stage Flash (SSF) test using two sets of data:
 - Laboratory defined vapor fractions (Yi), liquid fractions (Xi) and recombined reservoir fluid composition (Zi);
 - Mathematically recombined Zi, using the GOR, vapor and liquid fractions from SSF test.
- 2) Thermodynamic consistency check using equilibrium ratio K-value (Eq. 1.65) behaviour to verify qualitatively the consistency of the compositions.

2.1.1 Material Balance Check

Material balance check is suggested as the most accurate technique to analyse compositional consistency of flashed fluid compositions. Considering the component material balance, [Seyed Mohammad et al., 2020] derives the equation below:

$$\frac{Y_i}{Z_i} = \left(-\frac{L}{V}\right) \frac{X_i}{Z_i} + \frac{F}{V}, \tag{2.1}$$

where, F is the total mole of fluid entering the PVT cell, V is the total mole of vapor obtained at standard conditions (1 atm. and 15 °C), L is the total mole of liquid obtained at std.

Based on the above equation, a plot of $\frac{Y_i}{Z_i}$ vs $\frac{X_i}{Z_i}$ should yield a straight line with a slope of $-\frac{L}{V}$ and an intercept of $\frac{F}{V}$. As a result, any observed deviations from the straight line indicate that the reported data are inaccurate.

In order to validate the GOR it is recommended to calculate vapor, liquid factions and recombined fluid mol% using GOR from the SSF flash test. The recombination process is the following:

- 1) Calculation of gas mole fraction (Fg) (equation 2.2);
- 2) Recombination of vapor and liquid fractions to calculate total mole of the component (z_i) .

Gas mole fraction is identified by the equation below [Danesh 1998,; McCain 1990]:

$$F_g = F_g = \frac{n_g}{n_g + n_o},$$
 (2.2)

where, n_0 and n_g are respectively the moles of oil at stock tank per 1 sm³ of oil and the moles of gas at standard conditions and they are defined as follows:

$$n_0 = \frac{\rho_o}{M_o}; \tag{2.3}$$

$$n_g = \frac{R_s P_{\text{std}}}{Z_{\text{std}} R T_{\text{std}}},\tag{2.4}$$

where ρ_o is the oil density at standard conditions (std), M_o is the Molecular Weight (MW) of residual oil, R_s is the solution GOR, $Z_{\rm std}$ is the gas compressibility factor at std, $P_{\rm std}$ and $T_{\rm std}$ are pressure and temperature at std.

Using F_g , vapor and liquid fractions can be recombined as below [Seyed Mohammad et al., 2020]:

$$z_i = F_g y_i + (1 - F_g) x_i. (2.5)$$

Consistency is evaluated by plotting the ratios $\frac{Y_i}{Z_i}$ on y – axis and $\frac{X_i}{Z_i}$ on x – axis using laboratory and calculated data. An example of this diagnostic plot is shown in Figure 2.1.

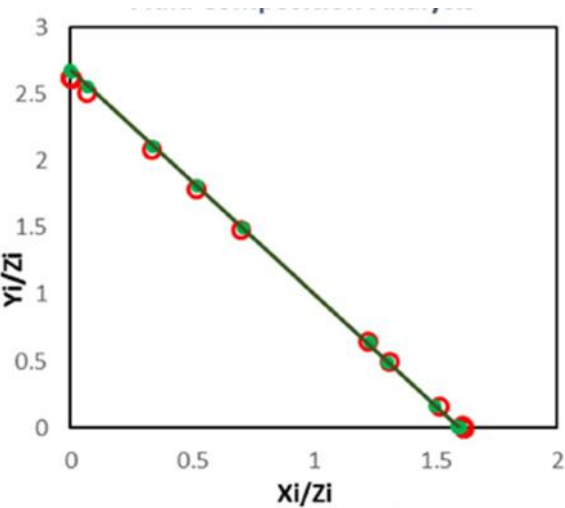


Figure 2.1: Material balance plot for PVT compositions. Green markers show $\left(\frac{Y_i}{Z_i} and \frac{X_i}{Z_i}\right)$ computed from laboratory data; red markers use $\left(\frac{Y_i}{Z_i} and \frac{X_i}{Z_i}\right)$ with calculated Z_i . Plotted data demonstrate alignment of laboratory and calculated data.

2.1.2 Thermodynamic Consistency Check of Composition

Reservoir Pressure decline and Temperature changes in upstream and downstream facilities causes live oil liberating some gases. Composition of the liberated gases and flashed liquids depend strongly on the equilibrium ratio - K value (Eq. 1.65). Different thermodynamic consistency methodologies have been developed to verify the fluid composition accuracy based on the K value. Hoffman plot and Buckley plot are examples of the techniques which use the concepts of the equilibrium check.

[Hoffman et al., 1953] extended earlier industrial correlation by introducing a component factor F_i to estimate K value (Eq 1.66) using measurable physical properties of each component They showed that K-value is related to a component factor F_i exponentially, providing a practical method to estimate K-values from component specific properties. The F_i is calculated as:

$$F_{i} = \frac{\log\left(\frac{P_{ci}}{P_{sc}}\right)}{\frac{1}{T_{bi}} - \frac{1}{T_{ci}}} \left(\frac{1}{T_{bi}} - \frac{1}{T_{sp}}\right),\tag{2.6}$$

where T_{bi} , T_{ci} and T_{sp} are the components normal boiling point, critical temperature and separator temperature measured in ${}^{\circ}R$, respectively. In addition, P_{ci} and P_{sc} are critical pressure and separator pressure in Psia, respectively. Semilog plot of K_i versus F_i for light to intermediate components of an equilibrium mixture is expected to follow a liner trend. Hoffman plot verifies if the equilibrium ratio applied in phase behavior and separation calculations are consistent with both theoretical expectations and observed laboratory data. Figure 2.2 is an example of Hoffman plot illustrating the expected alignment of valid data.

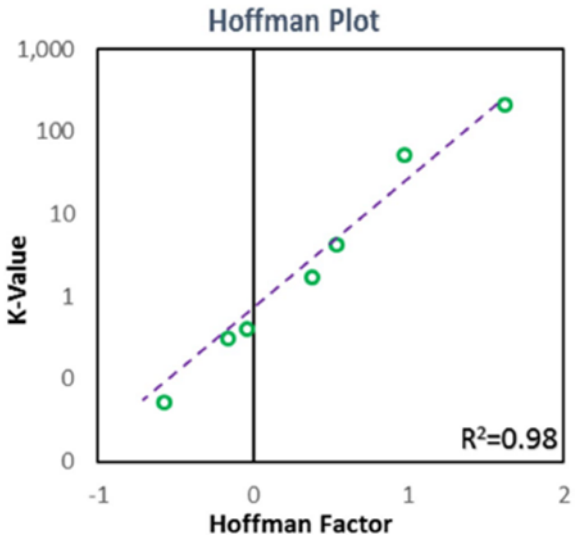


Figure 2.2: Demonstration of Hoffman plot with valid data [Seyed Mohammad et al., 2020].

Another thermodynamic method for checking the consistency of equilibrated mixtures is the Buckley plot. Like the Hoffman approach, it uses a semilogarithmic graph of K_i versus a component critical property-based parameter. Buckley defined this parameter as square of the critical temperature of hydrocarbon components. Buckley demonstrated that that $\log(K_i)$ versus T_c^2 results in a straight line. An example of Buckley plot is presented in the Figure 2.3.

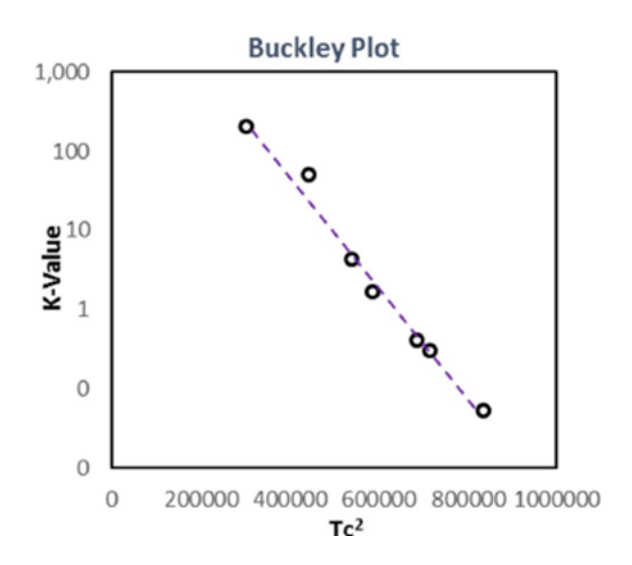


Figure 2.3: Demonstration of Buckley plot with valid data [Seyed Mohammad et al., 2020].

2.2 EoS Comparison and Definition of PVT Properties

This section outlines the workflow used to compare EoS and defines the PVT properties used in the evaluation. In particular, it is structured as follows:

- 1) Composition preparation for modelling: the detailed 23 component mixture was used for the modelling of PVT properties in PVT sim; PVT parameters modelling with untuned EoS on 23 components composition: SRK, SRK-Peneloux, PR and PR Peneloux were run with default parameters using the same components properties. In this way the differences in the results due to model "intrinsic" parameters are distinguishable.
- 2) Comparison of EoS results: simulated outputs were compared against experimental data. Observed differences were then interpreted in terms of EoS features.

2.2.1 Composition Preparation for Modelling

The laboratory report provides composition up to C20+ constructed using single stage flash data and additional data from distillation report. Composition up to C10+ was carried out in gas chromatograph including N₂, O₂ and CO₂ [Lab. Report Well 15/9-19SR DST 1].

The data were loaded into PVTsim using a single-carbon-number (SCN) characterization for all components. Two adjustments were made: isomers iC4 and nC4 were lumped as C4, and iC5 and nC5 were combined as C5. In this way dimensionality was reduced but volatility ordering is preserved [Whitson et al., 2000]. Additionally, C20+ fraction was de-lumped into two pseudo-components—C20–C32 and C33–C80.

PVT sim [Calsep PVTsim13] provides two workflows for plus fraction characterization:

- 1) Standard oil characterization (up to C80);
- 2) Heavy oil characterization (up to C200).

In both cases, the critical properties T_c , P_c are estimated from empirical correlations that depend on density (ρ) and MW. The correlations have the following general forms [Pedersen et al., 1989 and 1992]:

$$T_c = c_1 \rho + c_2 \ln M + c_3 M + \frac{c_4}{M'}, \tag{2.7}$$

$$\ln P_c = d_1 + d_2 \rho^{d_5} + \frac{d_3}{M} + \frac{d_4}{M^2}, \tag{2.8}$$

$$m = e_1 + e_2 M + e_3 \rho + e_4 M^2. (2.9)$$

 c_i , $\underline{d_i}$, and e_i are empirically fitted coefficients provided in the tables below.

Sub-index/ Coefficient	1	2	3	4	5
С	1.6312×10^2	8.6052 x 10	4.3475 x 10 ⁻¹	-1.8774×10^3	-
d	-1.3408 x 10 ⁻¹	2.5019	2.0846×10^{2}	-3.9872×10^3	1.0
e	7.4310×10^{-1}	4.8122×10^{-3}	9.6707 x 10 ⁻³	-3.7184×10^{-6}	-

Table 2.1: Standard characterization -SRK [Pedersen et al.,1989 and 1992]

Sub-index/ Coefficient	1	2	3	4	5
С	7.3404 x 10	9.7356 x 10	6.1874×10^{-1}	-2.0593×10^3	-
d	7.2846×10^{-2}	2.1881	1.6391×10^{2}	-4.0434×10^3	1/3
e	3.7377×10^{1}	5.4927 x 10 ⁻³	1.1793 x 10 ⁻²	-4.9305 x 10 ⁻⁶	-

Table 2.2: Standard characterization – PR [Pedersen et al.,2002]

Sub-index/ Coefficient	1	2	3	4	5
С	3.04143×10^{2}	4.84052 ×10	7.10774×0^{-1}	3.80073×10^{3}	-
d	3.05081	-9.03352×10 ⁻¹	2.33768×10 ²	-1.27154× 10 ⁴	0.25
e	4.96902×10 ⁻¹	5.58442×10 ⁻³	1.01564×10 ⁻²	-5.24300×10 ⁻⁶	

Table 2.3: Heavy oil characterization – SRK [Pedersen et al.,2002]

Sub-index/	i	2	3	4	5
Coefficient					
С	3.26725×10 ²	5.23447×10 ⁻¹	5.77248×10 ⁻¹	1.77498×10 ³	-
d	2.68058	-5.32274×10	2.04507×10 ²	-9.45434×10 ³	0.25
e	1.89723×10 ⁻¹	7.42901×10 ⁻³	3.28795×10-2	-7.36151×10 ⁻⁶	

Table 2.4: Heavy oil characterization – PR [Pedersen et al.,2002]

M is MW in g/mol, ρ is in g/cm³, T_c is in Kelvin (K) and P_c in atm. The correlations are the same with and without volume correlation.

2.2.1.1 Extrapolation of Plus Fraction

Characterization of the plus fraction develops according to the following steps [Calsep PVTsim 13]:

- Estimation of the molar distribution (mole fraction versus carbon number);
- Estimation of the density distribution (density versus carbon number);
- Estimation of the boiling point distribution (boiling point versus carbon number);
- Estimation of the MW distribution (MW versus carbon number);
- Calculation of T_c , P_c and EoS inputs for the resulting pseudo-components.

Using a large set of reservoir-fluid compositions from around the world, [Pedersen etal., 1984]) observed that for components heavier than hexane (carbon number N>6), the mole fraction decreases roughly exponentially with carbon number. In other words, a plot of $\log z_N$ vs. N is approximately a straight line.

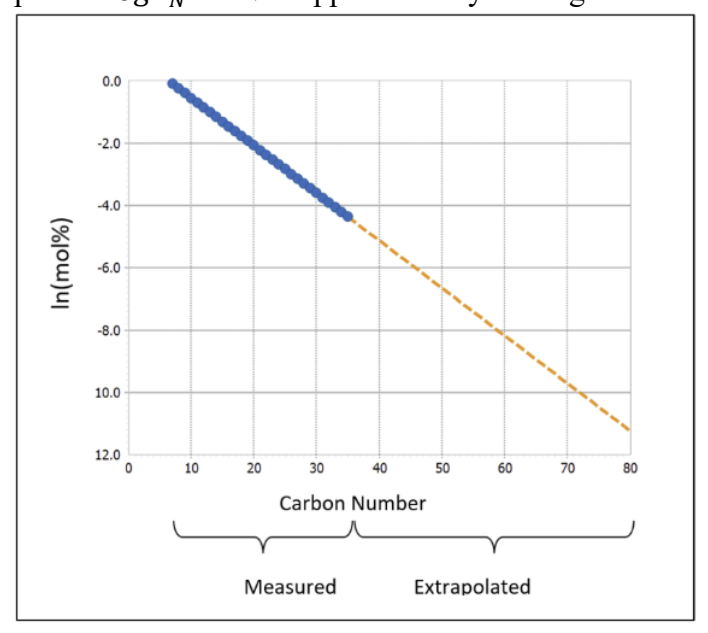


Table 2.5: Splitting of plus fraction into carbon number fractions [Calsep Tech Talk #19].

The molar composition of the true-boiling-point (TBP) residue is obtained by assuming a logarithmic relation between the mole fraction Z_N of a given carbon number cut and its carbon number cut:

$$C_N = A + B \ln Z_N. (2.10)$$

The constants A and B are determined from the overall mole fraction and measured average molecular weight of the plus fraction. The circles in Figure 2.5 plot the logarithm of the C7–C19 mole fractions versus carbon number. Therefore, the mole fractions for carbon numbers heavier than C19 can be estimated by extending the best-fit straight line obtained for C7–C19. Any extrapolated values must still satisfy the overall mass-balance constraints:

$$z_{+} = \sum_{i=C_{+}}^{C_{max}} z_{i}; (2.11)$$

$$M_{+} = \frac{\sum_{i=C_{+}}^{C_{max}} z_{i} M_{i}}{\sum_{i=C_{+}}^{C_{max}} z_{i}},$$
(2.12)

where C_+ is the carbon number of the plus fraction and C_{max} is the heaviest carbon number fraction considered. For ordinary reservoir fluids, C80 is reasonable the heaviest component to be considered.

Densities of the carbon number cuts within the plus fraction are estimated by assuming logarithmic dependence of the ρ on carbon number.

Boiling points recommended by [Katz and Firoozabadi 1978] are used up to C_{45} . For heavier cuts, the following correlation is applied:

$$T_B = 97.58M^{0.3323}\rho^{0.04609}, (2.13)$$

where T_B is in K, M is molecular weight in g/mol, ρ is in g/cm³.

In this study, we characterized the fluid composition up to C80. The C20+ fraction was grouped into two pseudo-components: C20–32 and C33–80. We also tested three- and four-lump splits of C20+, but these gave larger mismatches between EoS (SRK and PR) predictions and the laboratory data. The likely reason is a further uncertainty from introducing more lumps without true TBP data to anchor the split. Because no TBP was available for C20+, we could only constrain the overall properties of the C20+ cut—its average molecular weight, overall mole fraction, and density—rather than its detailed carbon-number distribution. For this reason, we adopted the two-lump scheme in the final model.

This workflow resulted in a 23-component detailed set to be used as common basis for subsequent EOS screening and plus fluid regression

2.2.2 EoS Simulation Before Parameters Tuning

The PVT properties were simulated with SRK, SRK-Peneloux, PR and PR-Peneloux in PVT sim using 23 component composition. Experimental data available for comparison include Single Stage Flash (SSF), Constant Composition Expansion (CCE) and Differential Liberation (DL) from [Lab. Report Well 15/9-19SR DST 1]. In this study, we assess the following PVT parameters:

- Saturation pressure (Psat), relative volume and compressibility from CCE;
- Oil formation volume factor (B_o) , solution GOR (R_s) , gas formation volume factor (B_g) , oil density (ρ_0) , gas Z-factor, gas viscosity (μ_g) from DL;
- Oil viscosity (μ_0) ;

2.2.2.1 Physical Meaning and Definitions of PVT Experiments

PVT properties describe how a reservoir fluid's phase and volumes change with pressure and temperature. A key quantity is the saturation pressure Psat. When the reservoir pressure falls below Psat, phase separation occurs and the produced well stream composition typically changes, as production comes primarily from either gas or liquid zone [Pedersen&Christensen, 2007].

The subsequent sections provide a description of the PVT test parameters.

2.2.2.1.1 Constant Composition Expansion (CCE) parameters

CCE is a standard depletion test performed at constant temperature on a sealed PVT cell containing a fixed mass of sample. After loading the PVT cell with well-known mass of fluid pressure is initially set slightly above the reservoir pressure (Pr). During the test, the pressure is gradually decreased, which causes the volume of the cell to increase step by step (Figure 2.5). The pressure volume measurements are reported in the PVT report.

Psat is identified either by the first visual appearance of a second phase in the visual cell or by interception of the two volume pressure trends (Figure 2.5 (b))

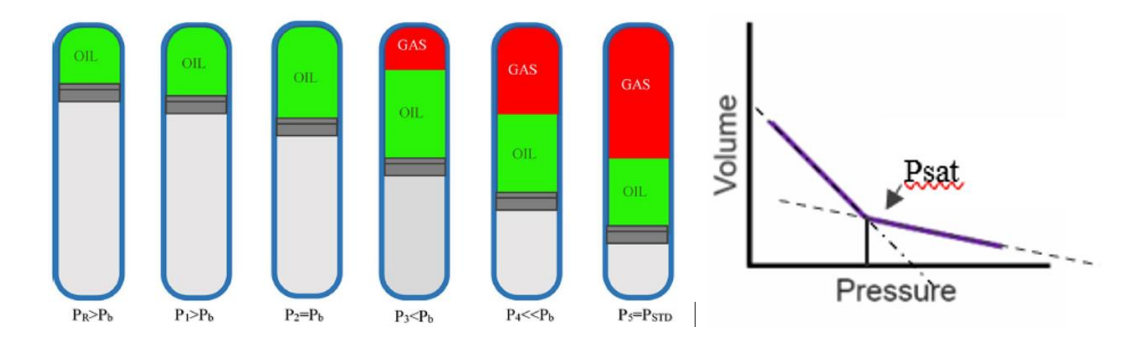


Figure 2.4: CCE (a) experiment [Seyed Mohammad et al, 2020]; (b)general volume versus pressure behaviour in CCE test [Whitson wiki].

At each step, the relative volume is recorded as the ratio of the current volume to the volume at saturation pressure (V_{sat}) [Pedersen&Christensen, 2007]:

$$V^{\rm rel} = \frac{V_{\rm tot}}{V_{\rm cat}}. (2.14)$$

The volume versus pressure data can be used to derive the compressibility:

$$c_o = -\frac{1}{V} \left(\frac{\partial V}{\partial P} \right)_T. \tag{2.15}$$

The Y-factor (Eq. 2.16) is a CCE volatility indicator and is a measure of the ratio between the relative changes in pressure and total volume in the two-phase region. The Y-factor is cited in textbooks ([Standing, 1952]; [Amyx et al., 1960]; [Whitson and Brulé 2000]) as a tool for checking the consistency of the black oil CCE. Because gas occupies far more volume than liquid, once the sample is below Psat, the total volume grows rapidly as gas is liberated.

$$Y = \frac{\frac{P^{\text{sat}} - P}{P}}{\frac{V_{\text{tot}} - V_{\text{sat}}}{V_{\text{sat}}}}.$$
 (2.16)

2.2.2.1.2 Differential Liberation (DL) parameters

The differential liberation test is carried out for oil mixtures and it approximates the volumetric changes during reservoir depletion at reservoir condition. [Dake 1978]. A PVT cell is loaded with an oil sample at reservoir temperature. The experiment is typically started at Psat. The pressure is reduced stepwise and at each stage the system is allowed to reach phase equilibrium before proceedings. As the pressure decreases below Psat, gas begins to liberate from the liquid. At each pressure stage, the system volume expands, and all gas liberated at each step is removed (Figure 2.6) in order to maintain a constant cell volume.

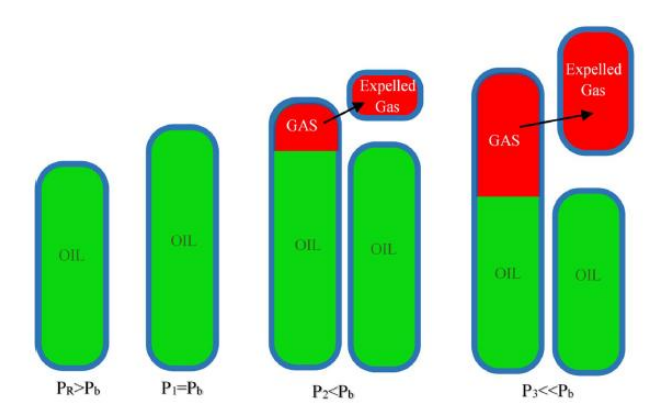


Figure 2.5: DL experiment [Seyed Mohammad et al, 2020].

The volume of liberated gas at standard conditions is measured at each DL stage, enabling calculation of the Bg as the ratio of the gas volume at the current conditions to its volume at std [Danesh 1988; Pedersen&Christensen, 2007]. The SI unit for Bg is m^3/Sm^3 .

$$B_g = \frac{V_g(P, T)}{V_{g, \text{st}}},\tag{2.17}$$

where $V_g(P,T)$ is the gas volume at cell condition and $V_{g,st}$ is the gas volume at std. The test continues until atmospheric pressure is reached and the cell is cooled to approximately 15 °C. The liquid volume at std is reported as the residual or stock tank volume of oil. Liquid volumes at the intermediate pressure steps are expressed relative to this stock tank volume (Bo). Knowing the oil volume at stage N, then Bo for stage N is defined as:

$$B_0(N) = \frac{V_N^{\text{oil}}}{V_{\text{std}}^{\text{oil'}}} \tag{2.18}$$

where $V_N^{\rm oil}$ is the oil volume at the current pressure (after gas removal) and Tr, and $V_{\rm std}^{\rm oil}$ is the residual oil volume at St. The R_s is another key parameter determined from a differential liberation test. At any stage R_s is calculated by summing the standard volumes of gas released in subsequent stages and dividing by the residual oil volume at that stage. The process is illustrated in Figure 2.7.

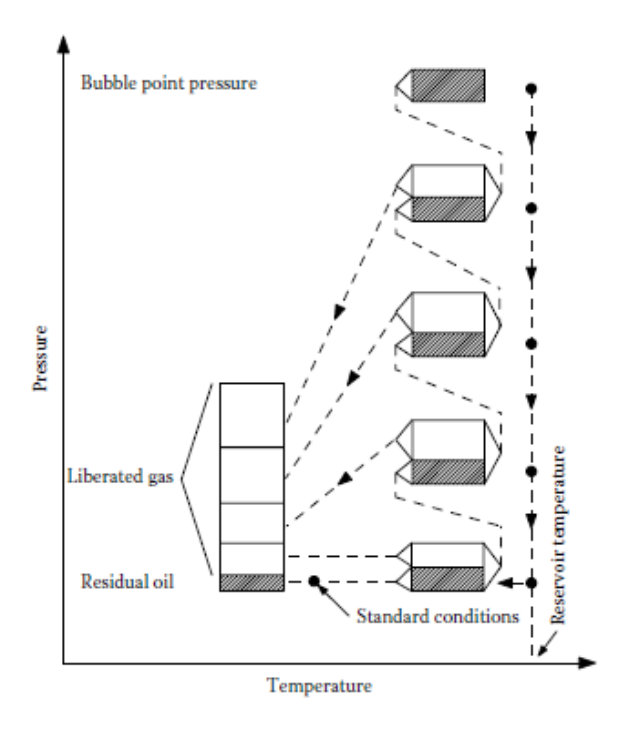


Figure 2.6: DL experiment in a pressure-temperature diagram [Pedersen et al., 2007].

At stage N of a DL test with a total of NST pressure steps, the Rs is estimated with Eq. 2.19. When the produced gas is flashed to std conditions, a small liquid dropout commonly forms. This volume should be added to gas volume, as an equivalent gas volume. The gas volume at std conditions of the gas released in stage N will be referred to as the stage-N standard gas volume ($V_{\text{std},N}^{\text{gas}}$). Rs is given by Pedersen&Christensen, 2007]:

$$R_s(N) = \frac{\sum_{n=N+1}^{\text{NST}} V_{\text{std},n}^{\text{gas}}}{V_{\text{std}}^{\text{oil}}}.$$
 (2.19)

Oil density at each pressure stage is obtained indirectly by combining the measured stock-tank oil density with the corresponding B_0 determined at that stage. Assuming mass conservation and complete gas removal, the in-situ oil density is calculated as:

$$\rho_o(P_i, T) = \frac{\rho_{ST}}{B_o(P_i)} -$$
(2.20)

Density of stock tank oil of the analysed sample is measured using a Paar DMA 62 frequency densitometer, thermos stated at 15 °C. Precision of the method is + /-0.0002 g/cm³ [Lab. Report Well 15/9-19SR DST 1].

Z-Factor is obtained indirectly from measurements made at the separator. First, the volume (V_s) of the flashed gas at the separator conditions is measured at a certain pressure (P_s) and temperature (T_s) . Then the volume of this same gas is measured

(or calculated) at standard conditions (V_{std}). Assuming the gas behaves nearly ideally at standard conditions (Z=1), the number of moles is calculated:

$$n_i = \frac{P_{std}V_{std,i}}{RT_{std}}. (2.21)$$

With fixed n the Z-Factor is calculated at each stage as:

$$Z_{s.i} = \frac{P_{s,i}V_{s,i}T_{std}}{P_{std}V_{std}T_{s.i}}. (2.22)$$

Viscosity measurements of the downhole sample were performed in ROP viscosimeter, viscosity standards from Cannon Instr. Corp. and some selected pure hydrocarbons. Precision of the method is about 3% [Lab. Report Well 15/9-19SR DST 1].

2.2.3 Comparison of Equations of State

Since this study analyses two families of EoS in their base formulation and with Peneloux correction, this section summarizes the key differences between the SRK and PR EoS. The summary of the SRK and PR EoS are provided in the table below. We use these points to interpret the simulation results in later sections.

Parmeter	SRK	PR
EoS	$P = \frac{RT}{V - b} - \frac{a(T)}{V(V + b)}$	$P = \frac{RT}{V - b} - \frac{a(T)}{V(V + b) + b(V - b)}$
Eqs. 1.37 and 1.50	V D V(V 1 D)	V B V(V B) B(V B)
Attractive term		
Eqs. 1.38 and 1.52	$a(T) = a_c \alpha (T)$	$a(T) = a_c \alpha (T)$
Eqs. 1.39 and 1.53	$a_c = \frac{0.42747R^2T_c^2}{P_c}$	$a_c = \frac{0.45724R^2T_c^2}{P_c}$
Co-volume (repulsive) parameter	$b = \frac{0.08664RT_c}{P_c}$	$b = \frac{0.0778RT_c}{P_c}$
Eqs. 1.49 and 1.56		_
Temperature function Eqs. 1.41 and 1.52	$\alpha(T) = (1 + m(1 - \sqrt{\frac{T}{T_c}}))^2$	$\alpha(T) = (1 + m(1 - \sqrt{\frac{T}{T_c}}))^2$
m	$m = 0.480 + 1.547\omega$	$m = 0.37464 + 1.54226\omega$
Eqs. 1.42 and 1.57	$\frac{-0.176\omega^{2}}{N}$	$-26992\omega^{2}$
Mixing rules (classical van der Waals, unless specified otherwise)	$a = \sum_{i=1}^{N} \sum_{j=1}^{N} z_i z_j a_{ij}$	i
Eqs. 1.30, 1.36 and 1.31	$a_{ij} = \sqrt{a_i a_j} (1 -$	k_{ij})

	$b = \sum_{i=1}^{N} z_i b_i$	
Pure fluid critical Compressibility	$z_c \approx 0.333$	$z_c \approx 0.307$

Table 2.6: Summary of the key differences between SRK and PR formulations [Soave 1972; Danesh 1998]; [Peng &Robinson 1976; Pedersen 2007].

SRK equation introduced temperature function to better estimate PVT behaviour and is widely applied to PVT calculations for condensate oils and natural gases [Soave 1972]. The PR equation modified both the attractive and co-volume terms to improve liquid phase properties and near critical behaviour [Peng, Robinson 1976; Li 2008]. Although many alternative EoSs exist, two parametric cubic models such as SRK and PR remain practical for predicting phase behaviour and vapor liquid equilibria [Nasrifar et al., 2006; Nazarzadeh et al., 2013].

2.2.3.1 Comparison of the Results Using AAD

In this study, the model -experimental data misfit was quantified by the average absolute percent deviation (AAD). For each pressure point, PVTsim reports the percent deviation of a simulated value

$$Deviation(\%) = \frac{\text{Experimental} - Simulated}{Experimental} x100$$
 (2.23)

To summarize the overall deviation across N points, the AAD is computed as the average of the absolute percent deviations:

$$AAD(\%) = \frac{1}{N} \sum_{i=1}^{N} |Deviation_i(\%)|$$
 (2.24)

2.3 Plus Fluid Regression

Plus fluid regression is the recommended procedure before main lumping to improve properties of the components. Regression for plus composition in PVT sim consist of two stages [Calsep PVTsim 13]:

- Adjustment of MW;
- Regression of the critical temperature (Tc), critical pressure (Pc), and acentric factor (m) for the C7+ components, in order to adjust the EoS parameters and improve the match with experimental PVT data. The default number of regression parameters is:

$$NPAR = 1 + ln(NDAT), (2.25)$$

where NDAT is the number of experimental data points not considering viscosity data. Additional upper limit 10 is imposed for NPAR to avoid overfitting. NPAR regression parameters are selected in the following order [Christensen, 1999]:

- 1. Coefficient c_2 in T_c correlation.
- 2. Coefficient d_2 in P_c correlation.
- 3. Peneloux volume shift parameter.
- 4. Coefficient c_3 in T_c correlation.
- 5. Coefficient d_3 in P_c correlation.
- 6. Coefficient e_2 in m correlation.
- 7. Coefficient e_3 in m correlation.
- 8. Coefficient c_4 in T_c correlation.
- 9. Coefficient d_4 in P_c correlation.
- 10. Coefficient e_4 in m correlation.

 T_c , P_c correlations and c_{1+i} , d_{1+i} , and e_{1+i} are empirically fitted coefficients defined in Eqs. 2.8 and 2.9, m parameter is defined in Eq. 2.10

The reference component, with a molecular weight of 94 g/mol and a density of 0.745 g/cm³, has its fixed assigned critical temperature ($T_{c,ref}$), critical pressure ($P_{c,ref}$) and acentric factor (ω_{ref}). At each iteration coefficients c_1 , d_1 and e_1 are recalculated so that correlation reproduces exactly the same $T_{c,ref}$, $P_{c,ref}$, ω_{ref} .

Then with these coefficients held fixed, the coefficients for the heavier cuts $(c_{1+i}, \underline{d_{1+i}}, e_{1+i})$ are regressed to produce updated estimates of T_c and P_c for $C_7 + cuts$. Anchoring the correlation at a physically meaningful reference component and then fitting the remaining coefficients — stabilizes the regression and ensures that the computed critical properties for the lowest C7+ fractions remain consistent with physically plausible values.

In pvt sim oil and gas viscosity can be modelled with Corresponding States (CSP) or Lohrenz-Bray-Clark (LBC). In our study we used CSP model. This software builds an effective mixture MW for viscosity from the composition and two internal constants, VISC1 and VISC2. The default values are:

- VISC1=1.304E-4;
- VISC2=2.303

the adjusted pair (VISC1, VISC2) yields the best agreement with the lab data leaving the EoS equilibria and densities unchanged.

2.4 Lumping and Calibration

In standard oil characterization, the extrapolated mixture can contain up to 80 components. In this study as described in the sections 2.2 and 2.3 analysed fluid was characterized up to C80. However, in order to reduce CPU time components

number should be reduced. For the comparison of the EoS it was used 23 components composition where C20+ was split to C20-32 and C32-80.

2.4.1 Lumping scheme

To reduce CPU time in compositional reservoir simulation, the EoS model should use the limited components that still reasonably capture phase and volumetric behaviour. A pseudoized EoS may have roughly 6-9 lumped components by combining "similar" components such N_2+C_1 , $iC_4+nC_4+iC_5+nC_5$ and some 3-5 C_6 fractions. Choosing which components to lump is challenging due to the huge number of possible combinations [Alavian et al., 2014].

[Lee et al.,1982] propose splitting the C7+ fraction into two pseudocomponents using a characterization factor computed as the average slope (tangent) of molecular weight, specific gravity, and Jacoby factor when each is plotted against boiling point. [Whitson, 1983] provides a procedure for selecting how many C7+ cuts to use and how to group them. [Coats, 1985] offers an in-depth treatment of lumping C7+ for modelling vaporization in gas-condensate cycling and, more broadly, presents fundamental criteria and formulas for calculating EoS parameters.

[Li et al., 1984] proposed grouping components using K values obtained from a flash calculation at the reservoir temperature and an "average" reservoir pressure. They first partition the mixture into "light" components (H_2S , N_2 , CO_2 , and $C_1 - C_6$) and "heavy" components ($C_7 +$), then apply different criteria to decide how many pseudo-components to form in each set. They also recommend validating the grouped fluid phase diagrams and compositional simulation.

[Schlijper 1986] addressed the inverse problem – recovering detailed compositions from pseudoized description. [Behrens&Sandler, 1986] introduced a C_7 + grouping method based on Gaussian quadrature within a continuous-thermodynamics framework, although they used a simple exponential distribution with two quadrature points. [Whitson et al., 1989] demonstrated that the approach is general and can accommodate other molar distribution models and any number of C_7 +groups. Additional pseudoization strategies have been proposed by [Montel&Gouel1984; Newley et al, 1991; Danesh&Todd, 1992; Hustad, 1993 and Liu, 2001]. In a comparison of twelve lumping methods, [Joergensen et al., 1995] suggested that no single method was consistently superior.

In this study the selection of lumping scheme was based on the groups proposed by [Pedersen&Christensen 2007; Alavian et al., 2014]. Several lumping schemes were tested, and the one that best reproduces the 23-component reference model of the plus fraction was selected.

2.4.2 Lumping in PVT sim

This lumping strategy [Calsep PVTsim 13] is designed to minimize the variability of the EoS parameters a (attraction) and b (co-volume) among components grouped

within each pseudo component [Lomeland and Harstad, 1994]. For a pure component i, the attraction parameter a_i is given in Eq.1.30

The expression for the parameter a of N component mixture may similarly be rewritten as:

$$\frac{a}{T} = \sum_{i=1}^{N} \sum_{j=1}^{N} z_i z_j \left(\frac{a_{1i} a_{1j}}{T} - \frac{a_{1i} a_{1j} \left(a_{2i} + a_{2j} \right)}{\sqrt{T}} + a_{1i} a_{1j} a_{2i} a_{2j} \left(1 - k_{ij} \right).$$
 (2.26)

For pseudo-component k, which groups the carbon number fractions from L_n to U_n , the average values of the parameters a_1 and a_2 are obtained as follows:

$$\overline{a_{1k}^{2}} = \frac{\sum_{i=L_{n}}^{U_{n}} \sum_{j=L_{n}}^{U_{n}} z_{i} z_{j} a_{1i} a_{1j} (1 - k_{ij})}{\left(\sum_{j=L_{n}}^{U_{n}} Z_{i}\right)^{2}};$$
(2.27)

$$2\,\overline{a_{2k}}\,\overline{a_{1k}^{2}} = \frac{\sum_{i=L_{n}}^{U_{n}} \sum_{j=L_{n}}^{U_{n}} z_{i}\,z_{j}\,a_{1i}\left(a_{2i} + a_{2j}\right)a_{1j}\left(1 - k_{ij}\right)}{\left(\sum_{i=L_{n}}^{U_{n}} z_{i}\right)^{2}}.$$
 (2.28)

Similarly, the average co-volume parameter *b* for pseudo-component k is the same mole fraction-weighted average of its member cuts:

$$\overline{b_k} = \frac{\sum_{i=L_n}^{U_n} z_i \ b_i}{\sum_{i=L_n}^{U_n} z_i}.$$
 (2.29)

The sub-components of pseudo-component n is found by minimizing the following function:

$$S = \sum_{n=L_{0}}^{N_{\text{pc}}} \sum_{i=L_{0}}^{U_{n}} \left(\frac{a_{1i} - \overline{a_{1k}}}{a_{1i}} \right)^{2} + \left(\frac{a_{2i} - \overline{a_{2k}}}{a_{2i}} \right)^{2} + \left(\frac{b_{i} - \overline{b_{k}}}{b_{i}} \right)^{2}$$
(2.30)

Grouping is determined by varying the lower carbon number cut L_n along the SCN list. The upper bound U_n is then implied by the next lower cut (i.e., $U_n = L_n + 1 - 1$) or by the end of the plus fraction. Here, L_s is the smaleest carbon number eligible for grouping, and N_{pc} is the final number of pseudo components. For each group n, the average $\overline{T_{ck}}$, $\overline{P_{ck}}$, ω are calculated using the formulas below:

$$\overline{m_k} = \sqrt{\frac{\Omega_b}{\Omega_a}} \frac{\overline{a_{1k}} \, \overline{a_{2k}}}{\sqrt{\overline{b_k}}}; \tag{2.31}$$

$$\overline{T_{ck}} = \frac{\overline{m_k}}{\{(1 + \overline{m_k})\}}; \tag{2.32}$$

$$\overline{P_{ck}} = \frac{\Omega_b R \overline{T_{ck}}}{\overline{b_k}},\tag{2.33}$$

where m is a second order polynomial in acentric factor defined in the EoS. If non-zero binary interaction coefficients are used for hydrocarbon-hydrocarbon pairs, the binary interaction coefficient between pseudo components n and m is computed from the formula given below:

$$k_{mn} = \frac{\sum_{i=L_n}^{U_n} \sum_{j=L_m}^{U_m} z_i z_j M_i M_j k_{ij}}{\overline{M_n} \overline{M_m} \sum_{i=L_n}^{U_n} z_i \sum_{j=L_m}^{U_m} z_j},$$
(2.34)

where $\overline{M_n}$ and $\overline{M_m}$ are the average MW of pseudo-components m and n. For CH₄ interactions, a correction term must be added to the binary interaction coefficient k_{mn} obtained from the preceding formula:

$$C\left(\frac{\overline{M_n} - \overline{M_m}}{\overline{M_n} \overline{M_m}}\right) \tag{2.35}$$

where

$$C = \frac{0.003864}{N_{\rm pc}} \tag{2.36}$$

2.4.3 Calibration of the 8 component EoS

Calibration of the lumped model parameters was performed following the regression methodology outlined by Christensen (1999) [Christensen,1999] and presented in [Pedersen&Christensen 2007]. The calibration was designed to improve the match of the selected PVT properties. Rather than arbitrarily tuning properties of individual pseudo-components, Christensen proposes the following approach:

- 1) Perform regression to the saturation points, limiting adjustments to plus molecular weight (+-10%)-
- 2) Assess whether oil density match requires improvement. If that is the case, adjust volume translation parameter of the C7+ components to +-100%.
- 3) Identify the two or three most sensitive coefficients in Eqs. 2.8-2.10.
- 4) Perform parameter regression with the most sensitive coefficients identified in the preceding step (max adjustment +-20%).

Following the guidance above the following workflow was used for the calibration of the lumped EoS:

- 1) Step by step regression:
 - 1-step: Regression of Tc, Pc and viscosity coefficients 1 and 2. For Tc and Pc adjustments three groups with heavy ends were selected and individually regressed: C13-C19, C20-C32, C33-C80;
 - 2 step: Building on top the 1-step regression results, the binary interaction coefficients (kij) were further adjusted for the following pseudo component pairs: N2+C1 and C20-C32; N2+C1 and C33-C80; CO2+C2 and C20-C32; CO2+C2 and C33-C80.
- 2) Combined regression: All parameters regressed in 1-step and 2-step were optimized together in a single step.
- 3) Final regression: Peneloux translation adjustment for the groups C13-C19, C20-C32 and C33-C80 up to+-50%.

Based on the deviation weight factor-weight of observed value (WOBS) was assigned to the parameter used in the regression.

According to PVT sim manual [Calsep PVTsim 13] the object function is defined as:

$$OBJ = \sum_{j=1}^{NOBS} \left(\frac{r_j}{w_j}\right)^2, \tag{2.37}$$

where NOBS is the number of experimental observations used in the regression, w_j is the weight factor for the j'th observation, and r_j is the j'th residual calculated as:

$$r_{j} = \frac{OBS_{exp} - OBS_{calc}}{OBS_{exp}},$$
(2.38)

where OBS stands for Observed value, OBS_{exp} for experimental observed value and OBS_{calc} for calculated observed value. In tests like CCE or DL a constant is added to all observed values. This constant is equal to one third of the maximum liquid dropout measured. The reason for this is to make sure that data points with small liquid drop out don't get too much importance compared to those with higher values. The weighting factor w_j and user specified weight (WOBS) assigned to j'th observation are interrelated as follows:

$$WOBS = \frac{1}{w_j^2}.$$
(2.39)

Chapter 3

3 Parametric Analysis of EoS on Real data

This chapter applies the methodology developed in Chapter 2 to the Volve field laboratory PVT dataset and demonstrates the full workflow from validation of laboratory data to a calibrated EoS model

In 2018 Equinor released a comprehensive open access dataset from Volve field, including more than 40000 files covering geological models, well logs, assays, static and dynamic models, and production history [Equinor]. Among these PVT laboratory reports are available. For this study, a laboratory report containing SSF, CCE and DL tests were included. It allowed to proceed with the workflow using a data set obtained from the downhole sample acquired from the well 15/19 SR in 1993.

As described in chapter 2 the following workflow was applied to this study:

- 1) Quality control of black oil laboratory data.
- 2) Simulation of Experimental data and Parametric analysis of EoS;
- 3) Plus fluid regression;
- 4) Lumping and calibration of the 8 component EoS.

3.1 Quality Control of Laboratory Data

3.1.1 Material Balance Check

According to the methodology describe in Section 2.1 a material balance check was performed with two data sets:

- 1. $\frac{Y_i}{Z_i}$ and $\frac{X_i}{Z_i}$ are calculated with reported flashed components composition.
- 2. Z_i in $\frac{Y_i}{Z_i}$ and $\frac{X_i}{Z_i}$ is calculated using SSF parameters.

The laboratory data including calculated fluid composition (Z_i) are presented in Table 3.1. SSF parameters are provided in Table 3.2.

Com	positional Ana	alysis - Re	ecombinati	on Calcul	lation			
Well	15/9-19SR							
Num	Component	Stabil oil	Evolved gas	Reservo	Reservoir fluid		MW	RHO
		Mol%	Mol %	Weight %	Mol %	Mol %	g/gmol	kg/m ³
1	Nitrogen	0.00	0.71	0.13	0.46	0.46	28.0	810
2	Carbon Dioxide	0.00	7.65	2.15	4.95	4.95	44.0	827
3	Hydrogen Sulphide	0.00	0.00	0.00	0.00	0.00	34.1	796
4	Methane	0.25	67.10	6.88	43.50	43.46	16.1	300
5	Ethane	0.26	9.34	1.82	6.14	6.13	30.1	356
6	Propane	0.96	7.60	2.29	5.26	5.25	44.1	501
7	i-Butane	0.29	0.91	0.39	0.69	0.69	58.1	557
8	n-Butane	1.61	3.21	1.52	2.65	2.64	58.1	579
9	i-Pentane	1.11	0.82	0.66	0.92	0.92	72.2	620
10	n-Pentane	2.18	1.15	1.08	1.51	1.51	72.2	626
11	Hexanes	4.46	0.81	1.75	2.10	2.10	84.6	685
12	Heptanes	8.36	0.52	2.97	3.29	3.29	91.5	722
13	Octanes	8.92	0.14	3.37	3.24	3.24	105.5	745
14	Nonanes	6.75	0.02	2.82	2.39	2.40	119.7	764
15	Decanes	64.86	0.00	72.20	22.90	22.93	320.0	778
	Total:	100.00	100.00	100.00	100.00	100.00		
	Molecular weight g/mol	240.50	25.63		101.48			

Table 3.1: Composition of the bottom hole sample

Single Stage Flash results						
Gas oil ratio	159.1	sm3/sm3				
Flash FVFat Pb	1.505	m3/m3				
Density at Pb	0.701	g/cm3				
Density of	0.883	g/cm3				
stabilized oil						
Density AT 328	0.708	g/cm3				
bar						
Density of C10+	0.916	g/cm3				
Gas gravity	0.885					
(air=1)						

Table 3.2: Single stage flush results.

As can be seen from the material balance plot (Figure 3.1) the reported and calculated Yi/Zi versus Xi/ Zi are in close agreement and yield a straight line with a slope of – L/V equal to -0.545 and an intercept of F/V equal to 1.5457. The material balance confirms high accuracy and reliability of the reported composition and validates GOR.

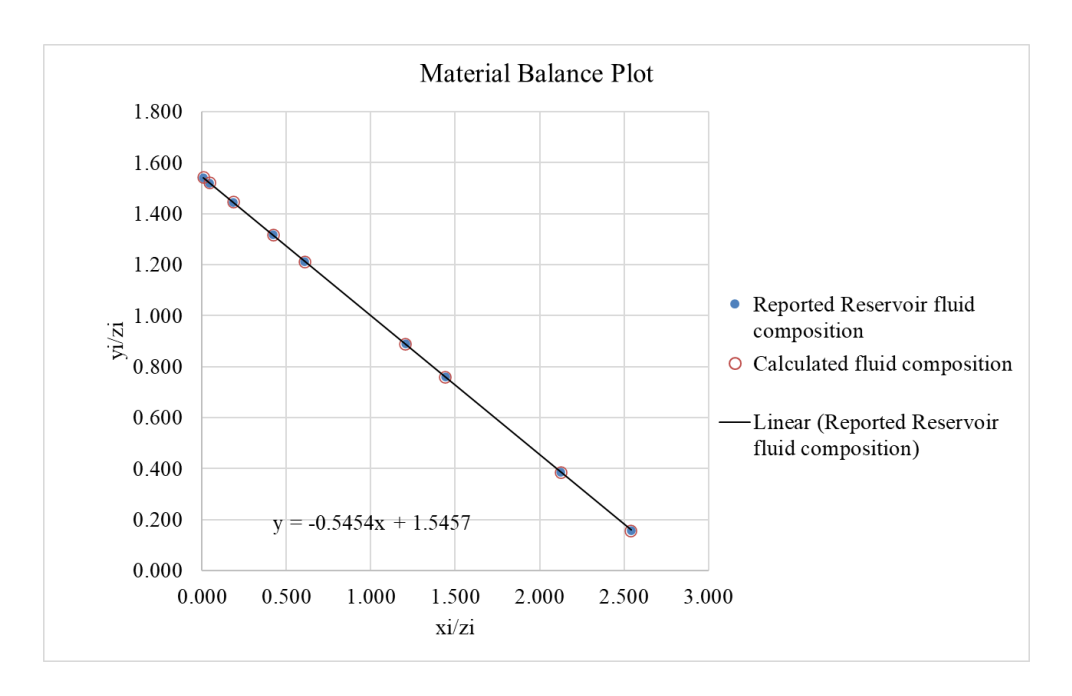


Figure 3.1: Material balance plot for the bottom hole sample (composition in Table 3.1)

3.1.2 Thermodynamic Consistency Check of Composition

The Hoffman plot was generated for the (C1-C8) components. As previously said, according to Hoffman et al. a plot of K_i versus F_i for light to intermediate components of an equilibrium mixture is expected to follow a liner trend. As shown in Figure 3.2 the analyzed composition yields a straight line in Hoffman plot suggesting that it corresponds to an equilibrated mixture.

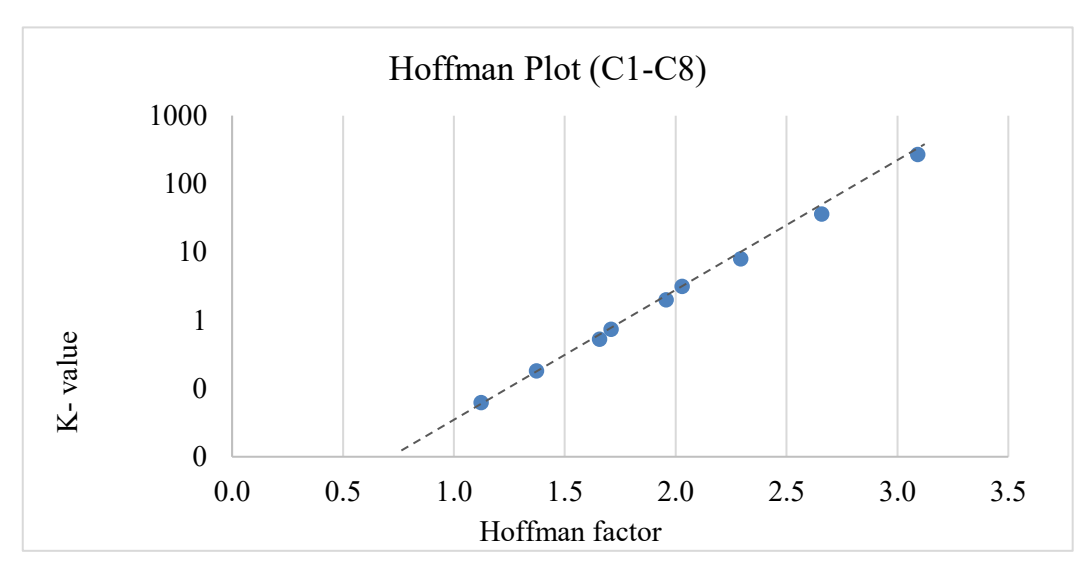


Figure 3.2: Hoffman plot

Buckley plot was used for the consistency check of the equilibrated mixtures too. The plot is shown in Figure 3.3.

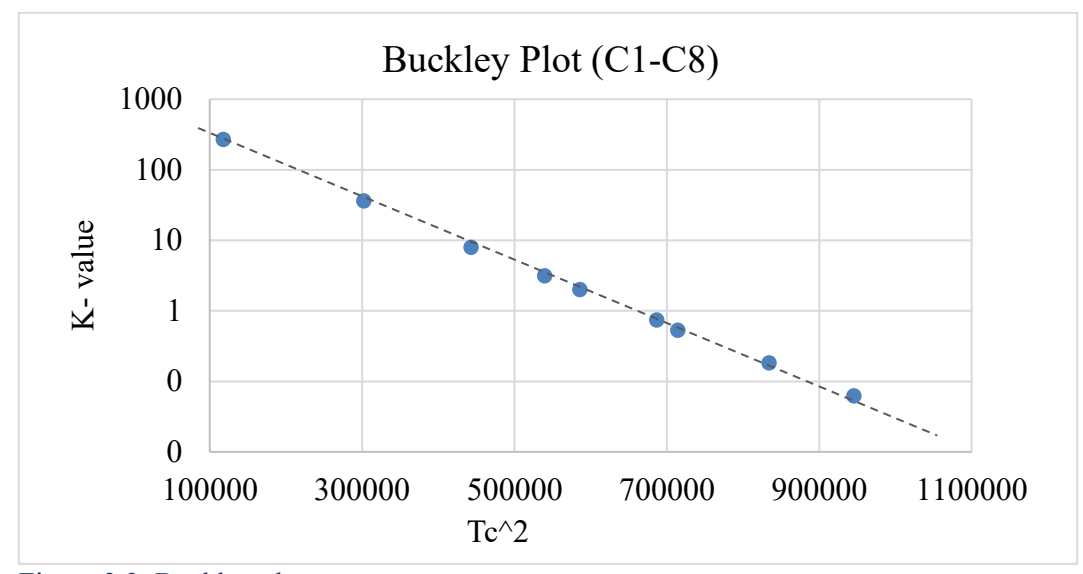


Figure 3.3: Buckley plot

The aforementioned techniques represent the principal approaches for evaluating the accuracy of reported reservoir fluid compositions. In particular, the analyses performed using the Hoffman plot, the Buckley plot, and the material balance check demonstrate that the composition data provided by the laboratory, obtained from bottom-hole sample 2 of well 15/9-19 SR, exhibit a high degree of accuracy and are consistent with thermodynamic equilibrium [Potsch et al., 2017].

3.2 EoS Comparison

3.2.1 Input Data for PVT Simulation

The laboratory report contained detailed compositional analysis up to C20+. As described in Section 2.2.1, a 23-component mixture (Table 3.3) was prepared and used as input for the modelling. The modelled results were compared with CCE and DL test results (Tables 3.4 and 3.5 (a and b)).

Analysed C	23 component co	mposition		
Num	Component	MW	RHO	Liquid Density
		Mol %	g/mol	kg/m3
1	N2	0.46	28.01	810.00
2	CO2	4.95	44.01	827.00
3	C1	43.50	16.05	300.00
4	C2	6.14	30.07	356.00
5	C3	5.26	44.10	501.00
6	iC4+nC4	3.34	58.12	574.31
7	iC5+nC5	2.43	72.15	623.71
8	C6	2.10	84.65	669.00
9	C7	3.29	91.45	742.00
10	C8	3.24	105.48	759.00
11	C9	2.39	119.68	776.00
12	C10	1.60	132.34	792.00
13	C11	1.71	143.40	793.00
14	C12	1.74	155.90	810.00
15	C13	1.51	170.40	821.00
16	C14	1.34	183.10	831.00
17	C15	1.22	195.30	839.00
18	C16	1.05	208.60	849.00
19	C17	1.06	223.00	852.00
20	C18	0.97	239.30	855.00
21	C19	0.88	252.30	863.00
22	C20-C32	4.93	350.08	902.31
23	C33-C80	4.87	663.56	989.00
	Total	100		

Table 3.3: 23 Component mixture used for the modelling of EoS [Lab. Report Well 15/9-19SR DST 1].

		CONSTANT MASS EX	PANSION AT 106.0 °C	
	PRESSURE BAR	REL VOL V/Vb	COMPRESSIBILITY 1/BAR	Y-FACTOR
Pb =	398.3 382.7 362.5 341.9 322.7 302.5 282.2 = 273.8	0.9776 0.9803 0.9836 0.9871 0.9906 0.9944 0.9984 1.0000	1.61E-04 1.66E-04 1.73E-04 1.79E-04 1.85E-04 1.92E-04 1.98E-04 2.00E-04	
	265.8 255.0 236.7 210.6 175.5 135.8 98.8 69.7	1.0068 1.0169 1.0375 1.0771 1.1577 1.3201 1.6237 2.1350		4.43 4.35 4.18 3.89 3.55 3.17 2.84 2.58
	FOR P < P	b $Y = 1.892$	+9.58E-03 x P 6783 -2.9501E-04xP +1	7264E-07xPx

Table 3.4: Constant mass expansion results [Lab. Report Well 15/9-19SR DST 1].

	CONSTANT MASS E	EXPANSION AT 106.0 °C	
PRESSURE BAR	REL VOL V/Vb	COMPRESSIBILITY 1/BAR	Y-FACTOR
398.3 382.7 362.5 341.9 322.7 302.5 282.2 Pb = 273.8 265.8 255.0	0.9776 0.9803 0.9836 0.9871 0.9906 0.9944 0.9984 1.0000 1.0068 1.0169	1.61E-04 1.66E-04 1.73E-04 1.79E-04 1.85E-04 1.92E-04 1.98E-04 2.00E-04	4.43 4.35
236.7 210.6 175.5 135.8 98.8 69.7 FOR P < P		+9.58E-03 x P 06783 -2.9501E-04xP +1	4.18 3.89 3.55 3.17 2.84 2.58

Table 3.5: Differential liberation results [Lab. Report Well 15/9-19SR DST 1].

DIFFERENTIAL VAPORIZATION AT 106.0 °C (Molecular composition of differentially liberated gas, mol%)									
(MOI	ecular	Composi	cion of	differ	entially	y liber	ated gas	s, mole)
P/Bar	255.0	230.8	200.8	160.7	120.7	81.7	51.6	25.2	1.0
CO2	1.36 6.70 76.96 6.39 4.29 0.47 1.57 0.43 0.63 0.58 0.15 0.15 0.02	6.76 76.60 6.52 4.37 0.48 1.60 0.43 0.64 0.60 0.52 0.18	77.18 6. 4 9	7.12 77.47 6.59 4.11 0.42 1.37 0.35 0.51 0.45 0.45 0.02	7.42 76.63 7.17 4.42 0.46 1.43 0.35 0.49 0.42 0.33 0.12 0.02	8.13 74.71 8.02 4.92 0.47 1.51 0.35 0.50 0.40 0.31 0.12 0.02	8.96 70.22 9.77 6.25 0.60 1.91 0.43 0.60 0.35 0.12	60.05 13.23 9.59 0.94 3.02 0.66 0.92 0.67 0.50	5.93 20.53 13.55 19.59 2.84 11.25 3.54 5.49 5.72 5.85 3.49 1.39
	100.00	100.00	100.00	100.00	100.00	100.00	100.00	100.00	
Molwt Gravity	22.52 0.778				22.38 0.773		24.05 0.830		50.27 1.735

Table 3.6: Differential liberation results [Lab. Report Well 15/9-19SR DST 1].

3.2.2 Comparison of EoS Results with Experimental Data

Four Cubic EoSs were tested with default parameters: SRK, SRK Peneloux, PR, and PR Peneloux. No regression was applied in this step. The aim was to quantify the "intrinsic" EoS behavior before tuning. The following properties have been compared:

- 1. Phase envelope;
- 2. CCE properties: P sat, Relative volume (V/Vsat), single phase compressibility, Y-factor;
- 3. DL properties: Solution Gas Oil Ratio (GOR), oil Formation Volume Factor (FVF), gas FVF, oil density, gas Z -factor;
- 4. Oil viscosity.

3.2.2.1 Phase Envelope

Phase envelopes were computed with the SRK and PR EoS with and without Peneloux volume correction (Figure 3.4). SRK and SRK-Peneloux provided identical results with complete overlap, as PR and PR-Peneloux. In general, SRK and PR equations give the same phase equilibrium results with and without Peneloux [Calsep PVTsim 13]. Given this, further comparison focuses on SRK versus PR. Both SRK and PR predicted a typical PT diagram with similar shape. Due to difference in attractive and repulsive terms, as compared in section 2.2.3, SRK and PR yield in different P_c and T_c . PR predicted lower P_c and higher T_c

relative to SRK. Accordingly, PR underestimated Psat by around - 9 % while SRK overestimated by +5% (Figure 3.4).

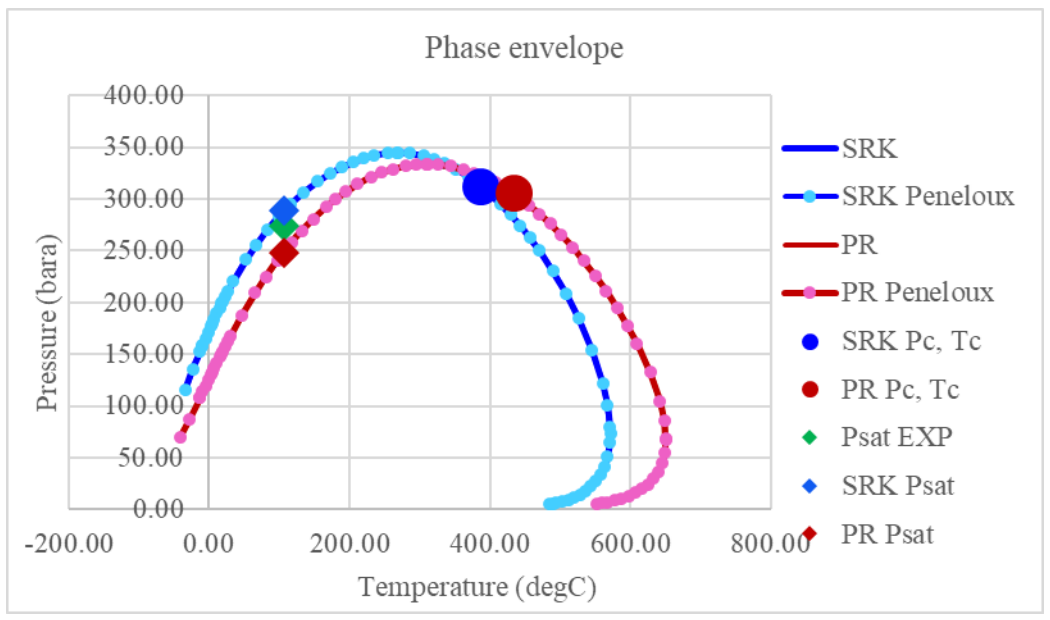


Figure 3.4: Phase envelope comparison modelled by PR and SRK. Deviation of the modelled Psat from experimental Psat.

3.2.2.2 Constant Composition Expansion (CCE)

3.2.2.2.1 Relative volume

The simulated V/Vsat values show good agreement with the laboratory data for both EoS (Figure 3.5). PR slightly underestimates V/Vsat (AAD is 0.96%), while SRK overestimates it (AAD is 1.39%). As pressure drops below Psat, deviations increase for both models. The effect of Peneloux correction appears below Psat, and for this parameter increases magnitude of deviations: SRK-Peneloux shows a larger positive deviation relative to SRK (AAD is 1.53%), and PR-Peneloux shoes similar deviation as PR (AAD is 0.93%).

3.2.2.2.2 Compressibility

Compressibility is calculated only for single phase, so up to a pressure equal toPsat (Figure 3.6). Compressibility is calculated for six pressure points till predicted Psat equal to 288.36 bara. For SRK, AAD is 14.03%, with the Peneloux correction AAD is similar 14.03%. For PR, AAD is 7.18%.

Both EoS overpredict compressibility relative to experimental data with SRK giving higher values than PR at all pressure points. For SRK, this aligns with its higher predicted Psat (greater volatility). By contrast, PR also overpredicts a higher compressibility, though its Psat is lower than the experiment.

3.2.2.2.3 Y-Factor

Both EoSs underpredict Y-factor. For PR the Y-factor is systematically low (AAD is 16.05%), and Peneloux translation only marginally reduces bias (AAD is 15.4). SRK is closer to the laboratory trend, although its deviation grows with pressure (AAD is 3.58%), with Peneloux correction the AAD is 4.96%[Figure 3.6].

Deviations can be interpreted based on the Eq. 2.16. A smaller Y can result either because the denominator is larger – the model predicts more two-phase expansion, hence more gas volume for a given pressure drop- or because the numerator is smaller – the model's Psat is too low. For SRK, model predicts both higher Psat (Figure 3.5) and higher V/Vsat (Figure 3.6) relative to experiment. The higher Psat increases numerator and would shift Y-Factor by itself, opposite to what is observed. Therefore, the remaining gap in Y-Factor must come mainly from the denominator. Thus, SRK overpredicts the two-phase expansion, leading to higher volume of gas liberation along the CCE path.

For PR, the model predicts a lower saturation pressure (Psat) than measured experimentally. This makes the numerator of the Y-Factor smaller, leading to underprediction of the Y-Factor. Also V/Vsat trend shows that PR underestimates volatility. In the end, PR mainly underestimates the Y-factor due to its low Psat prediction, not because of predicting high volatility.

The Peneloux translation affects density levels but not phase equilibria, so it has little influence on Y, explaining the small changes observed after applying correction [Pedersen&Christensen2007].

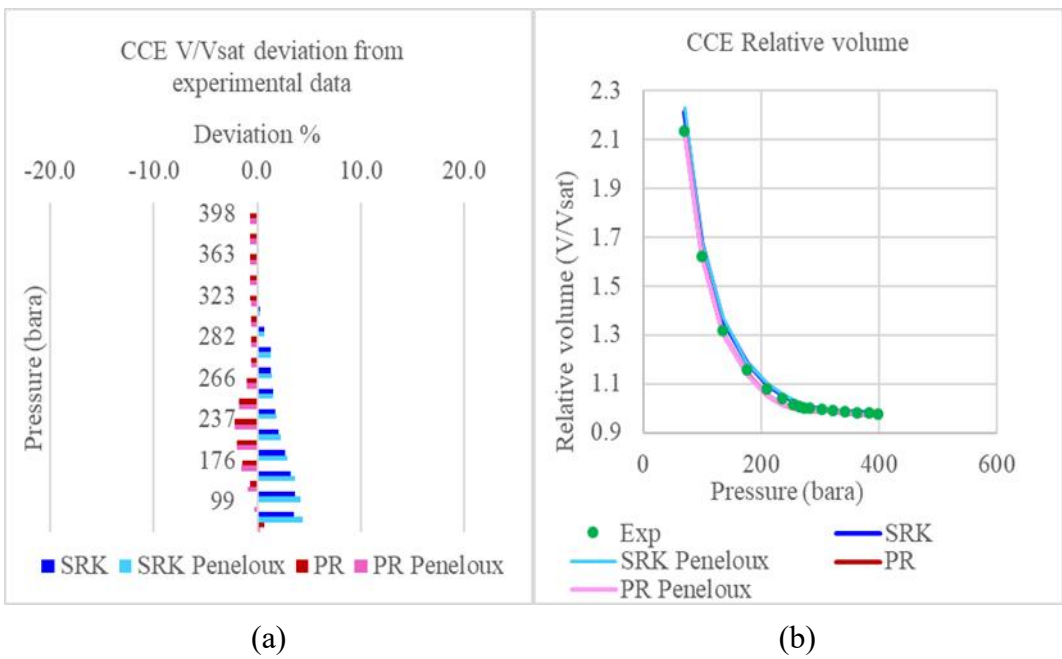


Figure 3.5: CCE. Relative volume comparison. (a) – Deviation from experiment (%). (b) – Relative volume vs. pressure (bar).

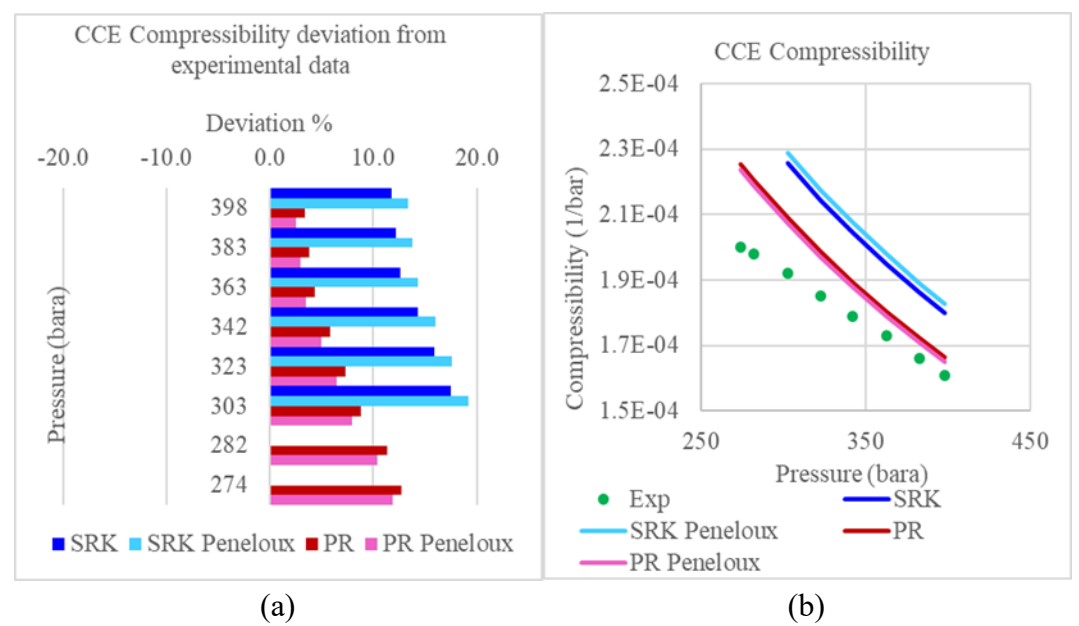


Figure 3.6: CCE. Compressibility comparison. (a) – Deviation from experiment (%). (b) – Compressibility vs. pressure (bar).

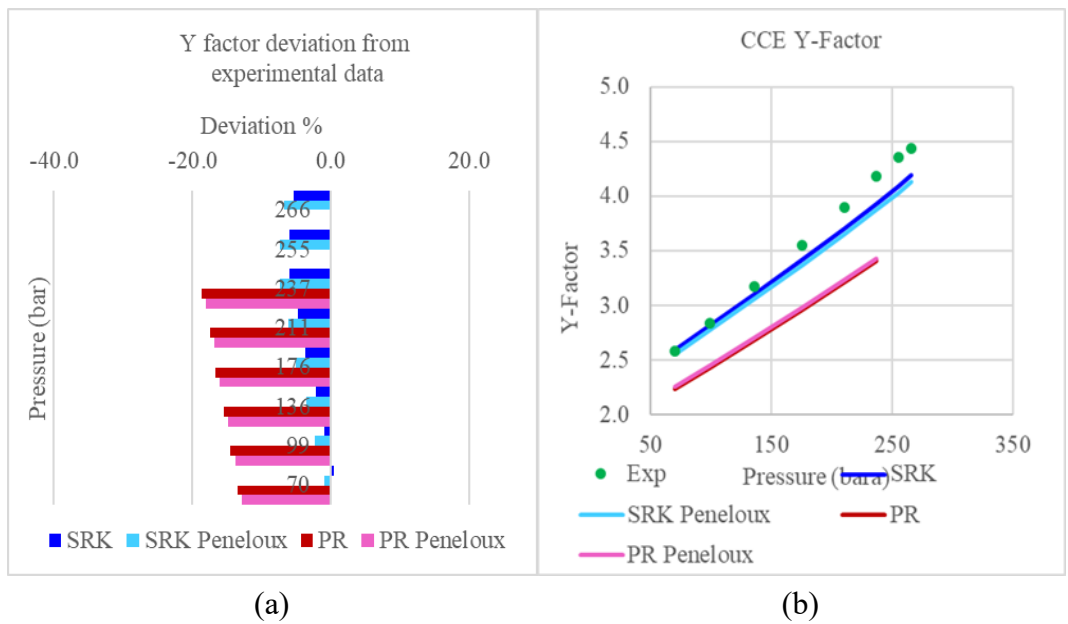


Figure 3.7: CCE. Y-Factor comparison. (a) - Deviation from experiment (%). (b) - Y-Factor vs. pressure (bar).

3.2.2.3 Differential Liberation (DL)

3.2.2.3.1 Oil Formation Volume Factor (Bo)

The oil formation volume factor Bo is slightly overpredicted by both EoSs across the pressure range (Figure 3.8). AAD for SRK is 1.2%, and it improves to 0.58% after applying Peneloux translation. For PR, the AAD is 1.74%, and with Peneloux it increases to 3.4%.

Bo trends are consistent with the CCE results. PR underestimates the volume of liberated gas, so at pressure steps below Psat it retains too high volume of dissolved gas in the liquid. So that extra dissolved gas swells the liquid and results

in larger volume in reservoir condition per stock tank barrel, consequently Bo is higher. The Peneloux translation adjusts the liquid volume, in this case it increases the PR liquid volume, and worsens the prediction.

SRK predicts higher volatility based on CCE results, which should reduce the Bo, however SRK also predicts a more expansive liquid, most likely due to higher single-phase compressibility, so the liquid volume remains slightly too large, and Bo ends up just above the data. Peneloux for SRK reduces liquid volume improving the Bo.

3.2.2.3.2 Solution GOR (Rs)

Both EoSs, SRK and PR, overpredict the Rs, but with different magnitude (Figure 3.9). SRK is close to the laboratory trend, with small positive bias, AAD is 4.24%. SRK-Peneloux yields the same Rs values, so MD is 4.24%. PR shows much larger systematic overprediction (AAD is 15.47%), and with Peneloux the bias increases slightly (AAD is 17.81%).

Overpredicted Rs means that model retains too much light gas dissolved in the oil at a given pressure (Eq. 2.19. This behavior aligns directly with Bo. For SRK modest Rs bias corresponds to a small Bo overprediction, whereas PR's high Rs bias correlates with large Bo overprediction due to under volatility prediction, consequently higher dissolved gas in solution, leading to Rs overestimation.

3.2.2.3.3 Oil Density

Oil density is overpredicted compared to the laboratory values across the pressure range by both EoSs, SRK and PR. The AAD for SRK is 2.46%, increasing to 3.56% with the Peneloux translation. For PR the AAD is 1.78%, rising to 2.4% after translation.

For SRK the density overestimation is aligned with previous observations for Bo and Rs. SRK overpredicts the volatility, therefore density of the remaining oil is overpredicted. On top, Peneloux translation increases liquid molar volume pushing the trend upward increasing the deviation. For the SRK it is intended to increase the liquid density, because unmodified SRK consistently underpredicts the liquid density [Pedersen&Christensen2007].

PR results in most accurate liquid phase density in this study, yet it still shows a small positive bias. This behavior is consistent with PR EoS formulation [Peng&Robinson, 1976]. Peneloux translation adds a constant shift to the liquid molar volume. However, for PR in this case it adds bias at lower pressure values.

3.2.2.3.4 Gas Formation Volume Factor (Bg)

The Bg is reproduced very well by both EoSs. SRK shows a small positive bias (AAD is 1.7%), which improves with Peneloux translation (AD is 0.88%). PR exhibits a small negative bias (AAD is 3.09%) improving to 1.03% with Peneloux translation. These magnitudes are minor and indicate that gas phase behavior is captured satisfactorily.

3.2.2.3.5 Gas Z-Factor

Gas Z factor deviation increases with increasing pressure for both EoSs. SRK deviates to positive side, while PR deviates to negative side. SRK resulted AAD is 1.41%, with Peneloux translation reduces to 0.76%, PR results give AAD equal to 3.71 which improved with Peneloux to 1.66%

Positive bias in Z-factor means lighter gas more ideal than laboratory measurement at the same pressure and temperature. For SRK it is consistent with higher volatility (leaner evolved gas). PR yields a slightly lower Z factor consistent with its under volatility (heavier evolved gas). Z factor estimations improve for both EoSs with Peneloux volume correction.

3.2.2.3.6 Gas Viscosity

Gas viscosity is computed using the corresponding states principles (CSP) viscosity model. The CSP model uses inputs such as composition, temperature, pressure and gas density (through Z-factor) and reference fluid properties. EoS is only used to provide phase behaviour and densities, which are then used as an input to the CSP correlation. This is why Peneloux translation has no effect, and why SRK and PR give nearly the same viscosity bias: for SRK AAD is 9.19%, and for PR AAD is 9.53%.

3.2.2.3.7 Oil Viscosity

The same as gas viscosity, the oil viscosity is computed by CSP. Both EoSs overpredict oil viscosity across the entire pressure range. The AAD is 13.9% for SRK, for PR the bias is larger, 24.72%, and as expected Peneloux does not impact oil viscosity calculation.

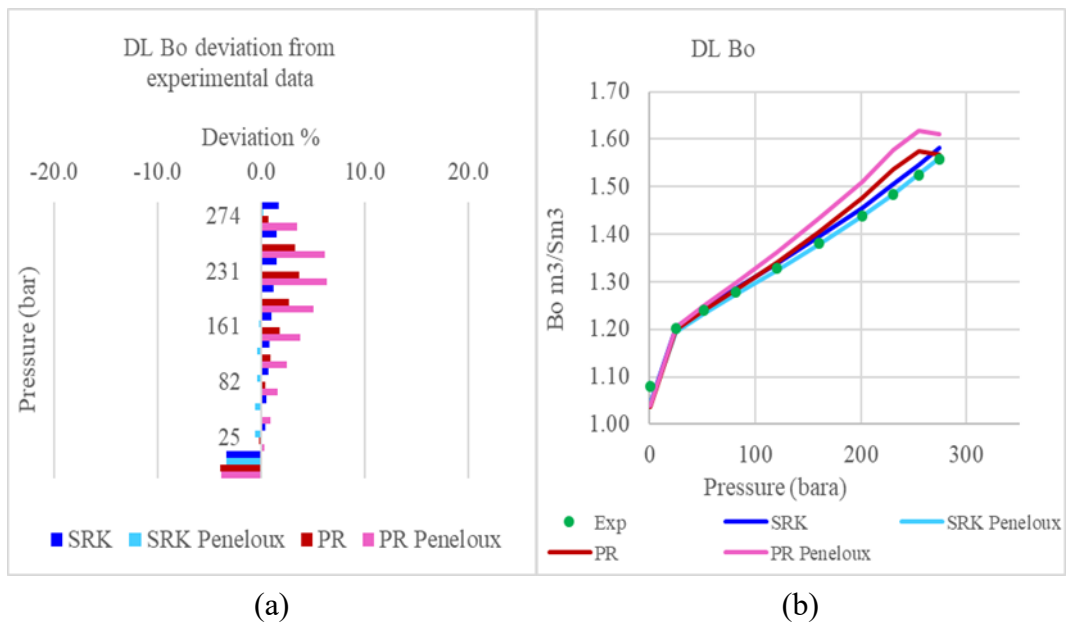


Figure 3.8: DL oil formation volume factor. (a) – Deviation from experiment (%). (b) – Oil formation volume factor vs. pressure (bar).

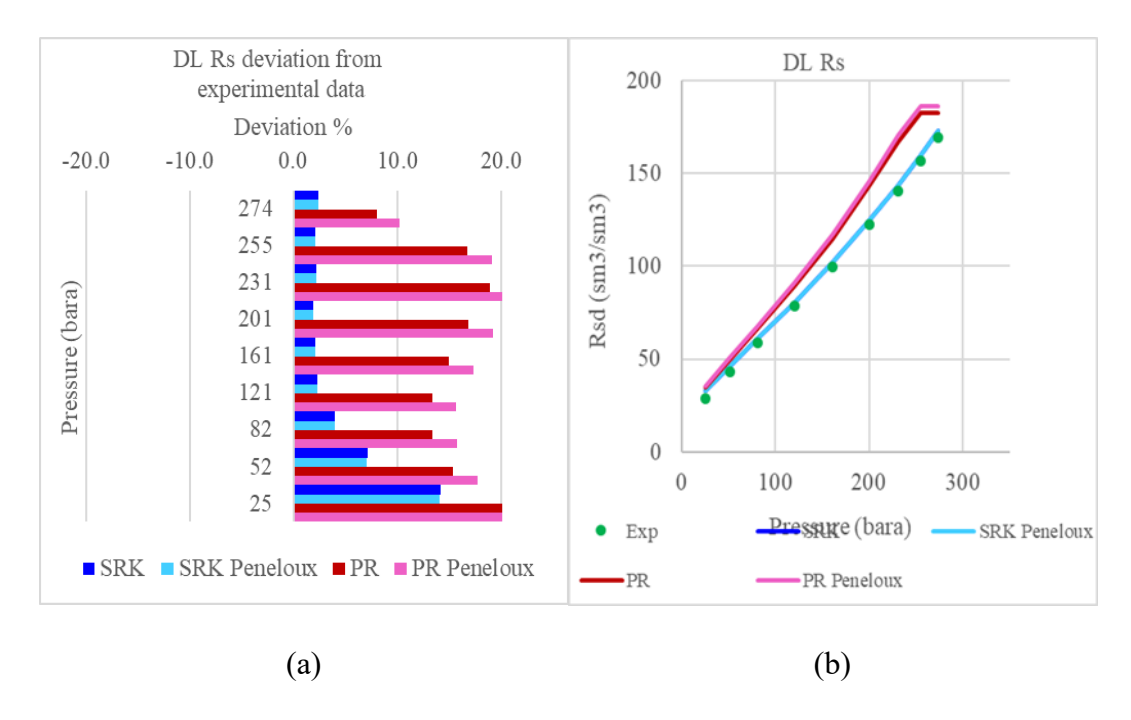


Figure 3.9: DL Solution GOR. (a) – Deviation from experiment (%). (b) – Solution GOR vs. pressure (bar).

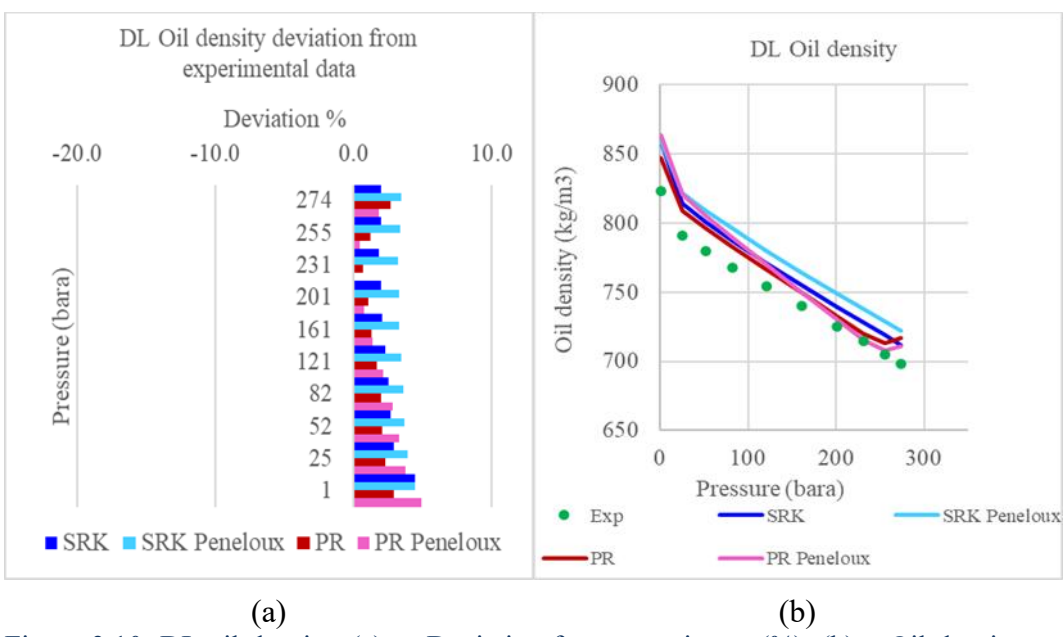


Figure 3.10: DL oil density. (a) – Deviation from experiment (%). (b) – Oil density vs. pressure (bar).

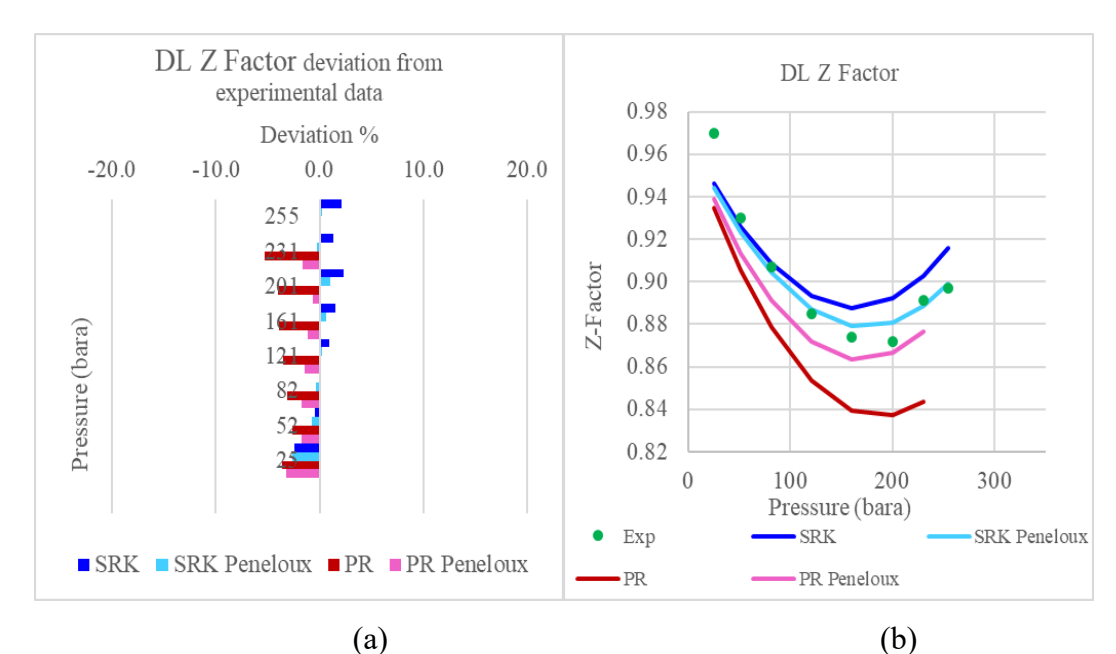


Figure 3.11: DL Z- factor. (a) – Deviation from experiment (%). (b) – Z- factor vs. pressure (bar).

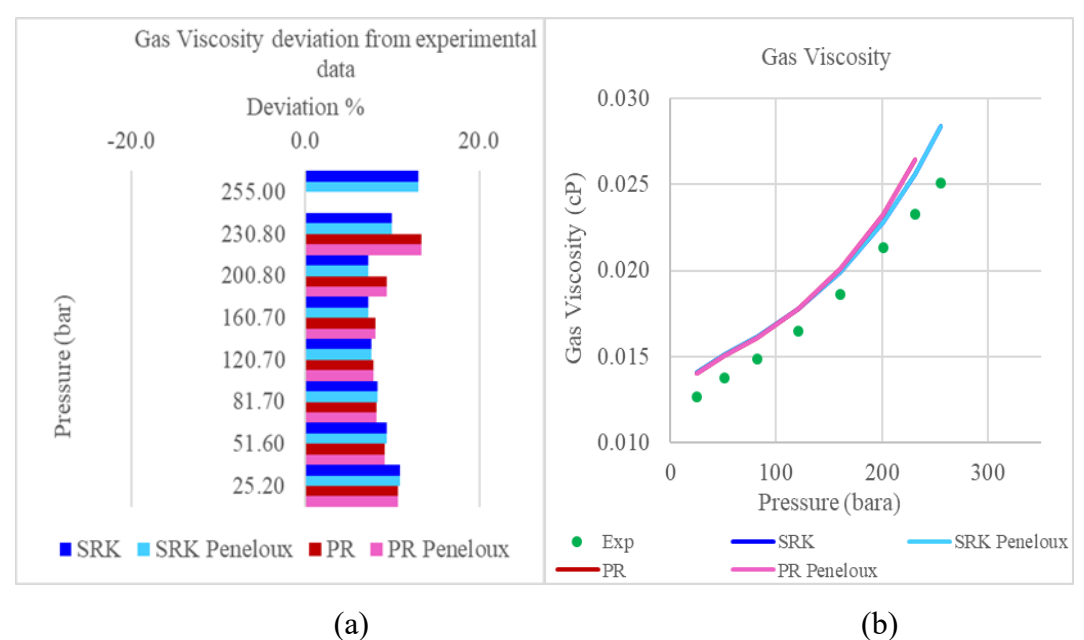


Figure 3.12: DL Gas viscosity. (a) – Deviation from experiment (%). (b) – DL gas viscosity vs. pressure (bar).

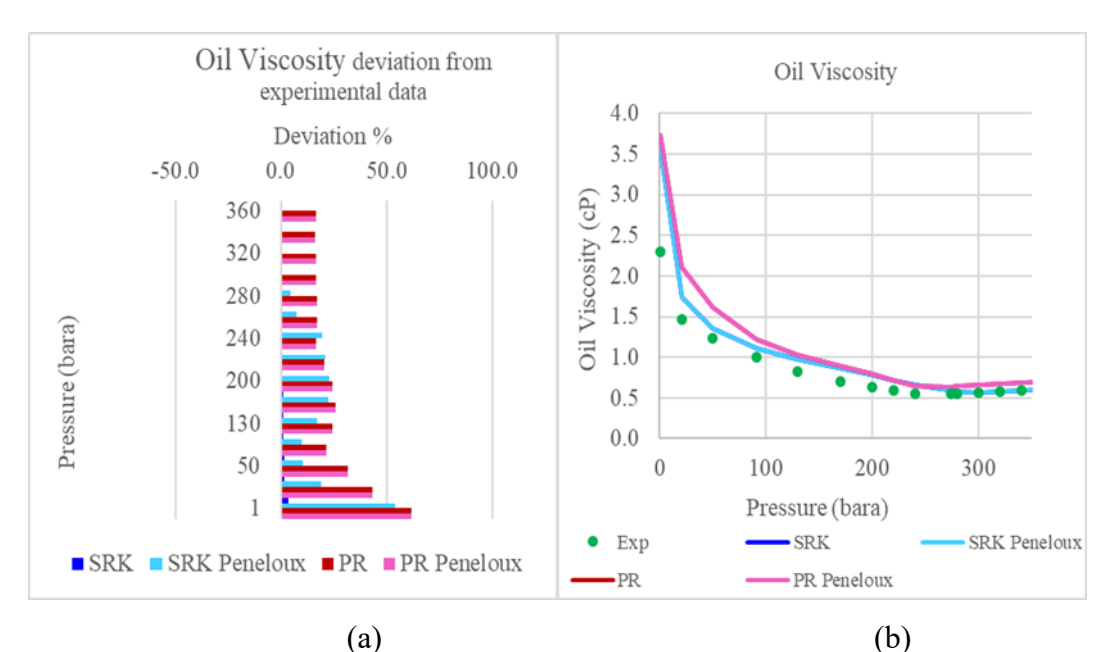


Figure 3.13: Oil viscosity. (a) – Deviation from experiment (%). (b) – Oil viscosity vs. pressure (bar).

3.3 Plus Fluid Regression

It is a common practice to perform plus fluid regression to improve characterization of C7+ heavy ends before lumping into a smaller set of components [Pedersen&Christensen, 2007]. Plus fluid regression workflow is described in Section 2.3.

The following regression range was set in PVT sim:

Molecular weight: 10%;
Critical temperature: 20%;
Critical Pressure: 20%;
Acentric Factor: 20%.

Also, regression weights were set up for the specific properties based on their deviation from the experimental data and their impact on EoS:

- Psat weight=5;
- CCE compressibility weight=4;
- DL Oil density weight =3;
- DL Oil FVF weight=2;
- DL Rsd weight =2;
- Oil viscosity weight=2.

During the plus fluid regression, the MW of the two pseudo-components C20-32 and C33-C80 were adjusted by 0.8% and 5.2.0% respectively(Figure 3.14).

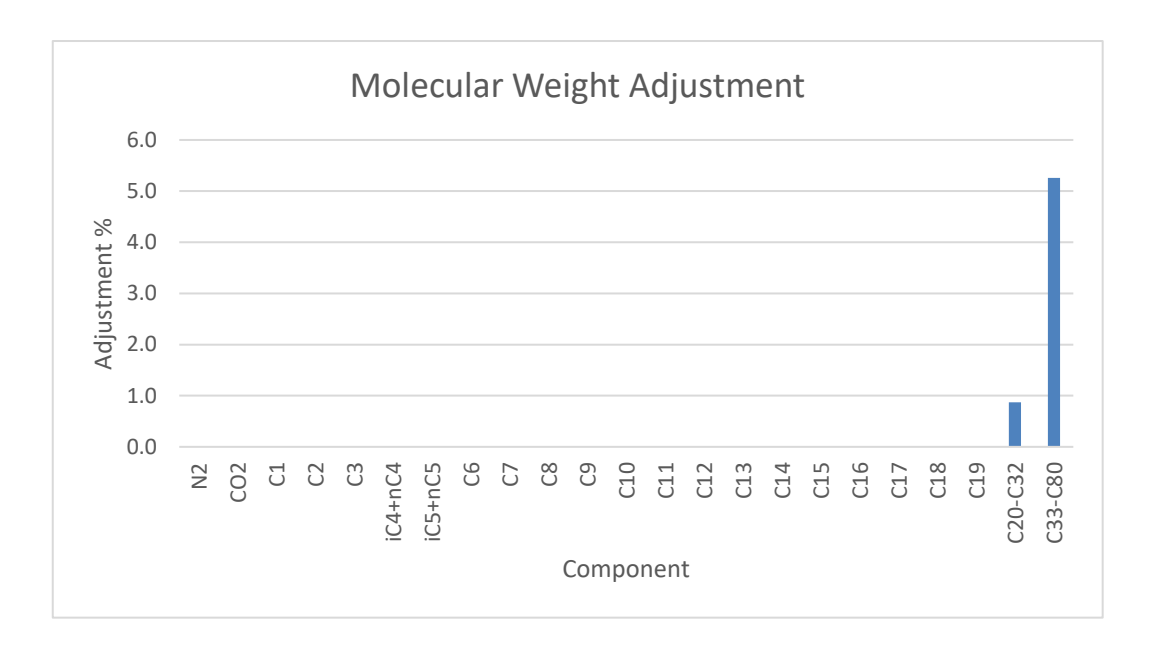


Figure 3.14: Molecular weight adjustment. Plus fluid regression

The plus fluid regression allowed for a broader adjustment of Pc (1.5–8.5%), while T_c adjustments were constrained to 0.5% for C7+, except for the C33-80 pseudocomponent where up to 2.5% adjustment has been reached. According to the literature, T_c is more strongly anchored by boiling point ranges and MW trends [Danesh.1998], while P_c is less constrained by those inputs. Therefore, P_c has higher uncertainty compared to T_c . The ranges of Tc and Pc adjustments are reported in the Figure 3.14 and Figure 3.15.

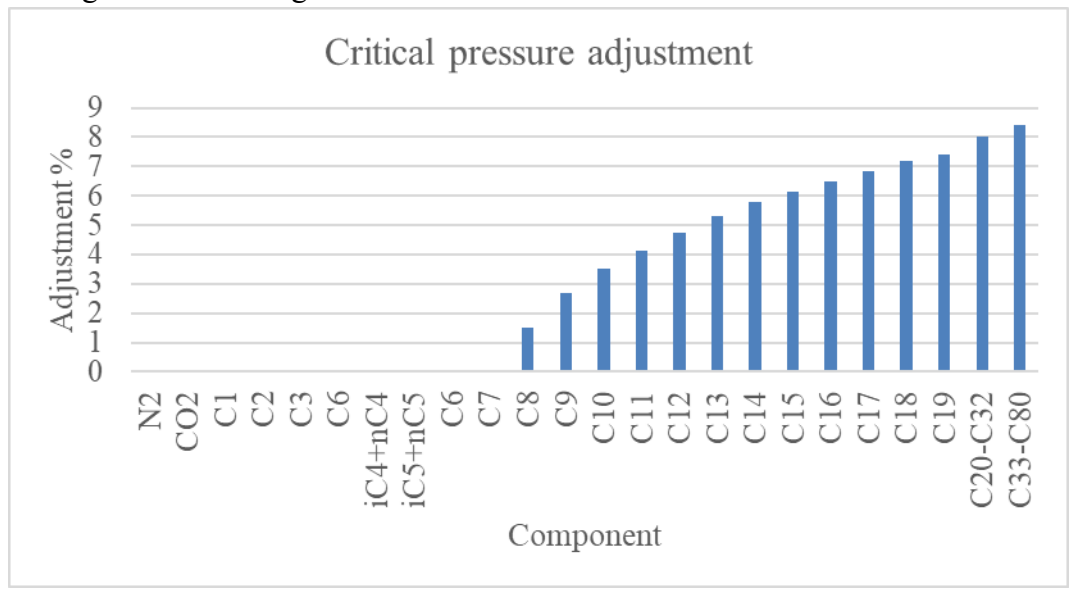


Figure 3.15: Critical Pressure adjustment. Plus fluid regression.

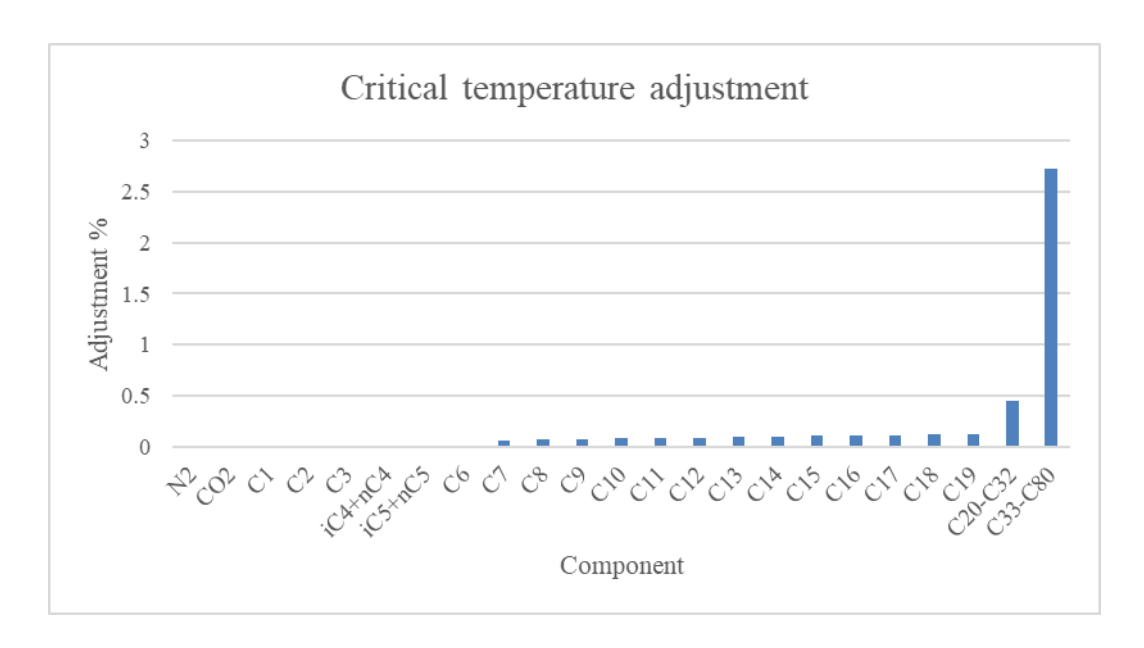


Figure 3.16: Critical temperature adjustment. Plus fluid regression.

In this section Peneloux volume shift (cPen) was recomputed due to MW change, not because of tuning cPen.

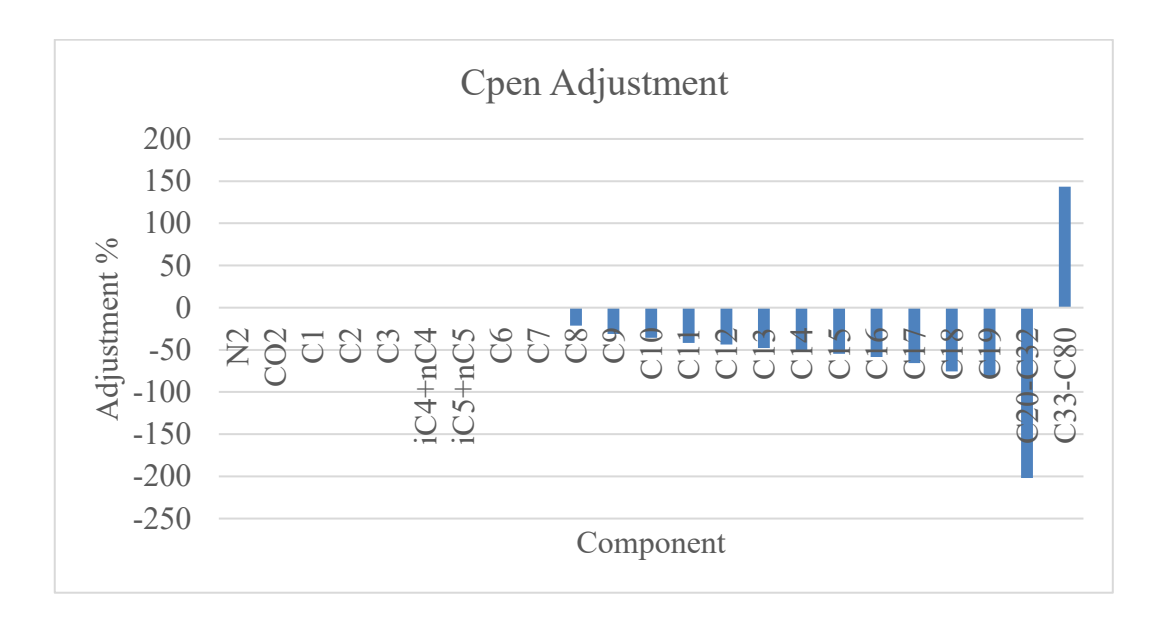


Figure 3.17: Recomputed cPen values due to MW change. Plus fluid regression.

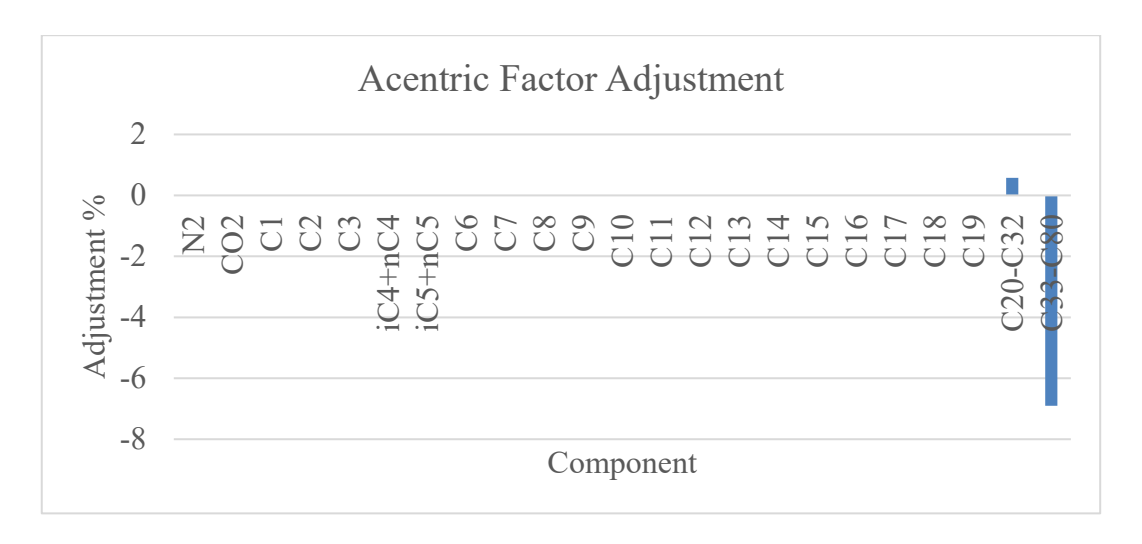


Figure 3.18: Acentric factor adjustment. Plus fluid regression.

Following adjustments were applied for viscosity correction factors to improve the match with the experimental data:

Viscosity correction factor (CSP)	Adjustment%
1 st	64.058
2 nd	-9.009
3 rd	49.260
4 th	12.745

Table 3.7: Viscosity correction factor adjustment. Plus fluid regression

The fit to experimental data improved due to the combined effect of the regressed parameters. Applying plus-fluid regression to the PR—Peneloux EoS improved the predicted saturation pressure: Psat increased from 248.59 bar (before regression) to 273.82 bar (after regression), versus experimental value of 273.8 bar.

The match to CCE parameters (Figures 3.6–3.8) and DL results (Figures 3.9–3.10) also improved.

Despite assigning a regression weight of 3 to oil density, the deviation increased after regression (Figure 3.11); a similar trend is seen for the gas Z-factor and gas viscosity. We will retune these DL-related parameters after component lumping, with results reported in Section 3.4.

Plus-fraction regression also significantly improved the oil-viscosity match.

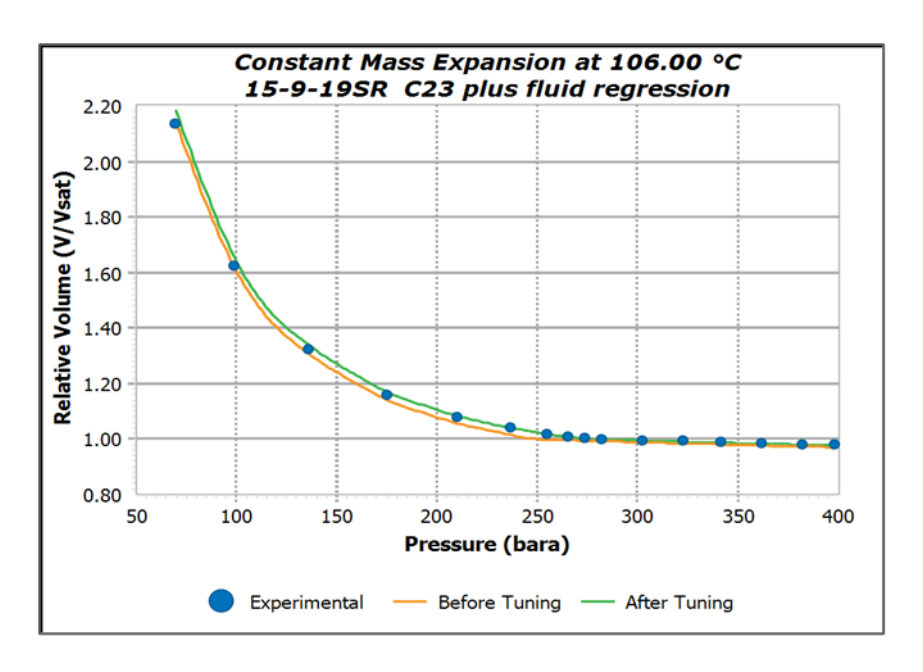


Figure 3.19: CCE Relative volume – before and after tuning.

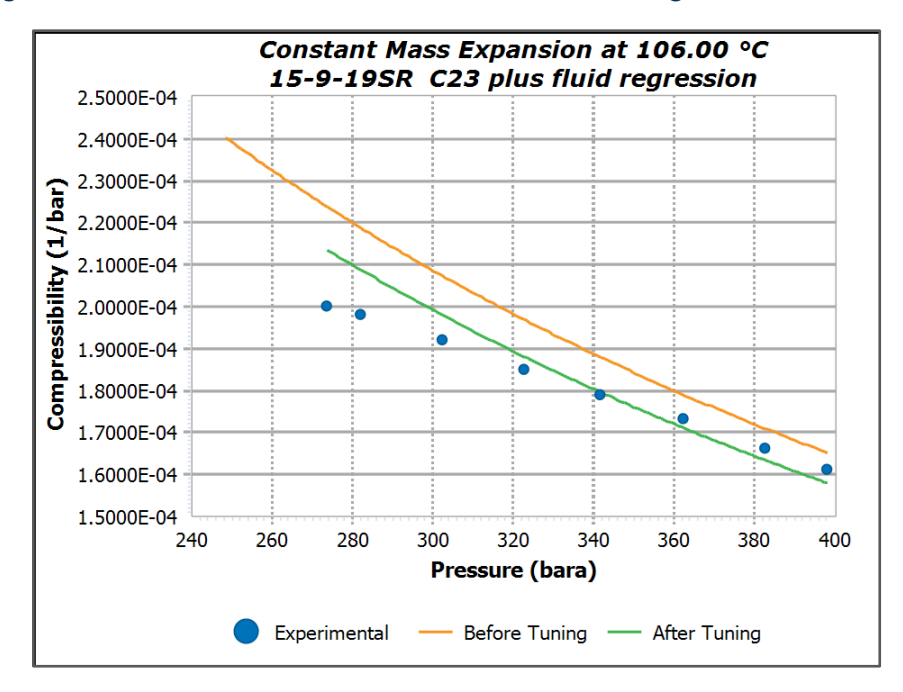


Figure 3.20: CCE Compressibility result – before and after tuning.

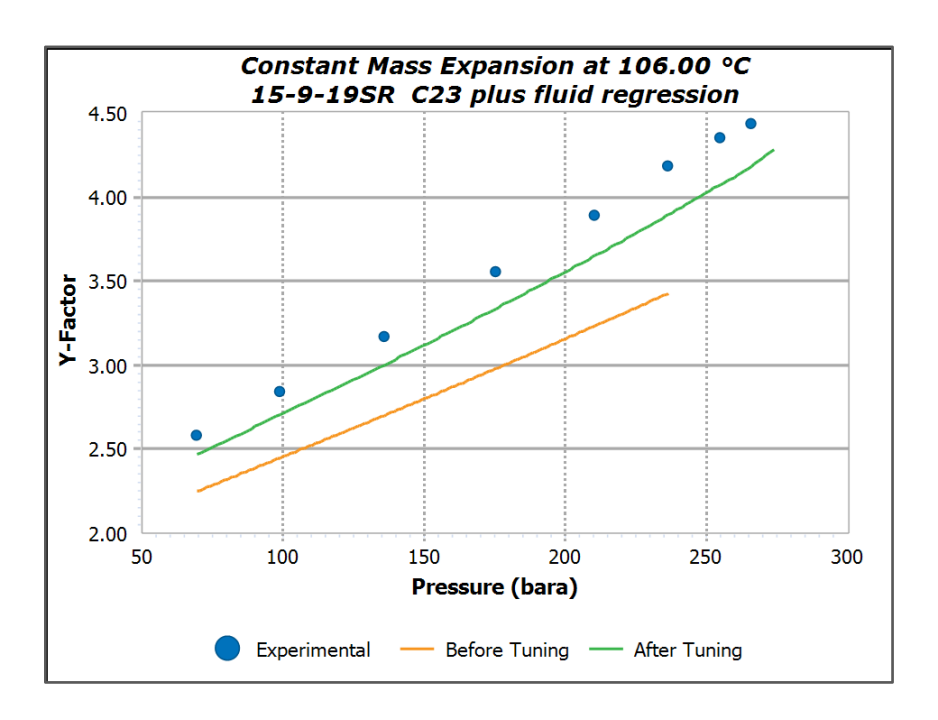


Figure 3.21: CCE Y-factor – before and after tuning.

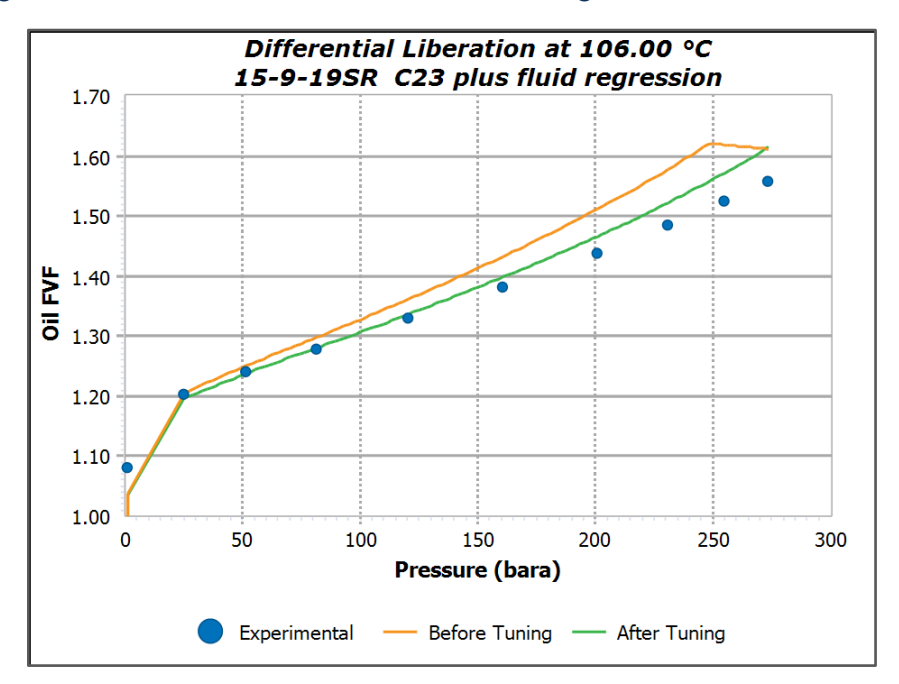


Figure 3.22: DL Oil FVF – before and after tuning

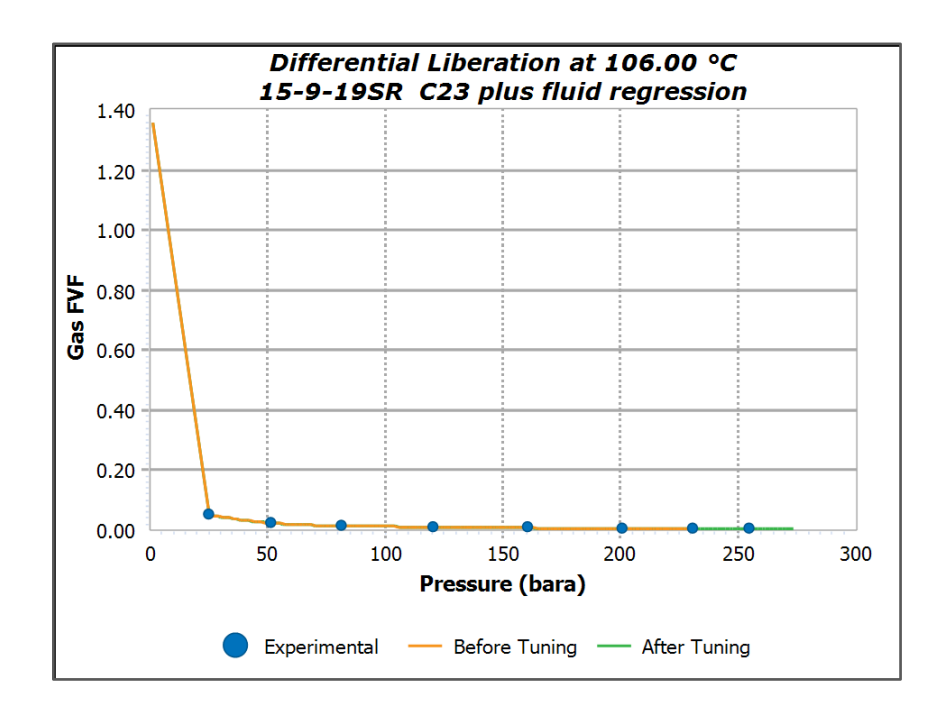


Figure 3.23: DL Gas FVF – before and after tuning

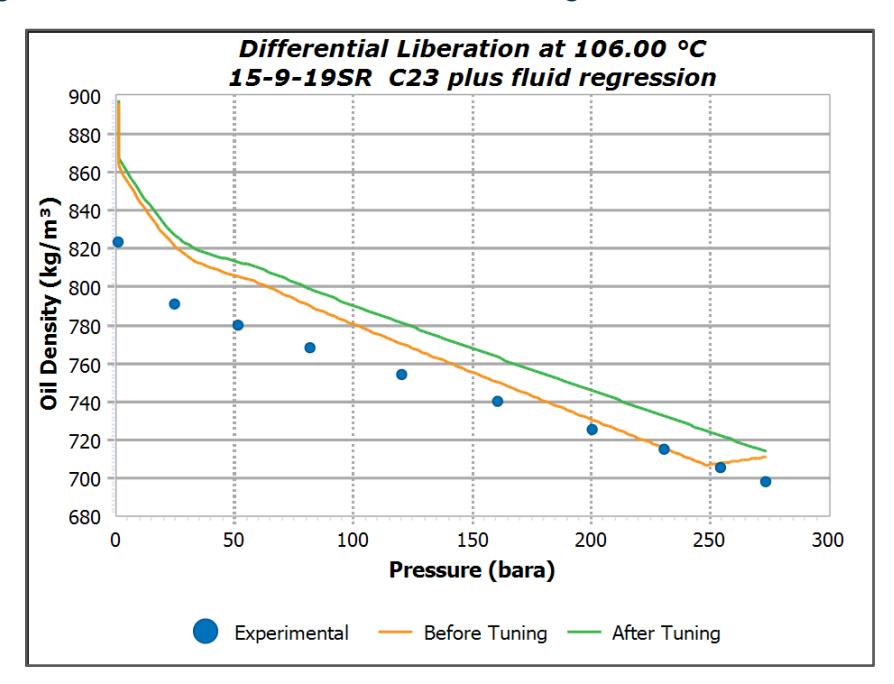


Figure 3.24: Oil density – before and after tuning

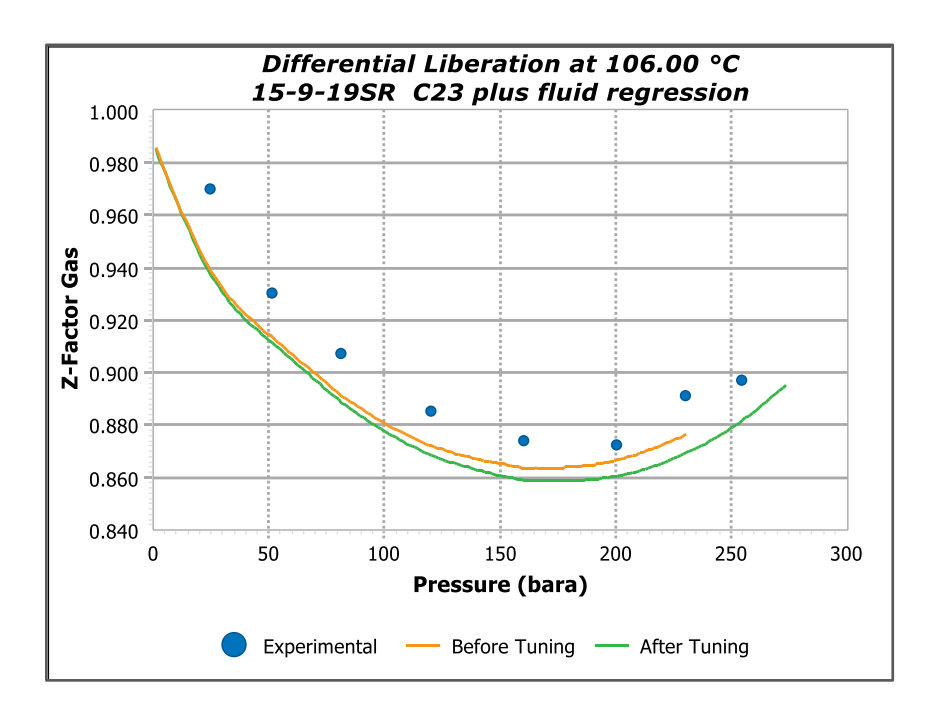


Figure 3.25: Gas Z-factor – before and after tuning

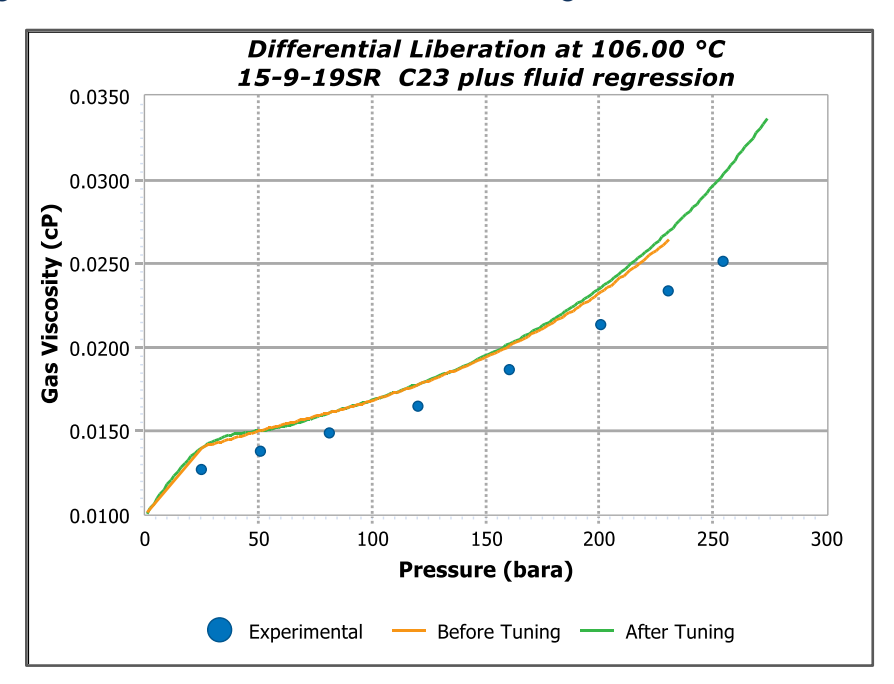


Figure 3.26: Gas Z-factor – before and after tuning

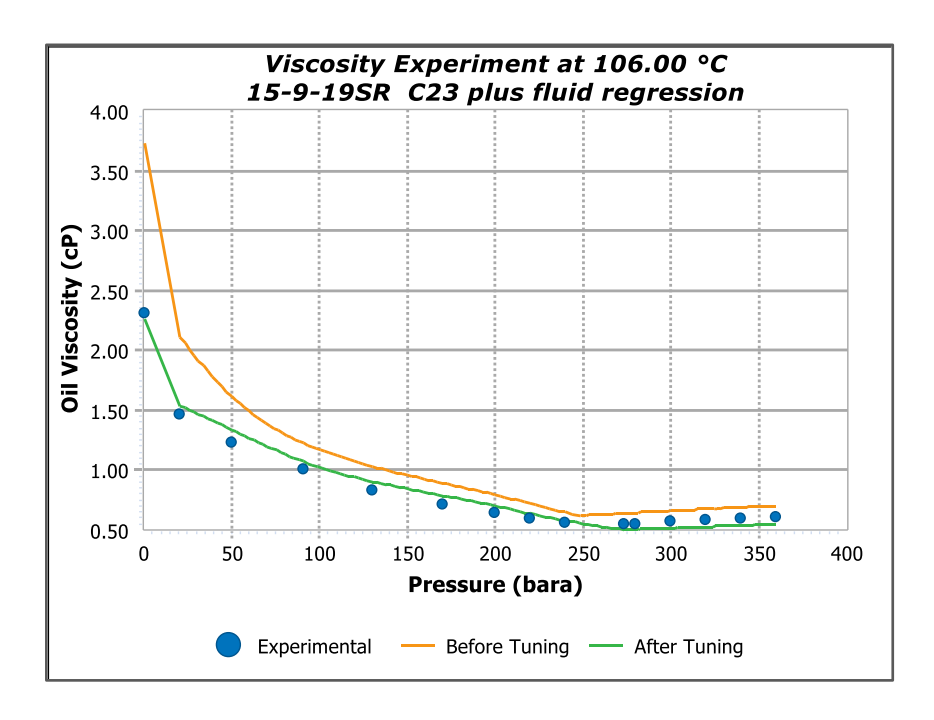


Figure 3.27: Oil viscosity – before and after tuning

3.4 Lumping and Calibration of PR-P

This section presents the results of component lumping and calibration. The aim is to investigate how heavy-end and other model-parameter regressions affect PVT predictions.

3.4.1 Lumping of 23 Components to 8 Components

To reduce CPU time in compositional reservoir simulation, the detailed fluid was lumped into a small set of pseudo-components. Field-scale models typically use 6–9 components. There are numerous lumping algorithms, as covered in Section 2.4, and no single method is optimal for all cases. Following the suggestions of [Pedersen 2007; Alavian et al., 2014], we assessed several grouping alternatives and chose the one that most closely matched the 23-component model post plus fluid regression:

- 1. N₂+CH₄
- $2. CO_2+C_2$
- 3. $C_3+iC_4+nC_4$
- 4. C5-C7
- 5. C₈–C₁₃
- 6. C₁₄-C₁₉
- 7. C₂₀–C₃₂ (plus)
- 8. C₃₂–C₈₀ (plus)

The selected lumping schemes roughly overlap the 23-component prediction as seen in Figures 3.28-3.36.

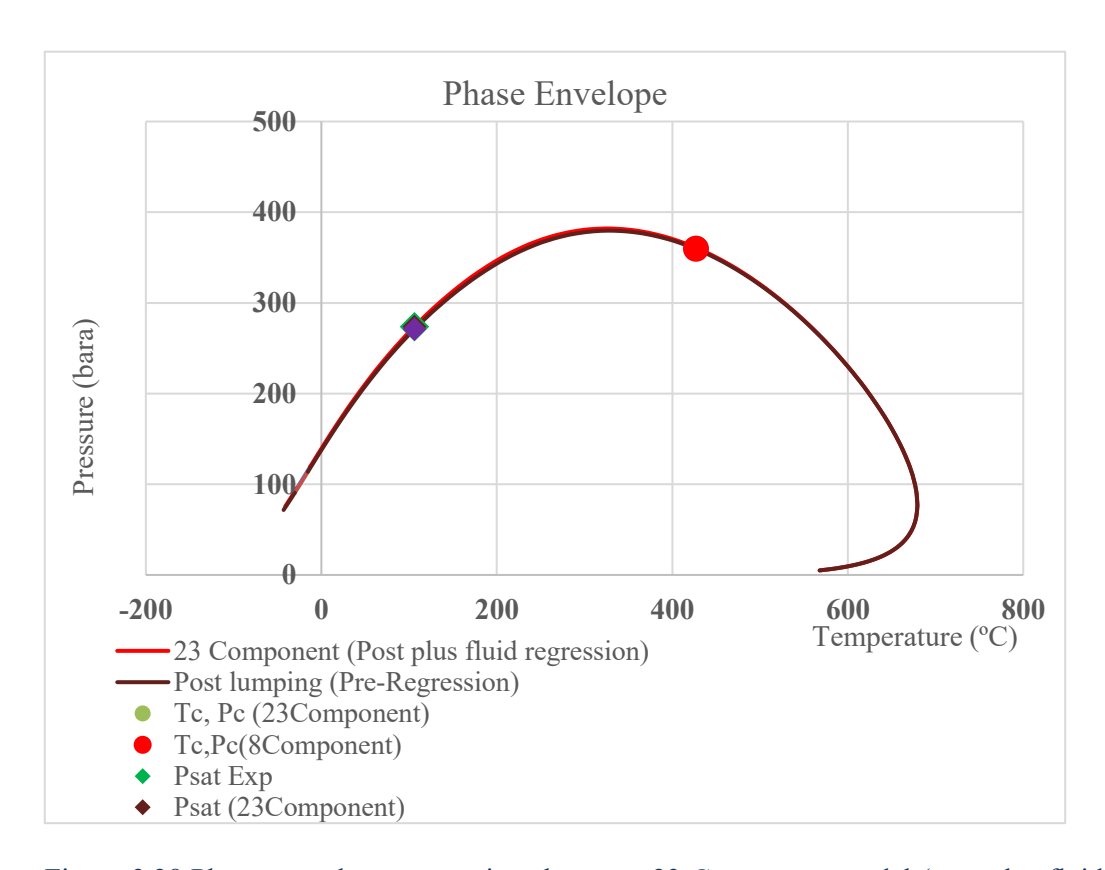


Figure 3.28:Phasae envelope comparison between 23 Component model (post plus fluid regression) and 8 component lumped model.

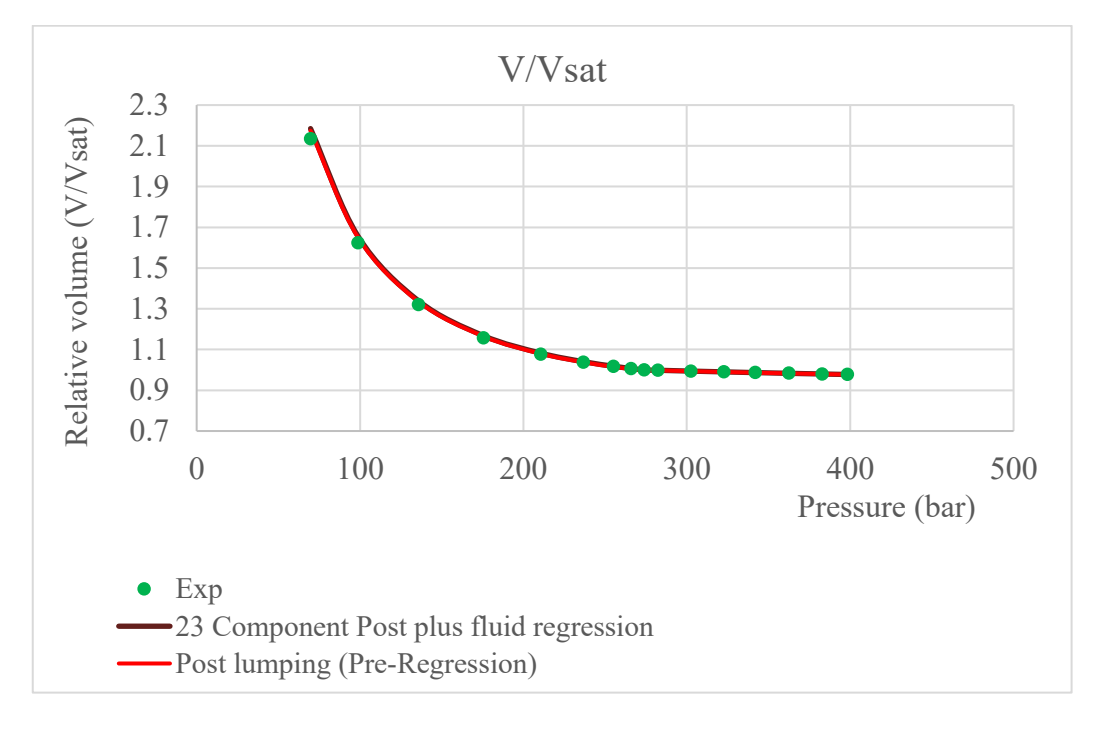


Figure 3.29: CCE Relative Volume comparison between 23 Component model (post plus fluid regression) and 8 component lumped model.

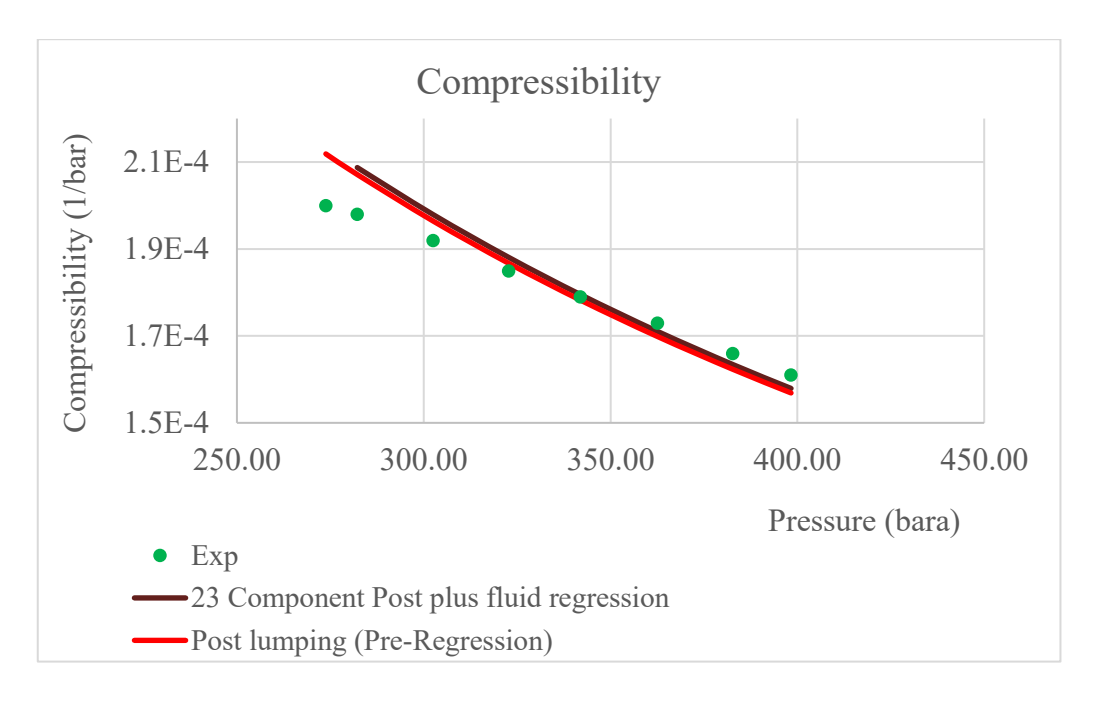


Figure 3.30: CCE Compressibility comparison between 23 Component model (post plus fluid regression) and 8 component lumped model.

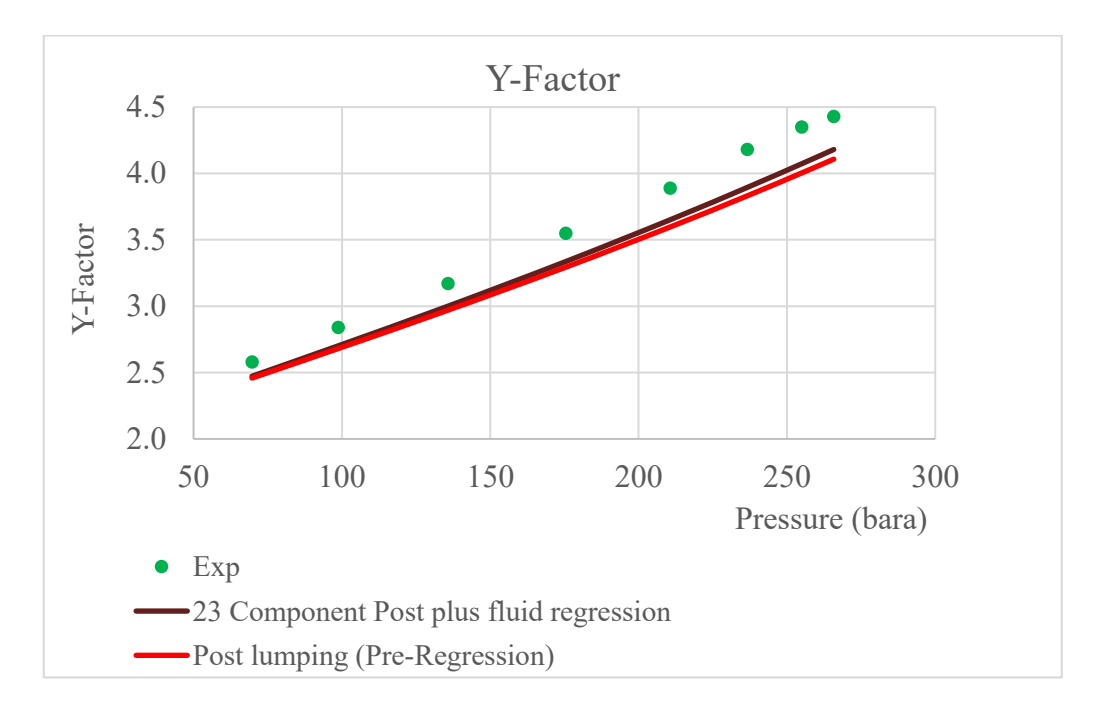


Figure 3.31: CCE Y-Factor comparison between 23 Component model (post plus fluid regression) and 8 component lumped model.

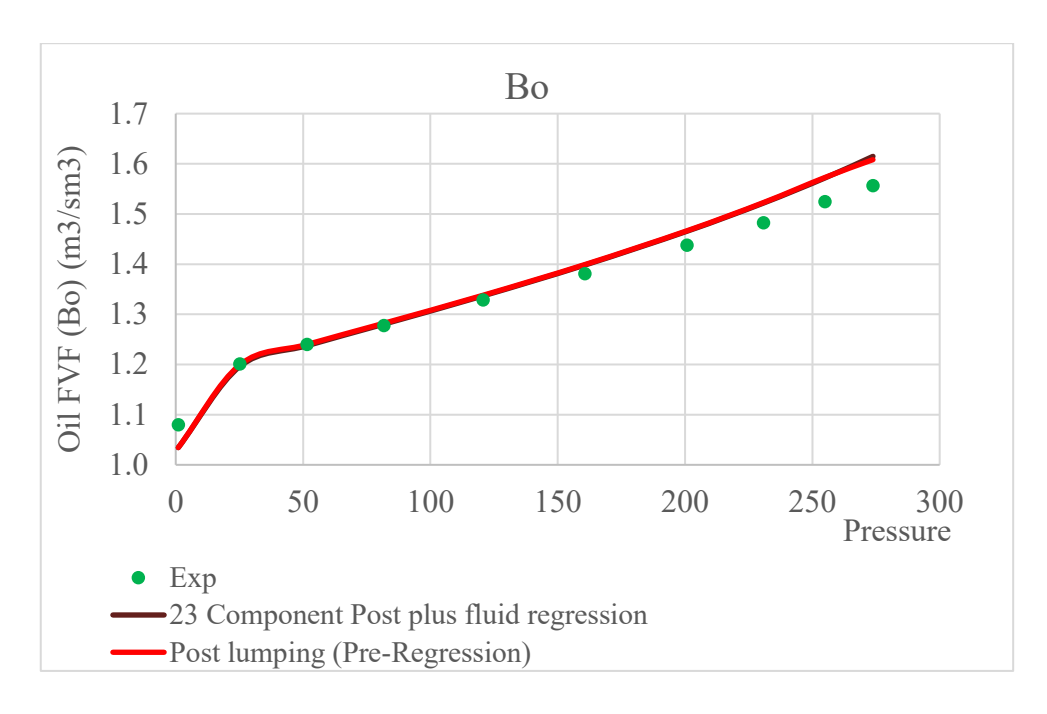


Figure 3.32: DL Oil formation volume factor comparison between 23 Component model (post plus fluid regression) and 8 component lumped model

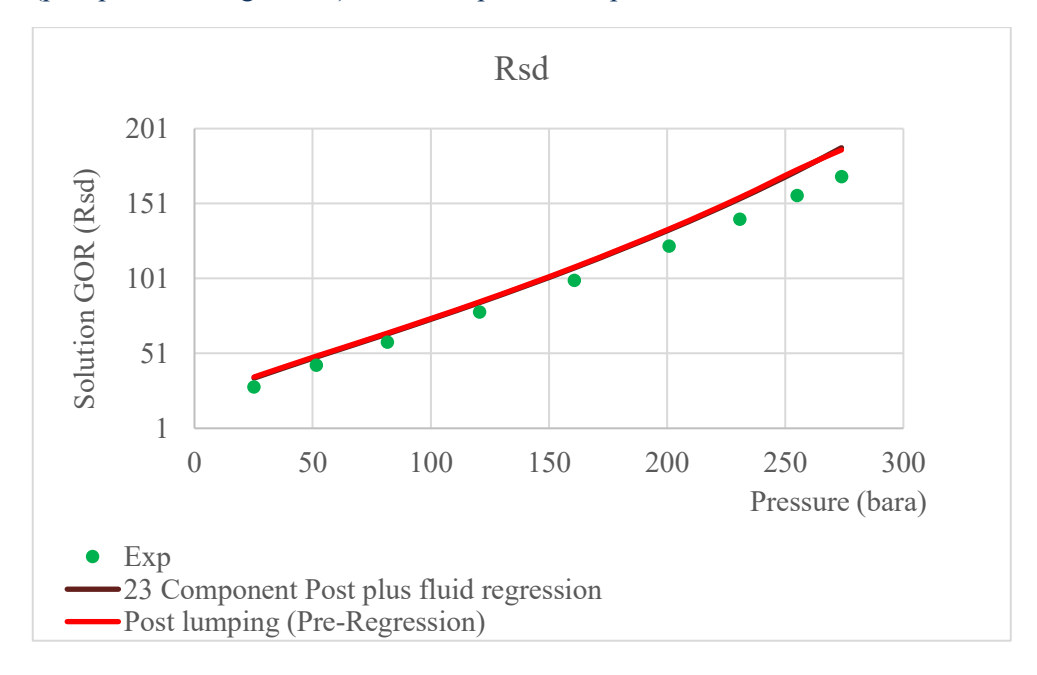


Figure 3.33: DL solution GOR comparison between 23 Component model (post plus fluid regression) and 8 component lumped model.

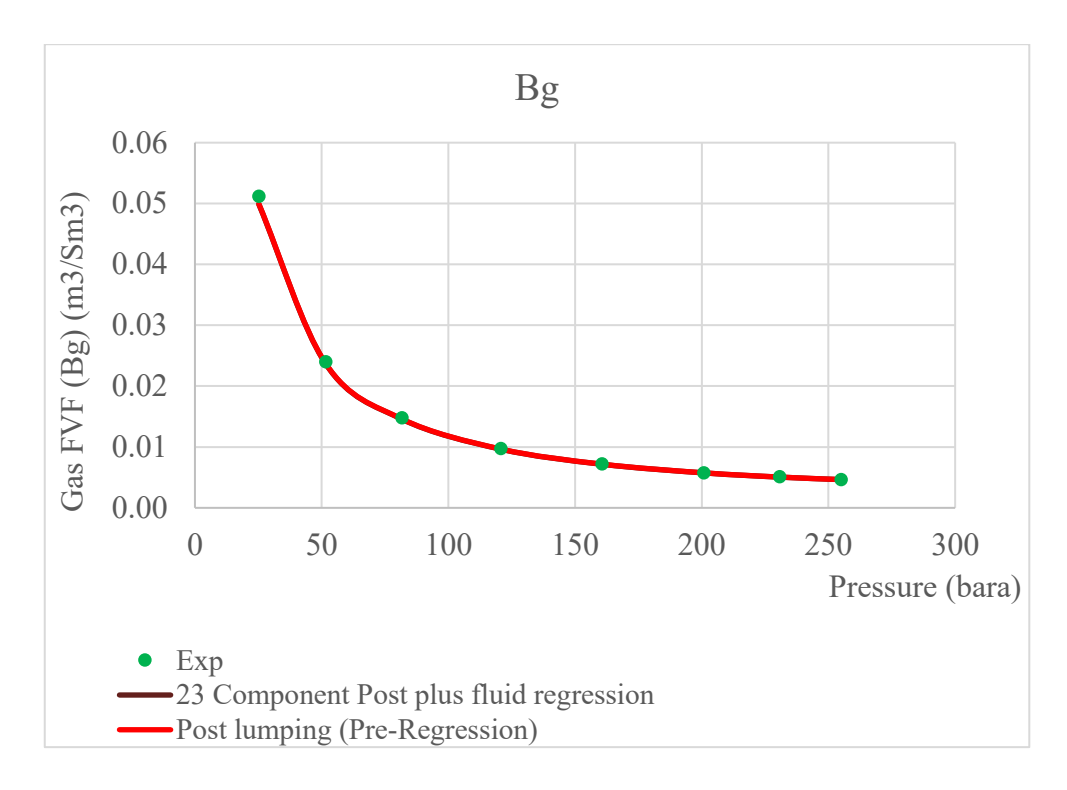


Figure 3.34: DL Gas formation volume factor comparison between 23 Component model (post plus fluid regression) and 8 component lumped model.

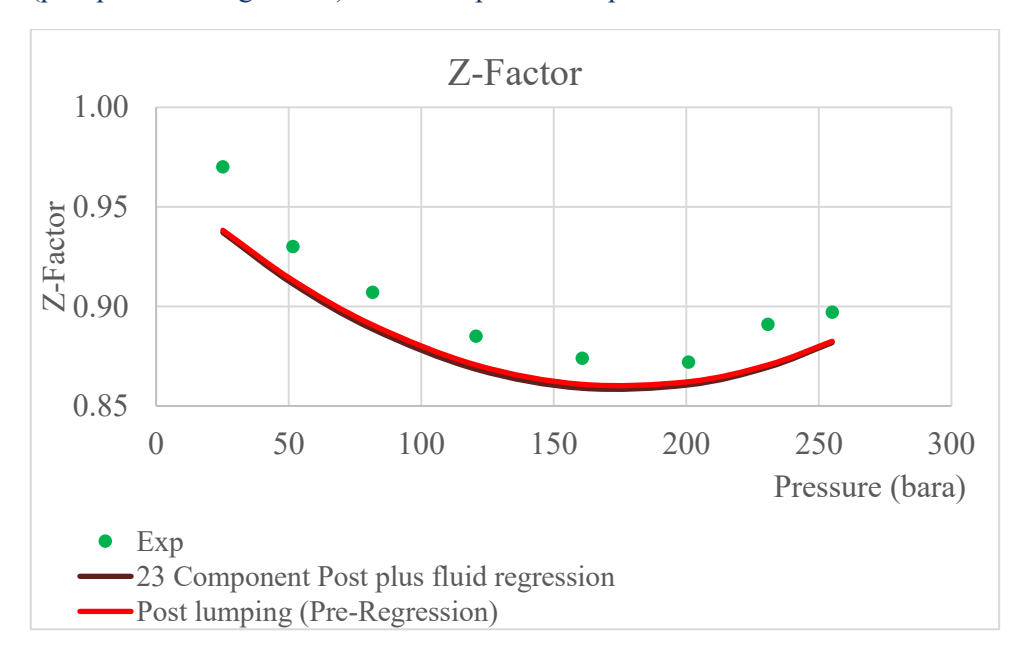


Figure 3.35: DL Z-Factor comparison between 23 Component model (post plus fluid regression) and 8 component lumped model.

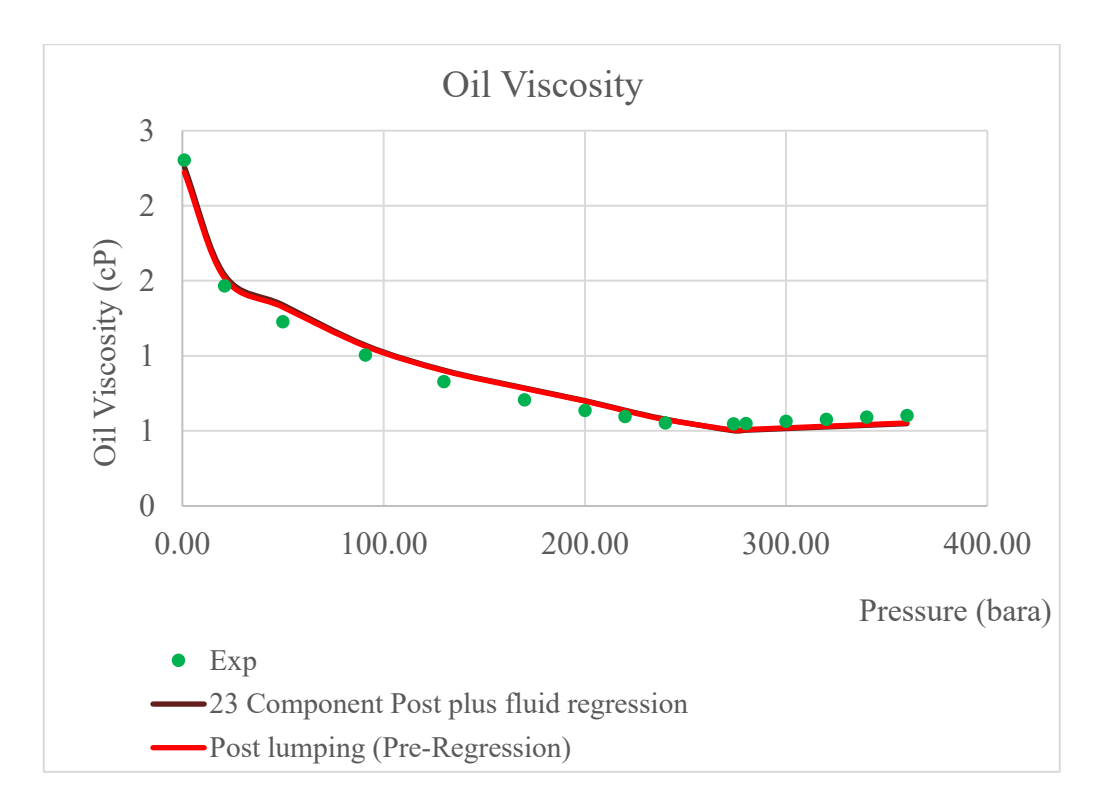


Figure 3.36: DL Oil viscosity between 23 Component model (post plus fluid regression) and 8 component lumped model.

3.4.2 Calibration of 8 Component EoS (PR-P)

The regression was performed in two ways:

- 1) **Option 1** represents a stepwise regression in two stages. In the first stage (1-step) T_c and P_c are regressed. In the second stage (2-step) binary interaction coefficient k_{ij} was tuned while parameters regressed at first stage were kept fixed.
- 2) **Option 2** corresponds to combined regression, where all parameters regressed in Option 1 were optimized together in a single step.

In the stepwise approach (Option 1), Tc and Pc were edited only in the first stage and only for the heavy pseudo-components (C13–C19, C20–C32, C33–C80), together with the two viscosity coefficients. The resulting Tc and Pc corrections were modest: for C13–C19, Tc increased by 2.6% while Pc decreased by 2.3%; for C20–C32, Tc changed by –0.002% and Pc by –0.8%; and for C33–C80, Tc increased by 2.4% and Pc decreased by 0.7%. Overall, Pc is essentially unchanged or shows a slight decrease for the heavier components (Figures 3.37-3.39).

In the second stage of the Option 1, only the binary interaction coefficients (kij) were tuned for the pairs N₂+CH₄ with C13–C19 and C20–C32, and CO₂+C₂ with C13–C19 and C20–C32. The adjustments were allowed within ±0.1 in absolute value, but some relative changes look very large because the initial values were close to zero. For example, the N₂+CH₄–C20–C32 coefficient moved from 0.0008 to 0.1000—an increase of about 12,400%—while the N₂+CH₄–C33–C80 term

shifted from 0.0008 to -0.0313, a change of roughly -4,013% (Figures 3.40 and 3.41). By contrast, the CO₂+C₂ terms changed only slightly, with small, sign-consistent adjustments mostly affecting C20–C32, with negligible changes elsewhere. Because kij values depend on the chosen EoS and on the P, T region used for fitting, there is no single "physical" range against which these numbers can be validated [Poling et al, 2014].

In the combined approach (Option 2), all parameters from the stepwise workflow are optimized together in a single step. Fitting everything at once allows Tc, Pc, the viscosity terms, and kij values to adjust simultaneously and to compensate for one another reducing the overall error. As a result, the heavy end shows larger adjustments: Tc increases for C13–C19 by 16.847% and decreases for C20–C32 and C33–C80 by about 4.537% and 7.475%, respectively. Pc is reduced mainly in the same cuts by 12.9% for C13–C19, 1.5% for C20–C32, and 7.437% for C33–C80. This combined regression can improve match, but it does so by allowing larger deviations of Tc and Pc from their post-lumping values. Analysing the results achieved with the two regression methods (Figures 3.37-3.41) shows that option 1 makes moderate adjustments of the regressed parameters, provides acceptable match and preserves phase envelope. On the contrary, option 2 achieves a stronger overall fit by making larger, coupled shifts to Tc and Pc in the heavy fractions.

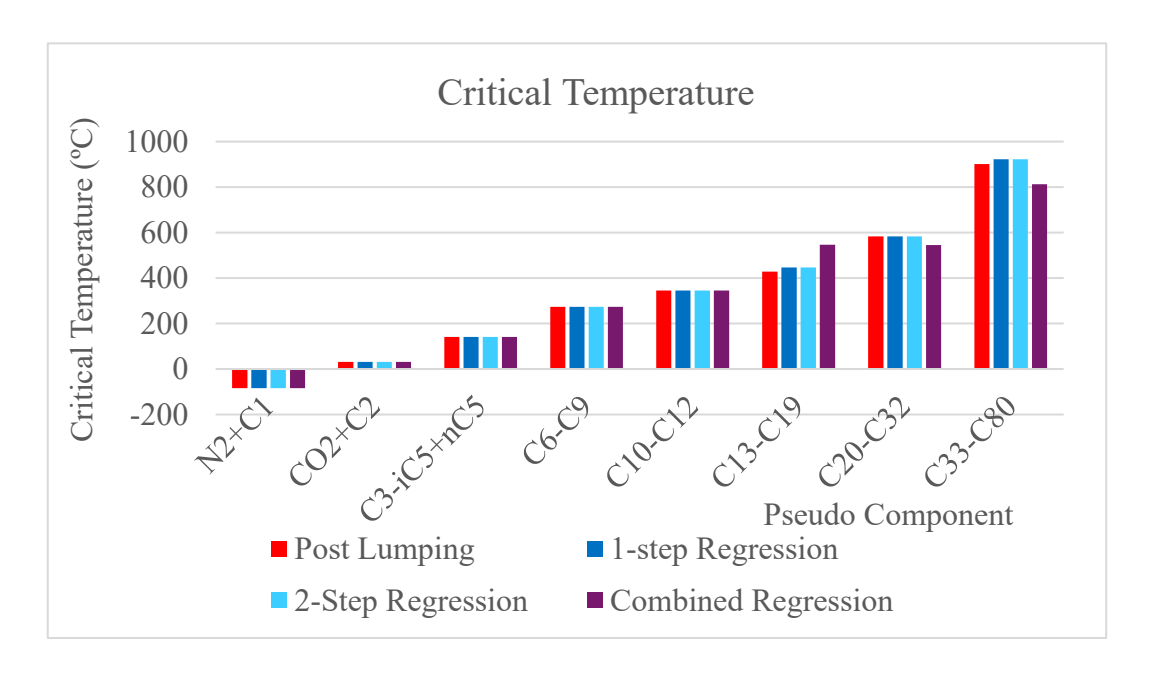


Figure 3.37: Critical Temperature values comparison for two regression options.

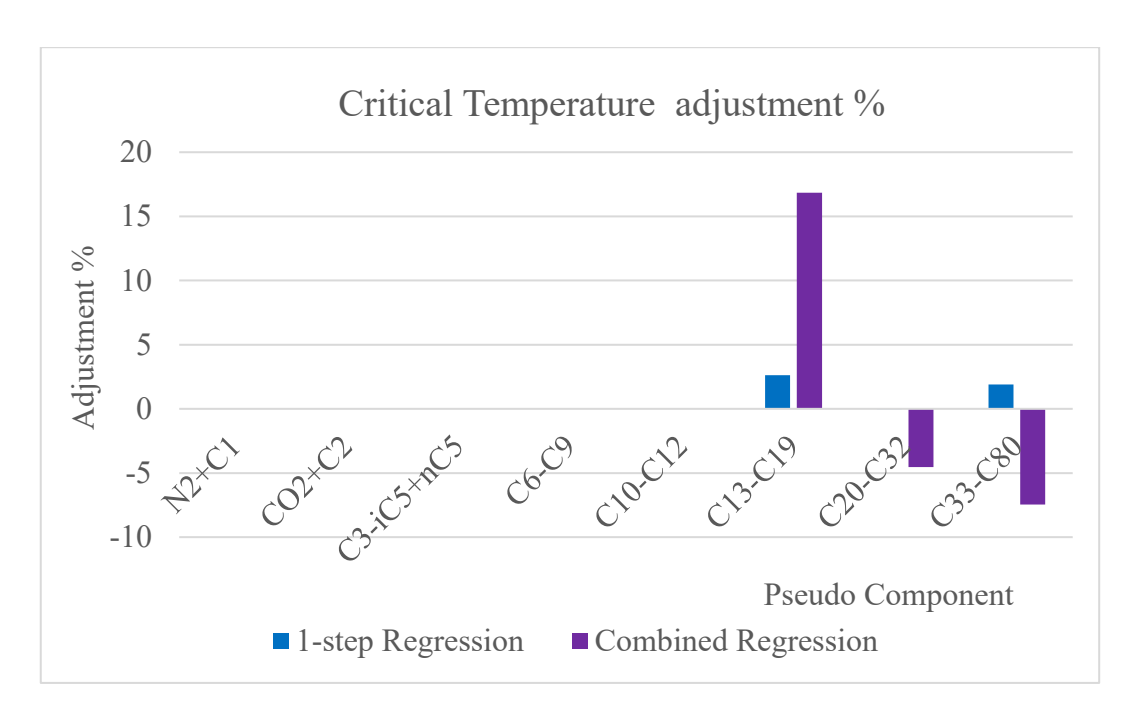


Figure 3.38: Critical Temperature adjustments. % Difference between Post lumping and Option 1(1-Step Regression) and Option 2 (combined Regression).

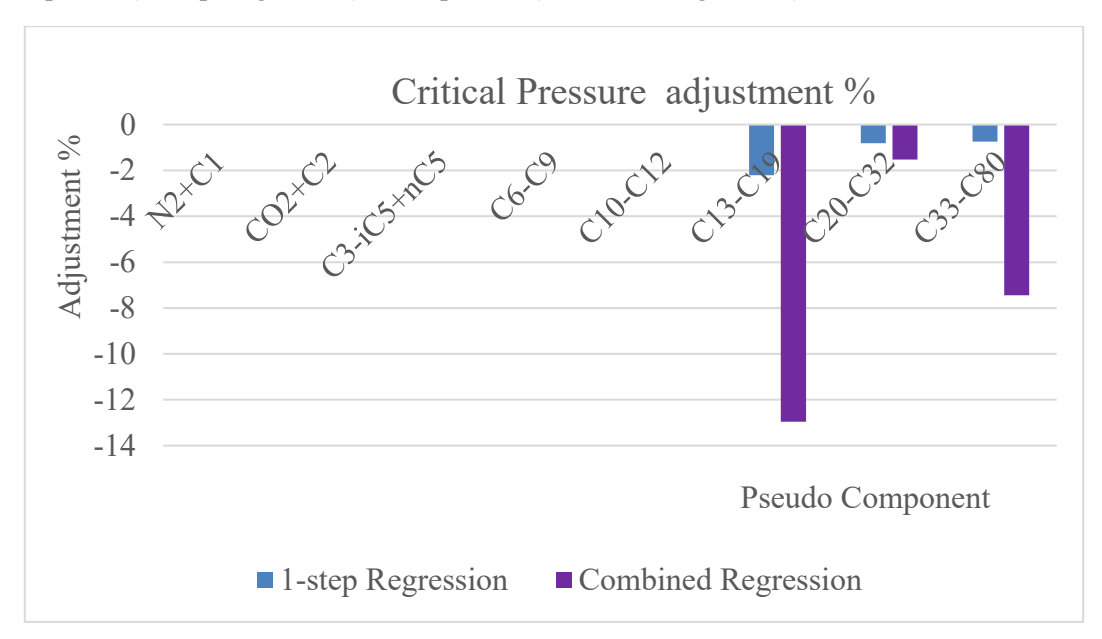


Figure 3.39: Critical Pressure adjustments. % Difference between Post lumping and Option 1(1-Step Regression) and Option 2 (combined Regression).

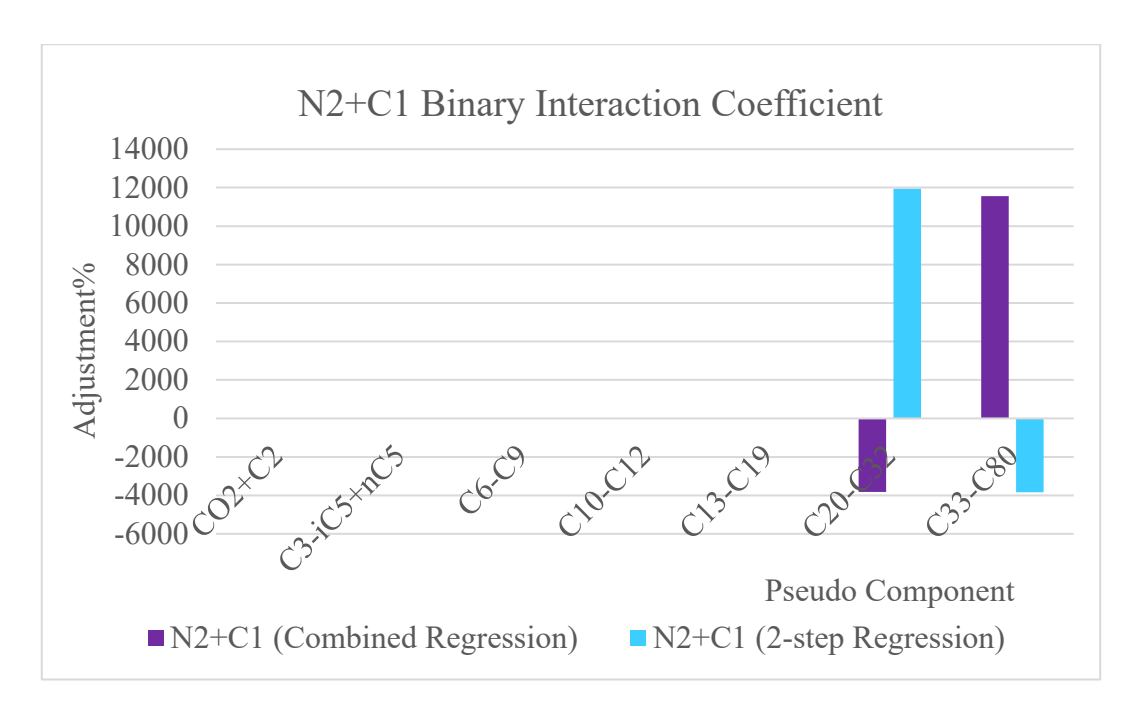


Figure 3.40: Binary interaction coefficient adjustments between N2+C1 and two heavy groups(C20-C32 and C33-C80). % Difference between Post lumping and Option 1(2-Step Regression) and Option 2 (combined Regression).

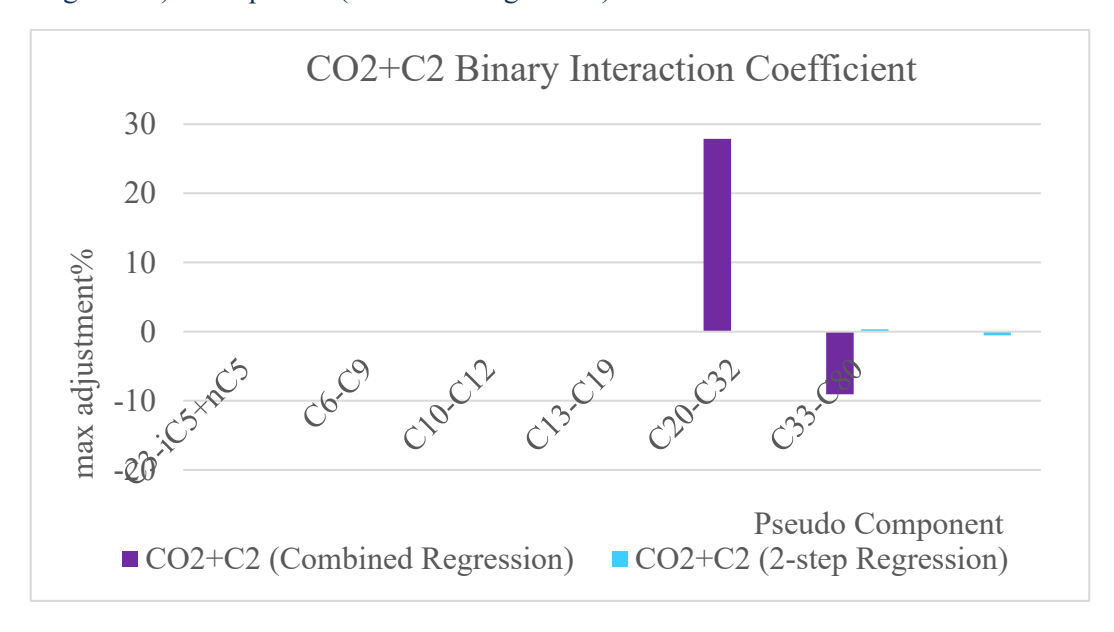


Figure 3.41: Binary interaction coefficient adjustments between CO2 +C2 and two heavy groups (C20-C32 and C33-C80). % Difference between Post lumping and Option 1(2-Step Regression) and Option 2 (combined Regression).

3.4.2.1 Option 1 and Option 2 regression results comparison

After post-lumping in Option 1, the Tc and Pc values are almost the same. The phase envelope moves a little higher and to the right, but its overall shape stays close to the post-lumping curve. In comparison, the combined regression (Option 2) makes a clear change in the heavy groups: the critical point moves from about 427 °C, 361 bar to 469 °C, 257 bar. This gives a separation between the envelopes above Psat and correlates with the better match to PVT behavior near saturation and at pressures above ~150 bar compared with Option 1.

For almost all PVT properties in Figures 3.42–3.51, the Option 1 and Option 2 results almost overlap. After the 2-step regression, the Psat deviation for Option 1 increased slightly to ~1%. The main difference is near saturation, where Option 2 follows the data more closely. Above 150 bar, Option 2 moves a bit away from Option 1: it predicts lower Rs and Bg, its Y-factor follows the data more closely, and it estimates slightly better volumetrics properties (higher Bo and a closer oildensity match).

Because we have limited data, we cannot make a final choice between the two options at this stage. To see the effect of a volume shift, we made a small Péneloux (Cpen) change to the heavy groups above C7+—specifically C10–C12, C13–C19, C20–C32, and C33–C80—with adjustments up to 50%, which is within the commonly recommended allowance (up to \sim 100%) for C7+ groups [Pedersen et al., 2007]. This gave a good oil-density match and improved Bo, and the phase envelope stayed essentially the same (Figure 3.58). Cpen changes calculated densities and volume factors but does not affect phase equilibrium [Péneloux et al., 1982; Pedersen et al., 2007].

Although we are not selecting a final option now, this analysis shows how the tuned parameters (Tc,Pc, kij,and Cpen) change the predicted PVT properties. Further tuning can be performed if compositions from more samples are available. Table 3.7 sums up the results and gives the simulations' average absolute deviation (AAD%).

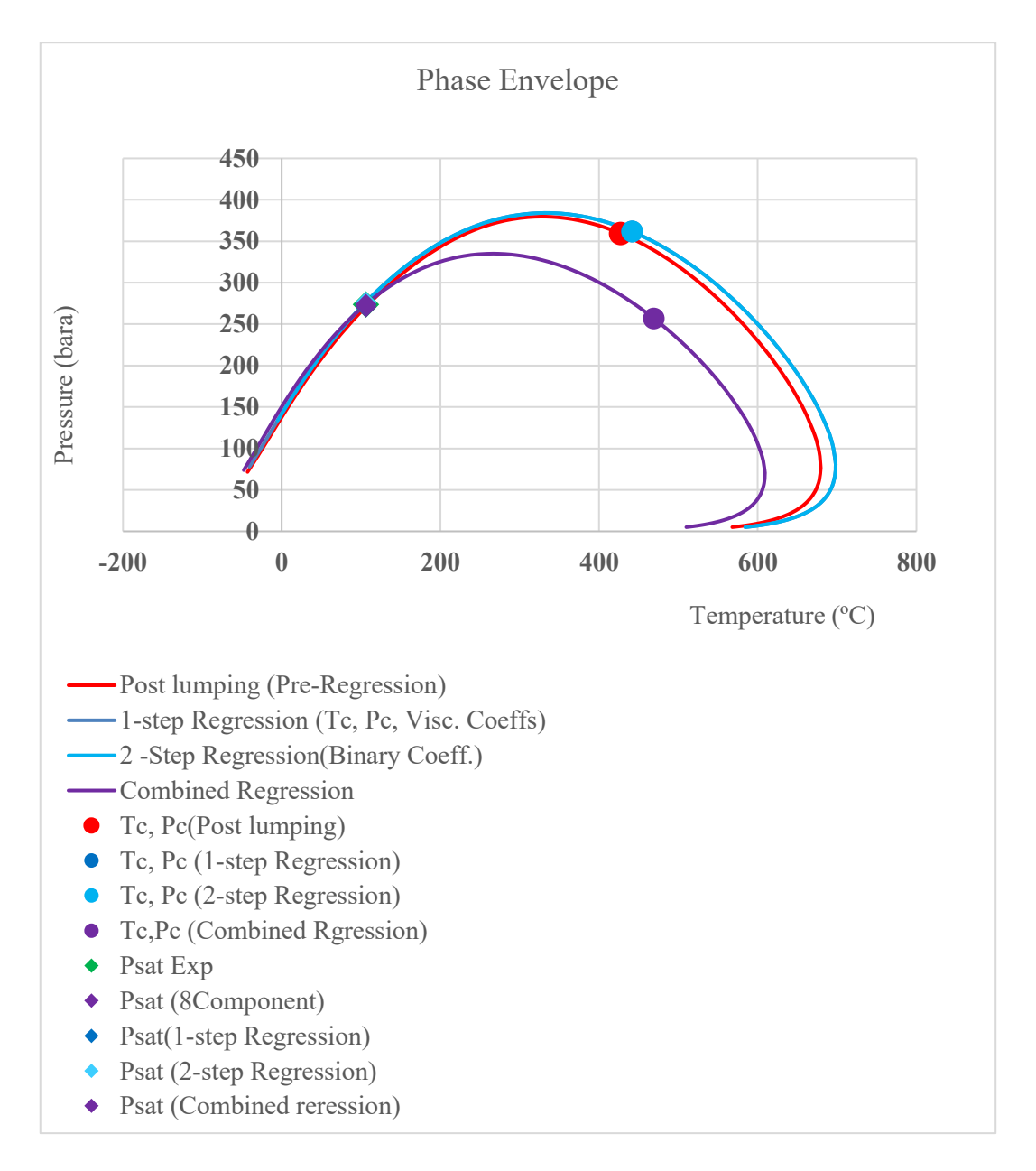


Figure 3.42: Phase Envelope. % Difference between Post lumping and Option 1(2-Step Regression) and Option 2 (combined Regression).

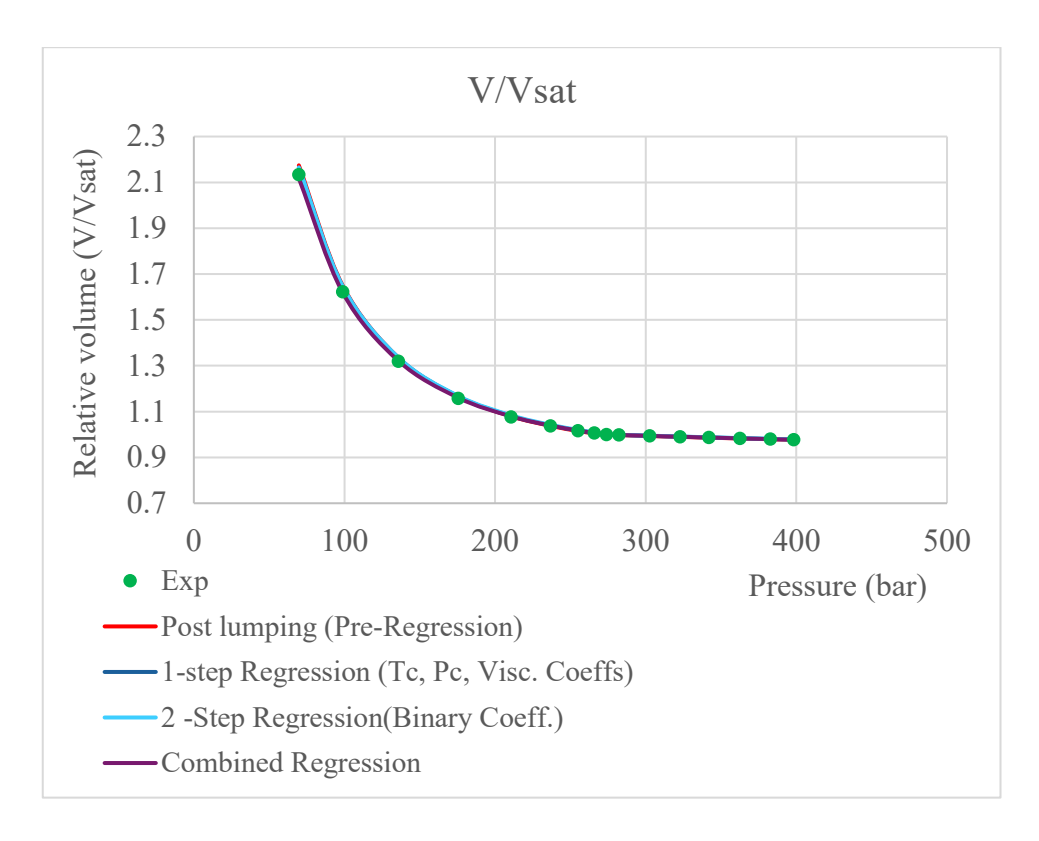


Figure 3.43: DL Relative volume. Difference between Post lumping and Option 1(1-Step and2-Step Regression) and Option 2 (combined Regression).

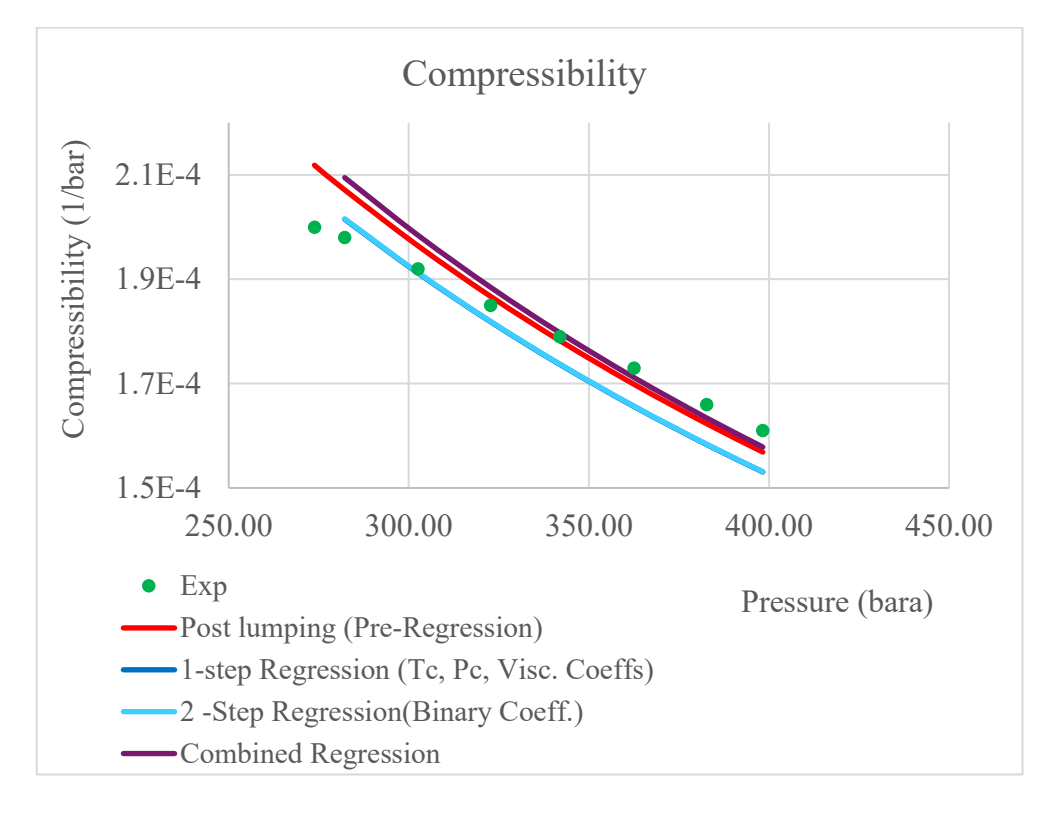


Figure 3.44: CCE Compressibility. Difference between Post lumping and Option 1(1-Step and2-Step Regression) and Option 2 (combined Regression).

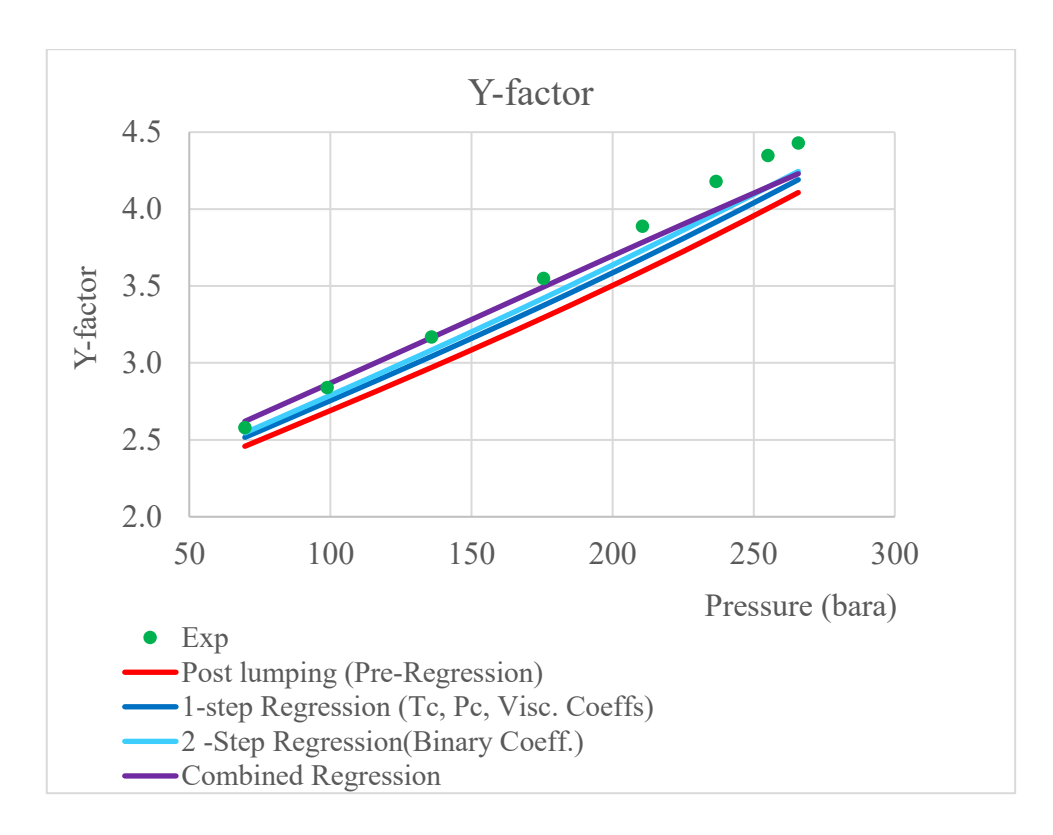


Figure 3.45: CCE Y-Factor. Difference between Post lumping and Option 1(1-Step and2-Step Regression) and Option 2 (combined Regression).

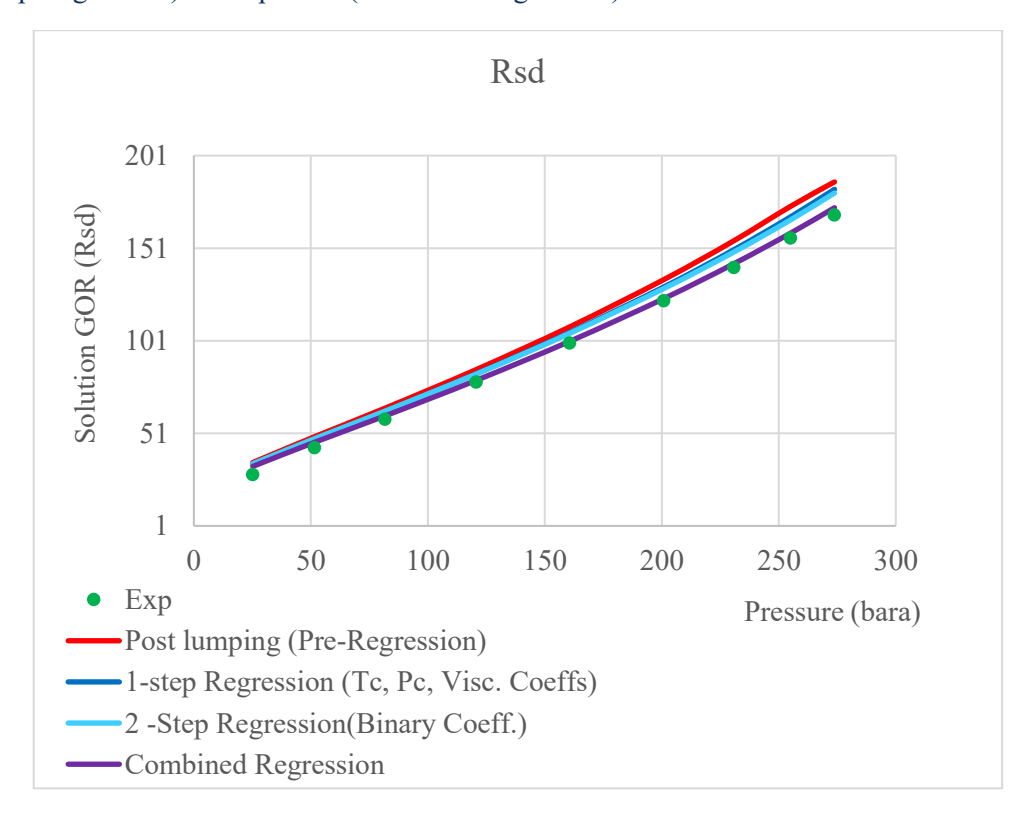


Figure 3.46: DL Solution GOR. Difference between Post lumping and Option 1(1-Step and2-Step Regression) and Option 2 (combined Regression).

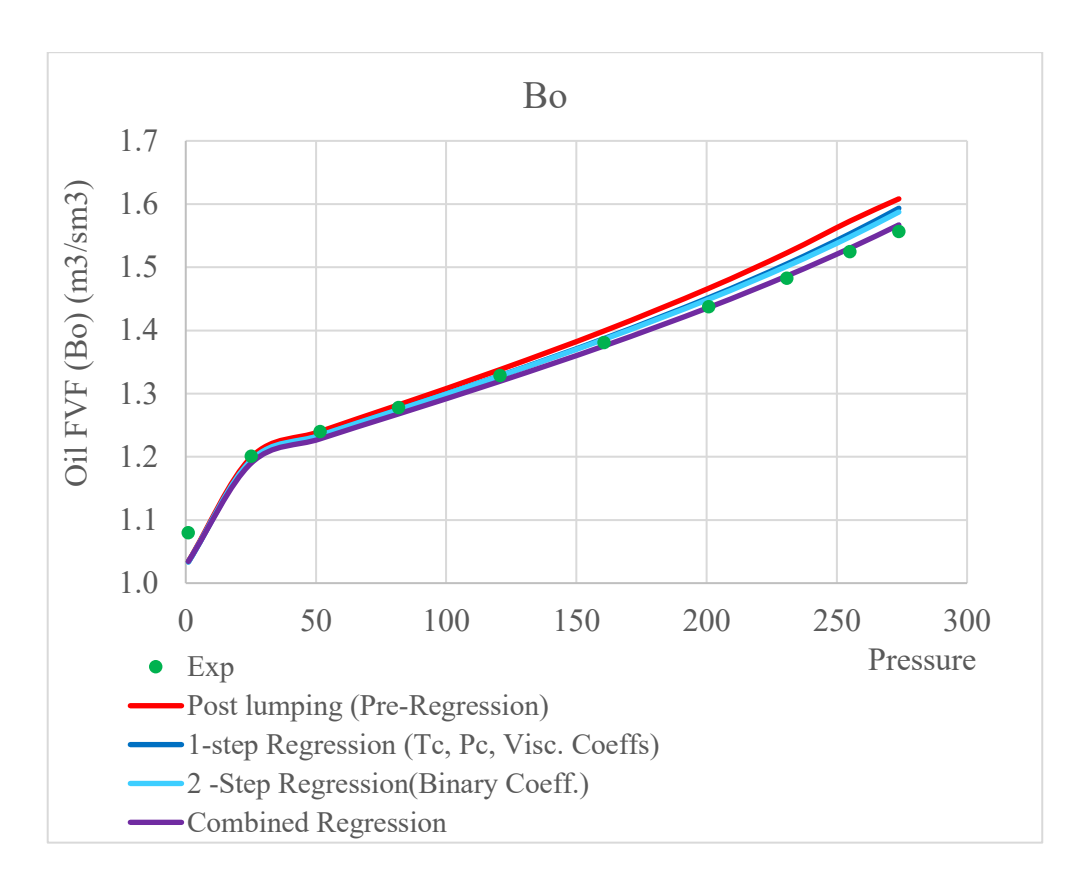


Figure 3.47: DL Oil Formation Volume Factor. Difference between Post lumping and Option 1(1-Step and 2-Step Regression) and Option 2 (combined Regression).

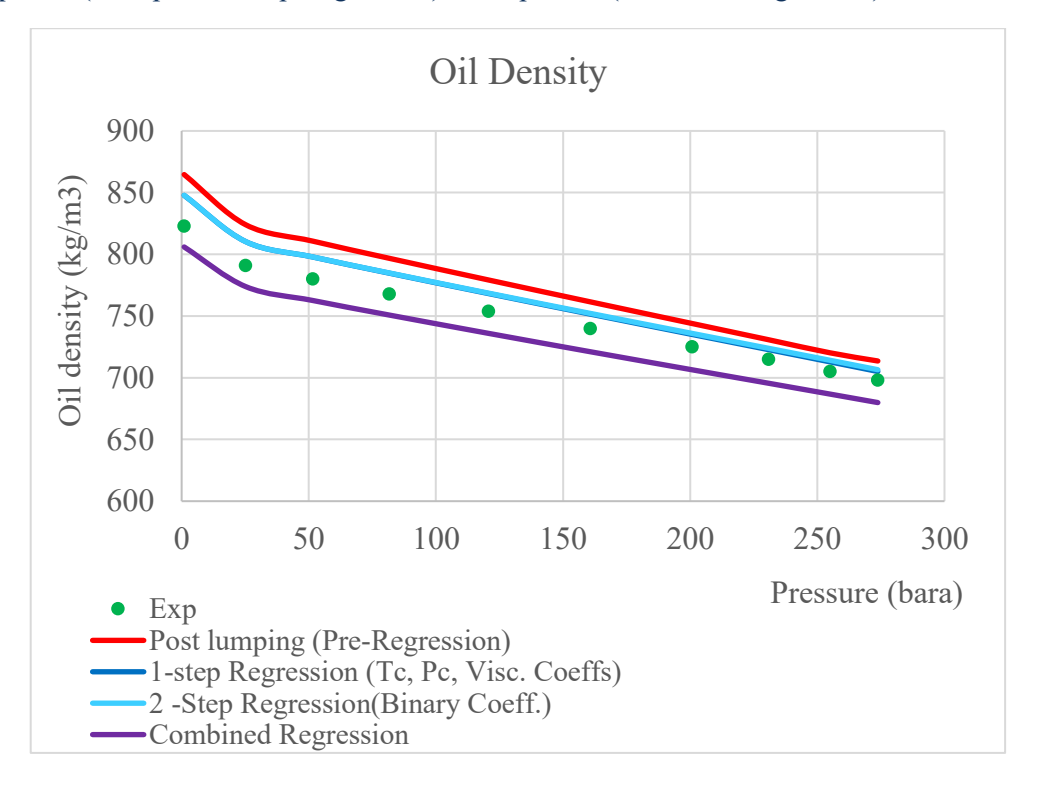


Figure 3.48: DL Oil density. Difference between Post lumping and Option 1(1-Step and2-Step Regression) and Option 2 (combined Regression).

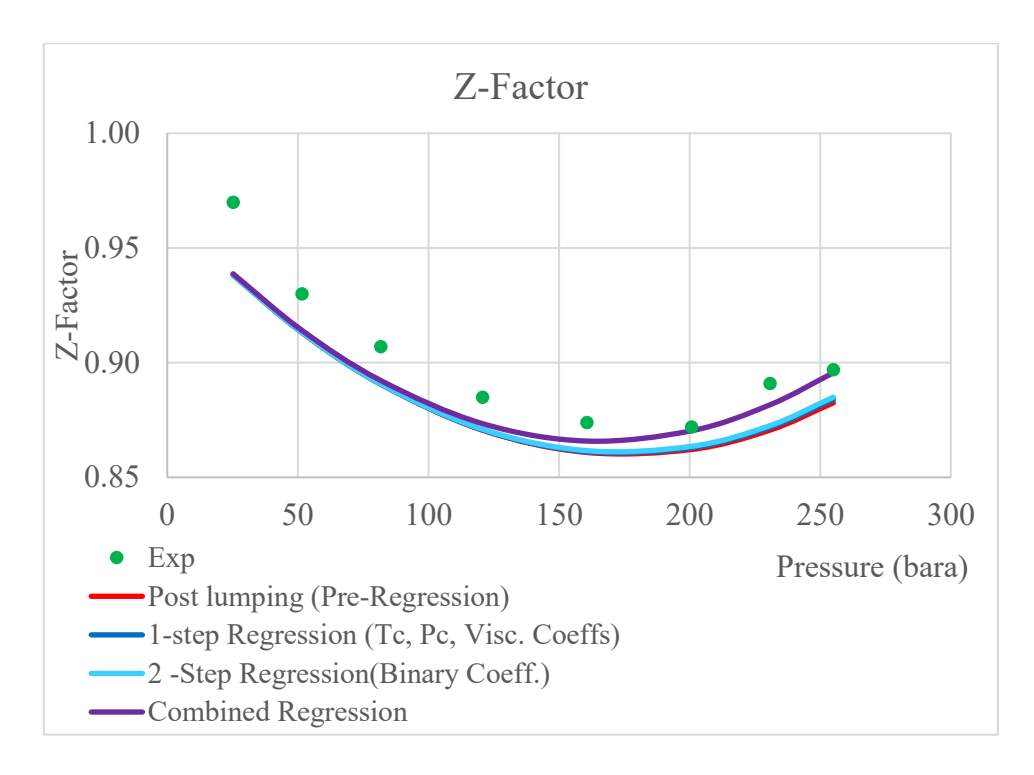


Figure 3.49: DL Gas Z-Factor. Difference between Post lumping and Option 1(1-Step and2-Step Regression) and Option 2 (combined Regression).

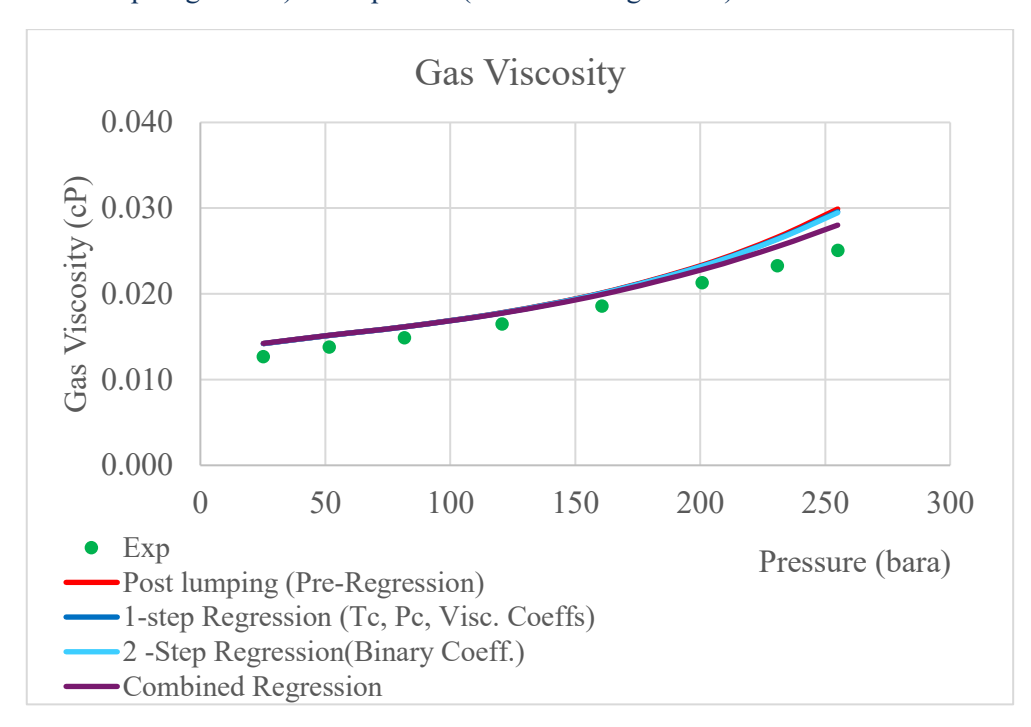


Figure 3.50: DL Gas Viscosity. Difference between Post lumping and Option 1(1-Step and2-Step Regression) and Option 2 (combined Regression).

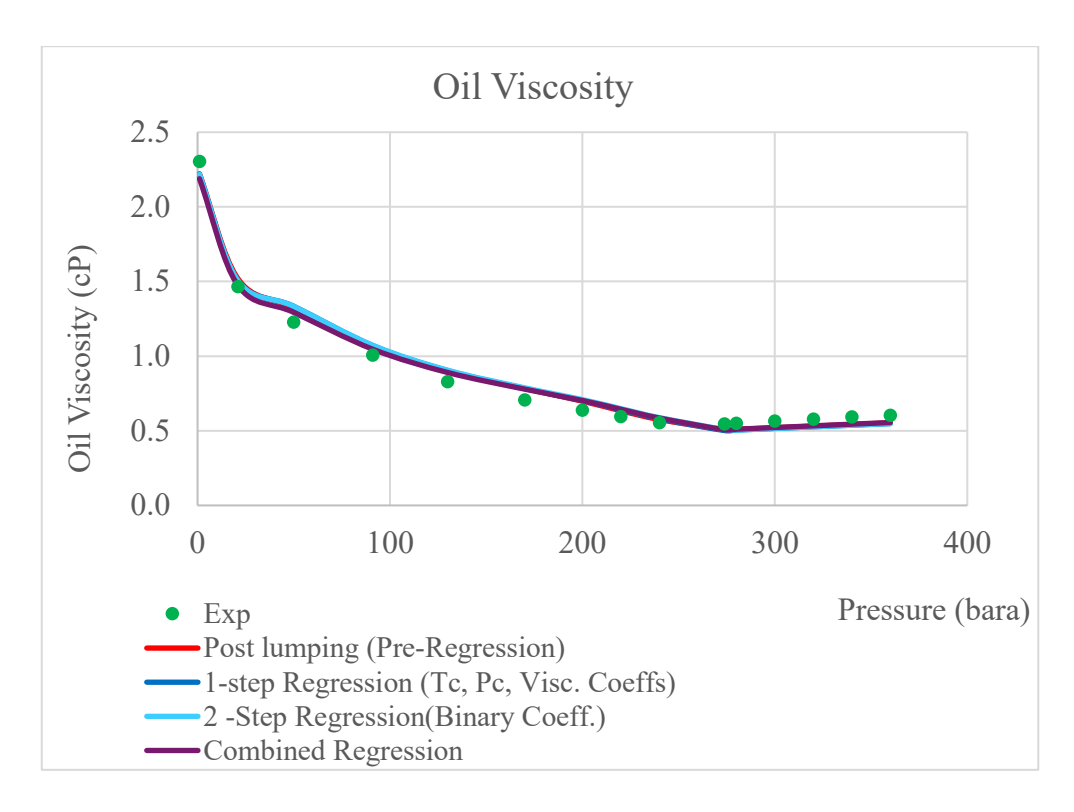


Figure 3.51: Oil Viscosity. Difference between Post lumping and Option 1(1-Step and2-Step Regression) and Option 2 (combined Regression).

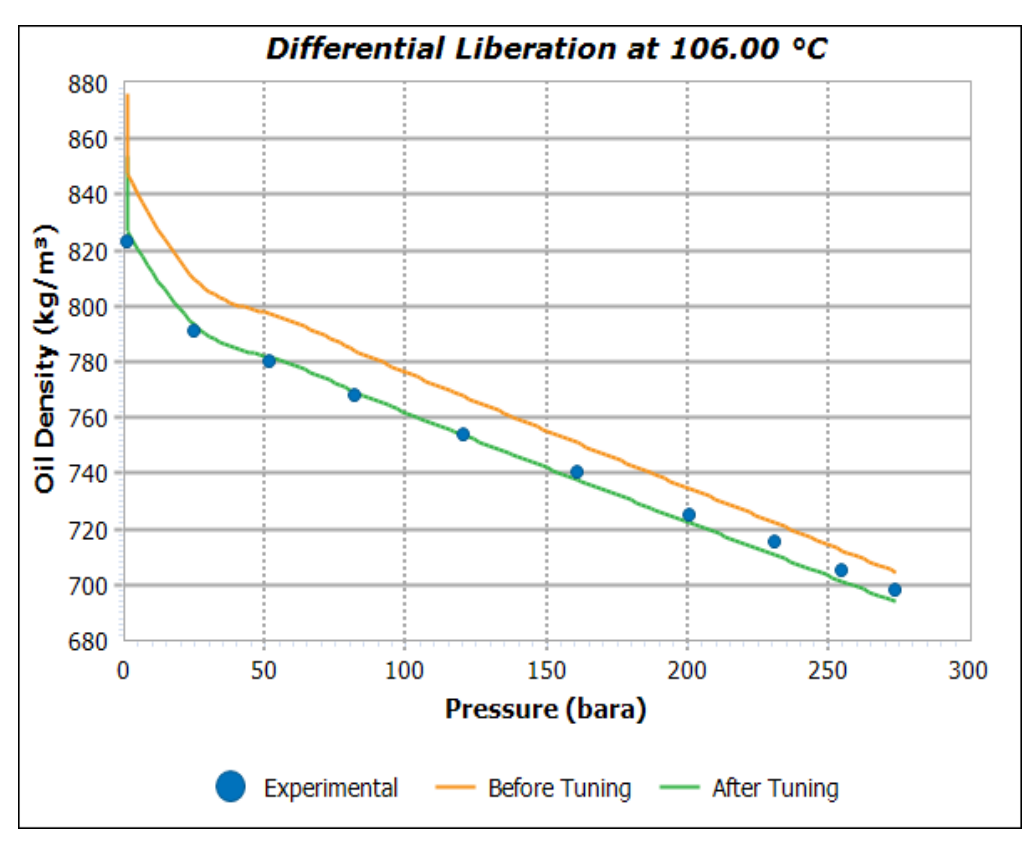


Figure 3.52: Oil density. Post Peneloux correction regression applied on Option 1.

		Num	Regression parameters	Regression groups		
Option 1	1-step regression	2	Tc, Pc max adjust 20% 1st Visc. Corr 2nd Visc Corr	1 group: C13-C19 2 group: C20-C32 3 group: C33-C80		
	2-step regression	1	kij max adjust 0.1	1 group:C20-C32 N2+C1 2 group: C33-C80 CO2+C2 1 group: C20-C32 CO2+C2 2 group: C33-C80		
Option 2	Combined regression	1	Tc, Pc max adjust 20%	1 group: C13-C19 2 group: C20-C32 3 group: C33-C80 N2+C1		
		2	kij max adjust 0.1	1 group: C20-C32 N2+C1 2 group: C33-C80 CO2+C2 1 group: C20-C32 CO2+C2		
		3	1st Visc. Corr 2nd Visc Corr	2 group: C33-C80		
	Final regression	1	cPen 0.1	1 group: C13-C19 2 group: C20-C32 3 group: C33-C80		

Table 3.8: Summary of regressed parameters of Option 1 (stepwise regression) and Option 2 (combined regression)

			CCE			DL						Oil	
				Comp ress.	V/Vsat	Y- factor	Oil density	Z- Factor	Gas visc.	Во	Rs	Bg	Viscosi ty
		Weight	5	4	1	1	4	3	3	2	2	1	2
	1-step regression	AAD %											
		before after	0.003		0.4		3.2 1.5		11.2 10.8		11.7 8.7		7.2 7.7
		Weight	1	4	1	1	1	4	3	3	2	2	1
Option 1	2-step regression	AAD %	0.0	2.6	0.3	4.7	1.5	1.8	10.8	1.3	8.7	1.2	7.7
		after			0.0		0.0		0.0		0.0		
			0.0		0.0	0.0	0.0				0.0	0.0	0.0
		Weight	5	4	1	1	4	3	3	2	2	1	2
Option 2	Combined regression	AAD % before after	1.1 0.006		0.4				11.2				7.2
		*** * 1 .	1				-	1	1	1	1	1	
		Weight	1	X	X	X	5	1	1	I	1	1	X
	Final regression	AAD % before after	0.006 0.006				2.4 0.0		9.2 0.0		3.8 0.0		

Table 3.9: Results of Option 1 (stepwise regression) and Option 2 (combined regression). Weight indicates the relative importance assigned during regression; AAD is the mean absolute difference between pre- and post-tuning predictions

Conclusion

This study carried out a three stages parametric analysis of cubic Equation of State using the Volve field PVT data set. A QA/QC of PVT composition confirmed high quality of the data.

In stage 1, SRK, SRK-Peneloux, PR and PR-Peneloux were compared in their default settings on the 23-component fluid. The comparison shows that both SRK and PR EoS reproduce the PVT trends with deviations acceptable for an untuned model parameters, nevertheless, consistent with their different formulations, systematic and expected differences appear in the simulated results. PR is less volatile, yielding a lower bubble point (248.5 bara) and smaller CCE expansion. By contrast, SRK is more volatile, predicting a higher bubble point (288.36 bara) and a "softer" liquid response. For reference, the experimental bubble point was 273.8 bara.

In Stage 2, plus-fraction regression was used to refine the heavy-end characterization. PR-Péneloux with modest adjustments to the heavy-end properties $(MW, T_c, P_c, and \omega)$ gave a clear improvement in the modelled PVT behaviour – better Psat match and CCE trends.

Stage 3 assessed the influence of key parameters, T_c , P_c and k_{ij} , under two tuning options and examined the effect of the Péneloux volume shift (cPen). A stepwise, constrained regression (heavy end T_c , P_c first, then k_{ij}) produced an acceptable match while keeping parameter deviations small and preserving the phase envelope. A simultaneous regression (optimizing T_c , P_c , and k_{ij} together) provided a more accurate fit, though it required larger adjustments. As expected, small, targeted Peneloux adjustment to C7+ groups effectively improved oil density.

To advance this work, the same workflow can be extended to multiple field samples. A field-wide, multi-sample calibration would help reduce deviations from experimental data while preserving key fluid characteristics, leading to a fit-for-purpose EoS suitable for reservoir-scale simulation.

References

- Alavian Sayyed Ahmad, SPE, PERA, Curtis Hays Whitson, SPE, NTNU/PERA, Sissel O. Martinsen, PERA. 2014: Global Component Lumping for EOS Calculations: SPE 170912
- Amyx, J. W., Bass, D. M., & Whiting, R. L. (1960). Petroleum Reservoir Engineering: Physical Properties (McGraw-Hill).
- **Bejan, A. 2006.** *Advanced Engineering Thermodynamics* (3rd ed.). Hoboken, NJ: John Wiley & Sons.
- **Behrens, R.A. and Sandler, S.I., 1986**: "The Use of Semicontinuous DescriptionTo Model the C7+ Fraction in Equation of State Calculations." paper SPE 14925 presented at the 1986 SPE/DOE Symposium on Enhanced Oil Recovery, Tulsa, Oklahoma, 23–23 April. doi:10.2118/14925-PA.
- **CALSEP, online.** Reservoir Fluid Characterization (Tech Talk #19):, https://www.calsep.com
- Calsep. PVTsim Method Documentation. https://calsep.com/pvtsim-method-documentation/
- **Chueh, P.L., and Prausnitz, J.M. 1967**. Vapor–liquid equilibria at high pressures: Calculation of critical temperatures, volumes, and pressures of nonpolar mixtures: AIChE Journal 13:1107–1116
- **Christensen, P. L. (1999).** Regression to experimental PVT data. Journal of Canadian Petroleum Technology, 38(13), 1–9. doi:10.2118/99-13-52.
- **Coats, K.H. 1870:** *Simulation of Gas Condensate Reservoir Performance*: JPT (October 1985) 1870.
- **Danesh, A., Xu, D., and Todd, A. C., 1992:** "A Grouping Method To Optimize Oil Description for Compositional Simulation of Gas-Injection Processes." SPE Res Eng 7(3): 343-348, August. doi:10.2118/20745-PA
- **Danesh, A. 1998.** PVT and Phase Behavior of Petroleum Reservoir Fluids. London: Elsevier Science B.V., 1998

- **Dake L .1978.** Fundamentals of reservoir engineering, no. 8. Amsterdam: Developments in Petroleum Science, Elsevier Science BV
- **Hoffman A, Crump J, Hocott C. 1953.** Equilibrium constants for a gascondensate system: J Petrol Technol 5(01):1–10
- **Hustad, O. S., and Dalen, V., 1993:** An Explicit Phase-Behavior Model for Pseudo-compositional Reservoir Simulation. Society of Petroleum Engineers. SPE Advanced Technology Series 1(1): 17-26, April, doi:10.2118/19806-PA
- **Joergensen, M., and Stenby, E. H., 1995:** "Optimization of Pseudo-component Selection for Compositional Studies of Reservoir Fluids": Paper SPE 30789 presented at the SPE Annual Technical Conference and Exhibition, Dallas, Texas. October 22-25, doi:10.2118/30789-MS.
- **Kay, W. B. 1936.** Gases and Vapors at High Temperature and Pressure—Density of Hydrocarbon Gases and Vapors: Industrial & Engineering Chemistry, 28(9), 1014–1019. DOI: 10.1021/ie50321a008.
- Katz, D. L., and A. Firoozabadi. 1978. "Predicting Phase Behavior of Condensate/Crude-Oil Systems Using Methane Interaction Coefficients." :Journal of Petroleum Technology 30 (11): 1649–1655. https://doi.org/10.2118/6786-PA
- **Laboratory report 93.104,1993**. *PVT analysis Well 15/9-19SR DST 1*. **PROLAB** 93.104. Volve field data set download Equinor
- **Lomeland, F., & Harstad, O. 1994**. Simplifying the task of grouping components in compositional reservoir simulation. Presented at the European Petroleum Computer Conference, Aberdeen, UK, March 15–17, 1994 (paper accepted Feb 10, 1995). (SPE Paper SPE-27581).
- Li, Y.-K., Nghiem, L.X., and Siu, A. 1984 "Phase Behavior Computation for Reservoir Fluid: Effects of Pseudo Component on Phase Diagrams and Simulations Results,": CIM 84-35-19 presented at the 1984 Petroleum Soc. of CIM Annual Meeting, Calgary, 10–13 June. doi.org:10.2118/85-06-02.
- **Liu, K., 2001**: "Reduce the Number of Components for Compositional Reservoir Simulation.", paper SPE 66363 presented at the 2001 SPE Reservoir Simulation Symposium, Houston, Texas, February 11-14, doi:10.2118/66363-MS.
- Lee, S.T., Jacoby, R.H., Chen, W.H., Culham, W.E., 1982. "Experiments and Theoretical Simulation on the Fluid Properties Required for Simulation of Thermal Processes": SPEJ (October) 535. doi.org:10.2118/8393-PA.

- **McCain WD Jr .1990.** Components of naturally occurring petroleum fluids. In: Properties of petroleum fluids, PennWell Books, Tulsa, pp 1–45
- Michelsen, M. L., & Mollerup, J. .2007. Thermodynamic Models: Fundamentals & Computational Aspects (2nd ed.): Tie-Line Publications.
- **Montel, F., & Gouel, P. L. 1984**: "A New Lumping Scheme of Analytical Data for Compositional Studies. Society of Petroleum Engineers." paper SPE 13119 presented at the 1984 SPE Annual Technical Conference and Exhibition, Houston, Texas, September 16-19, doi:10.2118/13119-MS.
- **Nasrifar, K.; Bolland, O. 2006.** Prediction of thermodynamic properties of natural gas mixtures using 10 equations of state including a new cubic two-constant equation of state. J. Pet. Sci. Eng. **2006**, 51, 253–266.
- Nazarzadeh, M.; Moshfeghian, M. 1999. New volume translated PR equation of state for pure compounds and gas condensate systems: Fluid Phase Equilibria 2013, 337, 214–223.
- **Nelson, L.C. e Obert, E.F. 1954.** *Generalizedp-v-T properties of Gases.* s.l.: Trans. A.S.M.E., Vol. 76 p. 1057, 1954.
- Newley, T.M.J. and Merrill, R.C. Jr. 1991. Pseudo-component Selection for Compositional Simulation: SPERE (November 1991) 490; Trans., AIME, 291. doi:10.2118/19638-PA.
- **Peng, D.-Y. and Robinson, D.B.1976.** A new two-constant equation of state: Ind. Eng. Chem. Fundam. 15, 59–64,1976
- **Peng, D.-Y. and Robinson, D.B.** 1978. The Characterization of the Heptanes and Heavier Fractions for the GPA Peng-Robinson Programs: GPA Research Report RR-28, 1978.
- Peneloux, A., Rauzy, E., and Fréze, R., A. 1982 consistent correction for Redlich-Kwong-Soave volumes: Fluid Phase Equilibria 8, 7–23, 1982
- Pedersen, K.S., Thomassen, P., and Fredenslund, Aa., 1983. SRK-EOS calculation for crude oils: Fluid Phase Equilibria 14, 209-218, 1983.
- **Pedersen, K.S., Thomassen, P., and Fredenslund, Aa.,1984**Thermodynamics of petroleum mixtures containing heavy hydrocarbons. 1. Phase envelope calculations by use of the Soave-Redlich-Kwong equation of state: Ind. Eng. Chem. Process Des. Dev. 23, 163-170, 1984.

- **Pedersen, K.S., Thomassen, P., and Fredenslund, Aa. 1989.** *Characterization of gas condensate mixtures, Advances in Thermodynamics*: Taylor & Francis, New York, 1, 137–152, 1989.
- **Pedersen, K.S., Blilie, A.L., and Meisingset, K.K.** 1992. PVT calculations on petroleum reservoir fluids using measured and estimated compositional data for the plus fraction: I&EC Research 31, 1378–1384, 1992.
- **Pedersen, Karen Schou, and Peter L. Christensen. 2007**. *Phase Behavior of Petroleum Reservoir Fluids*. Boca Raton, FL: CRC Press.
- Pedersen, Karen Schou, Peter L. Christensen, and Jawad Azeem Shaikh. 2014. Phase Behavior of Petroleum Reservoir Fluids: 2nd ed. Boca Raton, FL: CRC Press
- **Pedersen, K.S., Milter, J. and Sørensen, H., 2002.** "Cubic Equations of State Applied to HT/HP and Highly Aromatic Fluids", SPE 77385, SPE ATCE in San Antonio, Tx, September 29-October 2, 2002.
- **Poling, B. E., Prausnitz, J. M. e O'Connell, J. P. 2001.** The properties of gases and liquids, 5th edition. s.l.: McGrall-Hill, 2001.
- **Potsch, K.; Toplack, P.; Gumpenberger, T. 2017.** A review and extension of existing consistency tests for PVT data from a laboratory. SPE Reservoir Evaluation & Engineering, 20(2), 269–284. SPE Paper SPE-183640-PA.
- Prausnitz, J. M., Lichtenthaler, R. N., & de Azevedo, E. G. 1998. *Molecular Thermodynamics of Fluid-Phase Equilibria (3rd ed.):* Prentice Hall.
- Rachford, H.H. Jr. and Rice, J.D.1952. Procedure for use of electronic digital computers in calculating flash vaporization hydrocarbon equilibrium: J. Petroleum Technol. 4, 1952, sec. 1, p. 19 and sec. 2, p. 3
- **Redlich, O. e Kwong, J.N. 1949.** On the thermodynamics of solutions. V. An equation of state. Fugacities of gaseous solutions. s.l.: Chemical Reviews 44 (1),pp. 233-244, 1949.
- S. Sajjadian, M.R. Ghafoori, M. Roostaeian, A. Hashemi, A. Asheghi, and V.A. Sajjadian. 2010: Thermodynamic Fluid Characterization in a Compositional Reservoir Model: A Field Gas Injection Study: National Iranian Oil Company, SPE 132949
- **Schlijper, A.G. 1986.** "Simulation of Compositional Processes: The Use of Pseudo-components in Equation-of-State Calculations," SPERE (September 1986) 441; Trans., AIME, 282

- **Seyed Mohammad Hossein Hashemi, Kazem Monfaredi, Behnam Sedaee.** *An inclusive consistency check procedure for quality control methodsof the black oil laboratory data*: Journal of Petroleum Exploration and Production Technology (2020) 10:2153–2173. https://doi.org/10.1007/s13202-020-00869-6
- **Soave, G.1972.** Equilibrium constants from a modified Redlich-Kwong equation of state. Chem. Eng. Sci. **1972**, 27, 1197–1203.
- **Standing, M. B. (1952).** The compressibility factor of natural gas and its application to the calculation of gas volumes: Journal of Petroleum Technology, 4(11), 1–8.
- Whitson, C.H. 1983. "Characterizing Hydrocarbon Plus Fractions," SPEJ (August 1983) 683; Trans., AIME, 275. doi:10.2118/12233-PA
- Whitson, C.H., Anderson, T.F., and Søreide,1989. "C7+ Characterization of Related Equilibrium Fluids Using the Gamma Distribution,": C7+ Fraction Characterization, Advances in Thermodynamics, Vol. 1 (1989), Mansoori, G.A., ed., Taylor and Francis, NY, 35-56.
- Whitson, C. H., & Brulé, M. R. 2000. *Phase Behaviour:* (SPE Monograph Series, Vol. 20).
- Van der Waals, J.D. 1873. Doctoral Dissertation, Over de Continuiteit van der Gas- en Vloeistoftoestand. Leiden University (On the Continuity of the Gaseous and Liquid States), The Netherlands, 1873. (In Dutch.)
- Van der Waals, J. D. 1913. The law of corresponding states for different substances. s.l.: KNAW, Proceedings, Vol. XV, 1913.